

**PHYSICS OF MELT COOLABILITY FOR CORE  
CATCHER DESIGN FOR ADVANCED NUCLEAR REACTORS**

*By*

**NITENDRA SINGH**

**ENGG01201204026**

**BHABHA ATOMIC RESEARCH CENTRE,  
MUMBAI 400085, INDIA**

*A thesis submitted to the Board of Studies in Engineering Sciences*

*In partial fulfilment of requirements for the Degree of*

**DOCTOR OF PHILOSOPHY**

*of*

**HOMI BHABHA NATIONAL INSTITUTE**



**March 2018**

**Certificate**

**Will be**

**Uploaded**

**Soon**

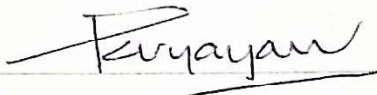
*“The true method of knowledge is experiment”*

— *William Blake (28 November 1757 – 12 August 1827)*  
*English poet, painter, and printmaker.*

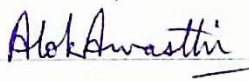
# Homi Bhabha National Institute

## Recommendations of the Viva Voce Committee

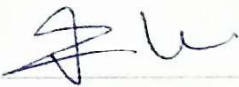
As members of the Viva Voce Committee, we certify that we have read the dissertation prepared by *Nitendra Singh* entitled "*Physics of melt coolability for core catcher design for advanced nuclear reactors*" and recommend that it may be accepted as fulfilling the thesis requirement for the award of Degree of Doctor of Philosophy.

Chairman – Dr P K Vijayan  Date: 03/03/18

Guide / Convener – Dr A K Nayak  Date: 3/3/18

Co-guide – Dr A Awasthi  Date: 03/3/2018

Examiner – Prof. Pradyumna Ghosh  Date: 3/3/18

Member 1- Prof Atul Sharma  Date: 3/3/18

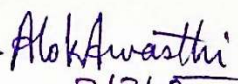
Member 2- Dr A K Nayak  Date: 3/3/18

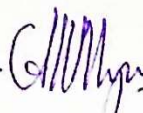
Final approval and acceptance of this thesis is contingent upon the candidate's submission of the final copies of the thesis to HBNI.

I/We hereby certify that I/we have read this thesis prepared under my/our direction and recommend that it may be accepted as fulfilling the thesis requirement.

Date:

Place:

<Signature>   
3/3/18  
Co-guide (if applicable)  
Dr A. AWASTHI

<Signature>  3/3/18  
Guide  
Dr. A. K. Nayak

## **STATEMENT BY AUTHOR**

This dissertation has been submitted in partial fulfilment of requirements for an advanced degree at Homi Bhabha National Institute (HBNI) and is deposited in the Library to be made available to borrowers under rules of the HBNI.

Brief quotations from this dissertation are allowable without special permission, provided that accurate acknowledgement of source is made. Requests for permission for extended quotation from or reproduction of this manuscript in whole or in part may be granted by the Competent Authority of HBNI when in his or her judgement the proposed use of the material is in the interests of scholarship. In all other instances, however, permission must be obtained from the author.

NITENDRA SINGH

## **DECLARATION**

I, hereby declare that the investigation presented in the thesis has been carried out by me. The work is original and has not been submitted earlier as a whole or in part for a degree / diploma at this or any other Institution / University.

NITENDRA SINGH

## List of Publications arising from the thesis

### Publications in Refereed Journal:

- [1] N Singh, P P Kulkarni, A K Nayak, “*Experimental investigation on melt coolability under bottom flooding with and without decay heat simulation*”, **Nuclear Engineering and Design**, 285 (2015), 48-57,  
<http://dx.doi.org/10.1016/j.nucengdes.2014.12.029>.
- [2] N Singh, A K Nayak, P P Kulkarni, “*Experimental investigation of melt coolability under bottom injection: effects of melt volume, melt composition, nozzle diameter, and inlet pressure*”, **Nuclear Technology**, 198 (2017), 306-318,  
<http://dx.doi.org/10.1080/00295450.2017.1305764>.
- [3] N Singh, A K Nayak, P P Kulkarni, “*Numerical modelling and experimental validation of melt pool coolability under bottom flooding with decay heat simulation*”, **Nuclear Technology**, (2018)  
<http://doi.org/10.1080/00295450.2018.1426961>.
- [4] N Singh, A K Nayak, P P Kulkarni, “*Experimental investigation on fuel coolant interaction using simulant ceramic melts in water: insights and conclusions*”. (In proof for publication, World Journal of **Nuclear Science and Technology**),  
<http://doi.org/10.4236/wjnst.2018.44025>.

### Publications in the conferences:

- [5] N. Singh, A. K. Nayak, “*Melt coolability under bottom flooding: A study to understand the effect of decay heat, melt simulants and geometrical parameters*”, PHWR International workshop **CANSAS-2016**, October 12-14, 2016, Korea
- [6] N. Singh, P. P. Kulkarni, A. K. Nayak, “*Modeling of ex-vessel melt pool coolability under bottom flooding with decay heat simulation*”, International Topical Meeting on Nuclear Reactor Thermal Hydraulics 2015, **NURETH 2015**, V-6, 5098-5111
- [7] N. Singh, A. K. Nayak, A. Awasthi, “*A model to understand physics of melt coolability under bottom flooding*”, 91p, 2014, **IW-NRTHS 2014**: International Workshop on new horizons in Nuclear Reactor Thermal Hydraulics and Safety; INIS V-45, INIS Issue34
- [8] N. Singh, A. K. Nayak, “*Physics of steam explosion*”, International symposium on Severe Accident Analysis & Management (**SAAM-2013**), 2013, IIT Kanpur, India

NITENDRA SINGH

# *Dedicated to*

## **“My Family”,**

*[Father: instilled me with leadership and fearlessness*

*Mother: taught me to stay calm and keep working*

*Brother: always encourages me to keep the curious child alive in me*

*Sister: my beloved “Megha”, my inner strength who always pushed me to gain perfection. (She'll remain alive within me, forever)]*



ॐ

असतोमा सद्गमय। तमसोमा ज्योतिर् गमया।  
मृत्योर्मा मृतं गमय ॥ ॐ शांति शांति शांति

(बृहदारण्यक उपनिषद् 1.3.28)

**"Aum Asato mā sad gamaya  
Tamaso mā jyotir gamaya  
Mṛtyormā amṛtam gamaya  
Aum śānti śānti śāntiḥ "**

(Bṛhadāranyaka Upaniṣad 1.3.28)

*O Lord, Keep me not in the **Unreality** (of the bondage of the Phenomenal World), but lead me towards the **Reality** (of the Eternal Self);*

*Keep me not in the **Darkness** (of Ignorance), but lead me towards the **Light** (of Spiritual Knowledge);*

*Keep me not in the **Fear of Death** (due to the bondage of the Mortal World), but lead me towards the **Immortality** (gained by the Knowledge of the Immortal Self beyond Death);*

*O Lord, (May there be) **Peace, Peace, Peace** (at the the three levels - Adidaivika, Adibhautika and Adhyatmika).*

## ACKNOWLEDGEMENTS

Foremost, I would like to express my sincere gratitude to my Guide Dr A K Nayak (RED, BARC) for the continuous support of my PhD study and related research, for his patience, motivation, and immense knowledge. His guidance helped me in all the time of research and writing of this thesis. I could not have imagined having a better advisor and mentor for my PhD study. During tough times and whenever I stuck in any way, he was always besides me.

Besides my guide, I would like to thank the rest of my thesis committee: Chairman of the committee, Dr P K Vijayan (BARC); Dr K Velusamy (IGCAR), Prof. Atul Sharma (IIT-Bombay) and Dr Umashankari Kannan (BARC), for their insightful comments and encouragement, but also for the hard questions which incited me to widen my research from various perspectives.

I would like to thank Dr R B Grover (Former Director HBNI) for the moral encouragement throughout this journey. He always managed to spare time amidst his busy schedule to listen to me, my issues and my views. His firm belief and vision towards my work, always, filled me with the confidence to make things happen.

I am grateful to my Co-guide, Dr A Awasthi (MPD, BARC), who have provided me through moral and emotional support in my life. His special guidance towards high temperature melts, thermite and scientific aspects of materials helped me a lot during my research. His faith in me and proud word like “he is my student” always instilled me with a feeling of joy and excitement.

A very special gratitude goes to Dr Parimal P Kulkarni (RED, BARC), for being there for a technical guidance, subjective inputs and above all a great friend whenever I needed him.

Without his precious support it would not have been a wonderful journey for me to conduct this research. He has been a great inspiration throughout this work.

Shri Sumit V Prasad (RED, BARC), is such a charming personality that I don't know how to thank him. His down to earth and humorous nature was a great emotional support. Also, he helped me in structural designs of test sections and its analysis. I have learnt a lot from him.

This section would be incomplete without mentioning Prof. Balraj Sehgal. A great persona, wonderful teacher and an inspiration in himself. I feel privileged to be able spend a few days with him during his last visit to Mumbai in February 2017. He asked me to call him after my final defence, but unfortunately we lost his physical presence forever. That too, 3 days before my final defence. May his soul rest in peace. I miss him a lot.

I am extremely thankful to Dr G Sugilal, (TDD, BARC), for letting me use his furnace for large amount of melt for the experiments and an efficient team to work with. Without his clear vision about my work and confidence in my experiments, it would have been difficult to perform such engineering scale experiments with that ease. I am also thankful to the team of furnace operators, electrical staff and other supporting staff members for their kind support during the experiments.

My sincere thanks also go to Dr P Chellapandi (RDG, IGCAR), who provided me an opportunity to work with their team at IGCAR, and who gave access to the laboratory and research facilities. I am also thankful to Dr B K Nashine, Shri S K Das, Shri Hemanth Rao, and all other scientific and technical staff at SED, IGCAR for helping me in FCI experiments in their SOFI facility. Because of all these people, IGCAR became homely place to work.

With a special mention to Prof. Kannan Iyer at IIT-Bombay for providing me the space and other logistics for letting me set-up my key experimental facility in their steam power laboratory. He is from southern India and I felt that special coconut like quality of him very

pleasing. He is hard shell from outside but very soft and kind from within. He always ensured us to follow all safety measures, and he himself kept visiting the facility for the same. I am also thankful to Shri Subhash and other fellow lab-mates at steam power lab for their kind support. It was fantastic to have the opportunity to work in that lab. What a cracking place to work!

I would also like mention and thank Dr D G Belokar (Retired, RED, BARC), who was the in-charge of all workshop activities. He not only helped me getting all fabrications done timely while maintaining quality, but also guided me to improvise my designing capabilities. His keen observations in my drawings were motivating. I am also thankful to his team of supervisors (Shri Amar Singh, Shri Rout, Shri Roshan Khedekar and Shri Chandraker) and workshop assistants for their efforts in machining and fabrication of my experimental facilities. Also, I am so thankful to drawing office in-charge and the staff for their immense help in drawings and various prints. They were always ready to help me even when they had their prior engagements.

I am immensely thankful to Shri S P Limaye (RED, BARC), for helping me in instrumentation of all my experimental facilities. I am also thankful to his entire team, especially Shri N A Patil, for their timely efforts.

I am also very thankful to Dr R D Kulkarni (RED, BARC), who was at the forefront with his team for all the electrical work of my experimental facilities. I am sincerely thankful to Shri Ramesh Parate and his efficient team for the same.

I am also thankful to Dr D K Chandrakar, Dr Naveen Kumar, Shri Alok Vishnoi, Shri Mukesh K Dhiman, Dr Arnab Dasgupta, Shri Bajaj, Shri Y Upreti, Shri Gorade and all Thermal Hydraulics Sections' members for their friendly support and wonderful encouragement.

I would also like to mention and thank my gentlemen's club. Shri Ganesh V, Shri Tipu Sultan, Shri Gaurav Srivastav, Shri Rakesh Chauhan, Shri Ganesh, Shri Avinash Mohrana and

Miss Garima (yes, she is a wonderful girl). They are young and dynamic fellows who are always willing and available for intellectual discussions and any kind of help. Three cheers to all of you guys.

I thank my all fellow mates for the stimulating discussions, for the sleepless nights we were working together, and for all the fun we have had in the last five years. My seniors Dr Rohit Singh Chauhan (my Godfather ☺), Dr Pankaj Kandwal, Dr Lokesh Gambhir, Dr Arvind Kumar, Dr Debes Ray, Dr Mohit Sharma, Dr Abhijit Deokule and Dr Sumit Chillar have introduced me with the life at HBNI. The cooking sessions, Daru party, dinner at TSH and the endless preaching are the precious memories with them. My dear friends at Annapurna: Vinay Rastogi, Vinod Belwanshi, Suryakant Gautam, Dr Sumit Mehan, Ravi Dhawan, Ganesh Maurya, Abhishek, Rahul, Tribeni Roy, Shankar, Anuj sharma, Ashish Shelke, Somenath Chatterjee, Suresh Sahu, Pankaj Jadhav and Harshit Jain were always the part of all birthday celebrations and the parties. I cannot forget to thank Dr Nitin Minocha, Dr Eshita Pal, Dr Jayaraj, Dr Archana Vallapil, Dr Amit Chandrakar, Dr Pradeep Tiwari, Dr Ankur, Vishal Bhusare, Parul Goel, Paridhi Goel, Amita Bedar, Sai Rajgopal, Rakesh, Samyak for being the wonderful friends and always there to help me. In particular, I am grateful to Ms. Sakshi Mukhija for helping me in conducting my experiments.

My best friend, roommate and the one who was always there in need; Sunil Kumar, has been one of the key person in my life during this entire journey. Love you bro. Another such person is Sapna Singh. She calls me ‘superman’ and believes that I can do anything. Always encourages me to stay ahead and whenever feels low, go to Marine drive and watch sunset. She is my sister from another mother.

I cannot thank this person. I call him ‘Anna’ meaning elder brother. Dr Naveen Kumar N, has always been there to take care of me. I have cried, laughed, screamed and even fought

in front of him during tough times. He stood by my side and used to say ‘Nitu, ho jayega...’. One of the best human being I have ever met.

I would also like to thank all Homi Bhabha National University Dean, Academic Dean, administration and staff members for their constant cooperation in all administrative activities related to my PhD.

Last but not the least, my family. Whosoever I am today, it is because of them only. My parents gave me the freedom to do anything I want. No words can explain the feeling, their sacrifice, pride and confidence in me. I can never forget the words of my sister Late Miss Megha Singh, “Bhaiya, aap ker loge...☺”. I miss her a lot. I would like to thank my entire family for supporting me spiritually and emotionally throughout this journey and my life in general.

Lastly, ‘Mlle Joyeux’, she is my family, my motivation, my life. She is above all relations. Her sacrifice and wish to see me graduating, always encouraged me to finish my work at the earliest. Her constant push kept me keep going without breaking. My parents made me a man and she made me a gentleman. Thank you for always being there, I love you.

Thanks for all your encouragement and motivation. This journey would not have been completed without each and every one of you!

# TABLE OF CONTENTS

<b>SYNOPSIS</b> .....	5
List of figures.....	18
List of tables.....	23
List of abbreviations .....	24
Nomenclature.....	26
<b>Chapter 1. INTRODUCTION</b> .....	29
1.1. Importance of nuclear energy .....	29
1.2. Core melt scenario and cooling strategies.....	35
1.3. Different core catcher concepts.....	38
1.4. Advanced Heavy Water Reactor (AHWR) core catcher.....	42
1.5. Dry conditions: Melt pool coolability .....	45
1.5.1. Top flooding.....	45
1.5.2. Side cooling .....	47
1.5.3. Bottom flooding .....	47
1.5.4. Unresolved issues in dry core catcher scenario with bottom flooding.....	50
<b>1.5.4.1. Influence of decay heat on melt coolability under bottom flooding</b> .....	50
<b>1.5.4.2. Scalability of melt coolability tests under bottom flooding</b> .....	50
1.5.4.2.1. Influence of melt volume .....	50
1.5.4.2.2. Influence of melt composition .....	50
<b>1.5.4.3. Effect of geometrical parameters</b> .....	51
<b>1.5.4.4. Lack of models for melt coolability under bottom flooding</b> .....	51
1.6. Wet conditions: Fuel coolant interaction .....	51
1.6.1. Current status and literature review .....	51
<b>1.6.2. Unresolved issues in wet core catcher scenario</b> .....	54
1.7. Objective of thesis.....	55
1.8. Strategy to address these unresolved issues .....	56
1.9. Outline of the thesis .....	57
1.10. Summary .....	59
<b>Chapter 2. EXPERIMENTAL FACILITIES</b> .....	61
2.1. Introduction.....	61
2.2. Simulant materials .....	61
2.3. Large scale bottom flooding test facility.....	62
2.3.1. Design details.....	62

2.3.2.	Instrumentation .....	64
2.4.	Small scale bottom flooding test facility.....	67
2.4.1.	Design details.....	67
2.4.2.	Instrumentation .....	68
2.5.	FCI test facility .....	70
2.5.1.	Design details.....	70
2.6.	Summary .....	71
<b>Chapter 3. INFLUENCE OF DECAY HEAT ON MELT COOLABILITY UNDER BOTTOM FLOODING.....</b>		<b>73</b>
3.1.	Introduction.....	73
3.2.	Experiment without decay heat.....	73
3.2.1.	Test facility .....	73
3.2.2.	Operating procedure.....	74
3.2.3.	Results and discussion .....	74
3.3.	Experiment with decay heat.....	79
3.3.1.	Test facility .....	79
3.3.2.	Operating procedure.....	79
3.3.3.	Results and discussion .....	80
3.4.	Comparative analysis .....	84
3.4.1.	Quench-front Analysis .....	88
3.4.2.	Debris comparison .....	91
3.5.	Summary .....	91
<b>Chapter 4. SCALABILITY OF MELT COOLABILITY EXPERIMENTS UNDER BOTTOM FLOODING.....</b>		<b>95</b>
4.1.	Introduction.....	95
4.2.	Influence of melt volume .....	96
4.2.1.	Details of the test sections.....	97
4.2.2.	Experiments conducted.....	97
4.2.3.	Comparative analysis .....	100
4.2.3.1.	Quench-front Analysis .....	104
4.3.	Influence of melt composition .....	104
4.3.1.	Details of the test section .....	104
4.3.2.	Experiments conducted.....	105
4.3.3.	Comparative analysis .....	105
4.3.3.1.	Quench-front Analysis .....	108
4.4.	Summary .....	110

<b>Chapter 5. EFFECT OF NOZZLE DIAMETER AND INJECTION PRESSURE ON MELT COOLABILITY WITH BOTTOM FLOODING .....</b>	<b>112</b>
5.1. Introduction.....	112
5.2. Influence of nozzle diameters .....	113
5.2.1. Details of the test sections.....	113
5.2.2. Experiments conducted.....	113
5.2.3. Comparative analysis .....	114
5.2.4. Quench-front analysis .....	119
5.3. Influence of inlet pressures .....	119
5.3.1. Details of the test sections.....	119
5.3.2. Experiments conducted.....	119
5.3.3. Comparative analysis .....	121
5.4. Quench-front Analysis.....	123
5.5. Summary .....	125
<b>Chapter 6. DEVELOPMENT OF MATHEMATICAL MODEL TO SIMULATE MELT COOLABILITY UNDER BOTTOM FLOODING .....</b>	<b>126</b>
6.1. Introduction of the model.....	126
6.2. Model Development.....	126
6.2.1. Limitations of Existing Model .....	126
6.2.2. Postulations .....	128
6.2.3. Model Assumptions .....	130
6.2.4. Description of Model .....	131
6.2.4.1. Governing equations for molten pool .....	131
6.2.4.2. Eruption Model .....	132
6.2.4.3. Equation in porous zone:.....	138
6.3. Solution Procedure.....	141
6.4. Results and Discussion .....	141
6.4.1. Case I: Decay heat scenario .....	141
6.4.2. Case II: Without decay heat scenario.....	144
6.5. Summary .....	147
<b>Chapter 7. MELT COOLABILITY DURING WET CONDITIONS IN A CORE CATCHER: FUEL COOLANT INTERACTION .....</b>	<b>148</b>
7.1. Introduction.....	148
7.2. Experiments conducted.....	151
7.2.1. Test section details.....	151
7.2.2. Operating procedures .....	151
7.3. Results and discussions.....	152

7.3.1.	Melt-to-water Ratio of 0.011 (Melt mass = 50 g; water mass = 4500 g).....	152
7.3.2.	Melt-to-water Ratio of 0.11 (Melt mass = 515 g; water mass = 4500 g).....	156
7.3.3.	Melt-to-water Ratio of 0.16 (Melt mass = 710 g; water mass = 4500 g).....	158
7.3.4.	Melt-to-water Ratio of 0.21 (Melt mass = 925 g; water mass = 4500 g).....	159
7.3.5.	Melt-to-water Ratio of 0.41 (Melt mass = 1846 g; water mass = 4500 g).....	161
7.3.6.	Melt-to-water Ratio of 0.51 (Melt mass = 2285 g; water mass = 4500 g).....	163
7.4.	Role of conversion efficiency .....	164
7.5.	Role of thermal cavitation in explaining steam explosion .....	167
7.6.	Summary .....	170
<b>Chapter 8. CONCLUSIONS .....</b>		<b>172</b>
8.1.	Influence of decay heat on melt coolability under bottom flooding .....	172
8.2.	Scalability of melt coolability under bottom flooding phenomena.....	173
8.3.	Influence of nozzle diameter and injection pressure on melt coolability under bottom flooding .....	174
8.4.	Development of model to understand melt coolability under bottom flooding .....	175
8.5.	Melt coolability during wet conditions in a core catcher: fuel coolant interaction.....	176
8.6.	Lessons learnt, Recommendations and Future work.....	177
<b>REFERENCES.....</b>		<b>180</b>

## **SYNOPSIS**

Core melting during severe accident scenario in a nuclear reactor is one of the major concerns. Corium, consisting of molten fuel and structural material, is highly radioactive, chemically reactive and has temperature around 2800°C. If the corium is not cooled down within stipulated time, it will ablate the reactor vessel (means 'pressure vessel' or 'calandria' or 'pressure tubes' depending on types of reactors) and then interact with the reactor pit concrete to breach into the ground, and may lead to severe environmental contamination. To mitigate such a scenario, core catchers are envisaged in new reactors and existing plants are being retrofitted for cooling of molten corium and its stabilization for prolonged period. The issue still remains is the efficacy of core catchers to cool the molten corium and terminate the accident progression. This is because the molten corium is highly aggressive material and thus, the cooling of the high temperature corium is one of the biggest challenges. This study focuses the coolability of molten corium in the core catchers for dry and wet conditions.

### **CASE I: DRY CONDITIONS IN THE CORE CATCHER**

In this case, the molten corium relocates into the core catcher and forms the melt pool. Literature suggests that injecting water from bottom directly into this melt pool is the most effective techniques for cooling the melt among various strategies. Considering this, the Advanced Heavy Water Reactor (AHWR) in India has conceptualized a core catcher in its design adopting the bottom flooding cooling technique.

However, a literature review suggests that there are various unresolved issues, mentioned below, which are important to design a core catcher. The main objective of my thesis is to resolve them. To address each issue, dedicated experiments have been performed and results have been analysed. It is difficult to perform the experiments using prototypic melts due to unavailability of prototypic material, radioactivity issues and of course the cost involved in

melting. In an actual scenario, when corium interacts with sacrificial concrete, it behaves as amorphous glass due to presence of metal oxides and silicates. Thus, oxides (glassy materials) having thermal diffusivity (transient heat transfer behavior is strongly dependent on thermal diffusivity) closer to that of corium, have been considered for the present experiments, which are also used by other researchers in the past.

### **Unresolved Issue 1: Influence of decay heat on melt coolability, debris formation and porosity under bottom flooding**

During severe accident in a nuclear reactor, the molten corium produces decay heat. Previous studies have never attempted to understand the influence of decay heat on melt coolability, debris formation and porosity under bottom flooding. To understand the above effects, experiments were conducted in an engineering scale test facility as shown in figure 1. The test section consists of a 300 mm diameter carbon steel pipe with 600 mm height.

The capacity of melt pool in the test section is about 25 litres corresponding to melt height of 500 mm.

The upper part of the test section has the capacity to contain a water pool up to 700 mm height and the steam outlet. At the bottom, a plate having six nozzles of 12 mm diameter was placed. Water was fed through an overhead tank under gravity flow. Total 27 K-type thermocouples were placed in 9 axial and 3 radial positions in the melt pool.

In addition, inlet water temperature and temperature of outgoing steam were also measured by thermocouples in the upper part of test section. The water inlet and steam outlet flow was

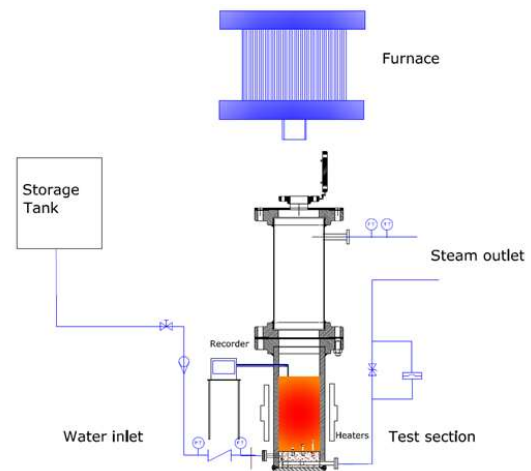


*Figure 1: Schematic of test facility for melt coolability under bottom flooding with decay heat simulation*

measured using differential pressure transmitter (DPT). Pressure gauge and transducer were used to monitor water inlet head and the pressure profile inside the test section, respectively. All these signals were recorded by a 48 channel multivariable recorder. The lower part of the test section was also surrounded by ten radiative heaters to impart decay heat. This was then insulated using ceramic wool so that the heat is imparted uniformly and concentrically into the melt.

Two experiments were performed in this facility, one with decay heat equivalent to  $0.5 \text{ MW/m}^3$  and other without decay heat. These experiments resulted in following insights.

- Propagation of quench-front was found to be similar in both the cases, as shown in figure 2. This is because, once the water is injected into the melt, it forms steam which pressurises the melt pool from bottom. If steam pressure exceeds the strength of the crust and the static head of the melt pool, steam erupts through the melt and converts the entire melt into debris. Thus, the influence of decay heat on melt coolability is insignificant.

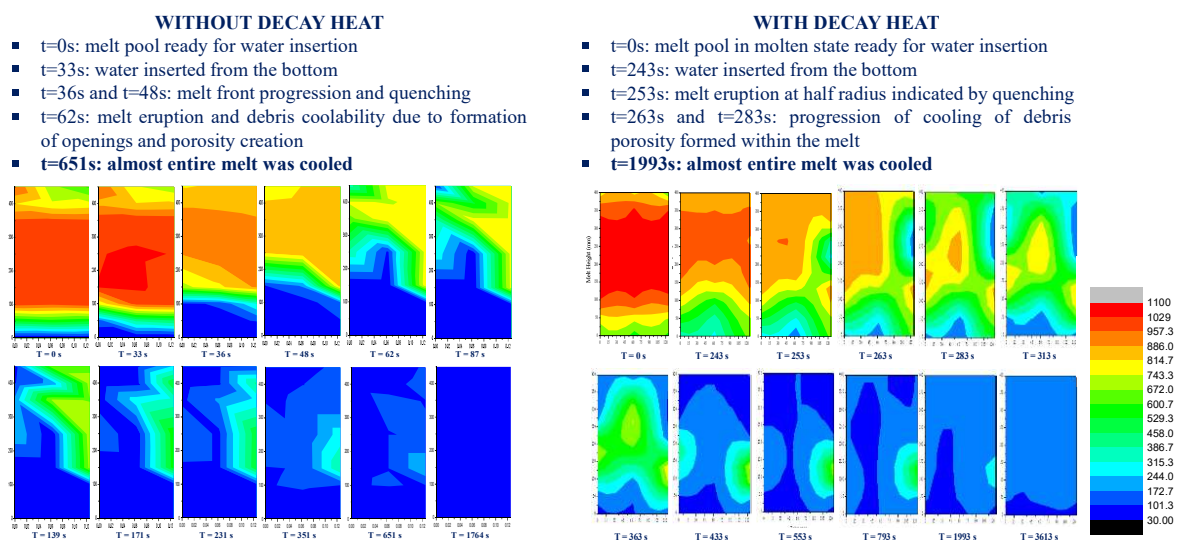


Figure 2: Quench-front propagation during water injection into melt from bottom with and without decay heat

- Due to debris formation there is an increase in interfacial area for better heat transfer. Also, due to eruption, water ingresses into the melt pool from bottom taking away the heat from

the molten debris by boiling. So during melt eruption, the rate of heat removal due to this process is inherently higher than the decay heat imparted. It can thus be concluded that the quenching characteristics of melt coolability under bottom flooding does not depend on decay heat, although coolability of debris take a bit longer duration as compared to stored heat scenarios.

- In both the cases, porous debris was found to consist of particles sizing from 0.5 mm fragments to 50 mm sized porous chunks. The hairs like strands known as “Pele’s hair” were also obtained which shows the high shear between steam and melt. The measured average porosity was 51% without decay heat and 67% with decay heat in the experiment. Radial variation in the measured porosity was observed.
- The average quenching time was 93s without decay heat and 96s with decay heat experiment, which is of similar order.

### **Unresolved Issue 2: Scaling effects – melt volume**

There are international concerns with regard to scaling of melt volume on quenching; that means by conducting a small scale experiments, can the data be extrapolated to large scale ones. To understand this aspect, experiments were performed in two different set-ups using the same melt and having the same melt height but different diameters. In one case, the melt was 25 litres and in other it was 3 litres. The test sections of diameter 300 and 130 mm and height of 500 mm were used to perform these experiments. The measured average quenching times and average porosities were compared for these experiments.

- Results show that melt erupted in both scales of experiments almost at the same time and once melt erupted, it converted the melt into porous debris and hence they got cooled.
- The average porosities measured in both the experiments were found to be nearly 51%. Debris in both the experiments were found to consist of very fine particles, numerous

Pele's hairs and porous chunks of sizes ranging from a few mm to 50 mm, as shown in figure 3.

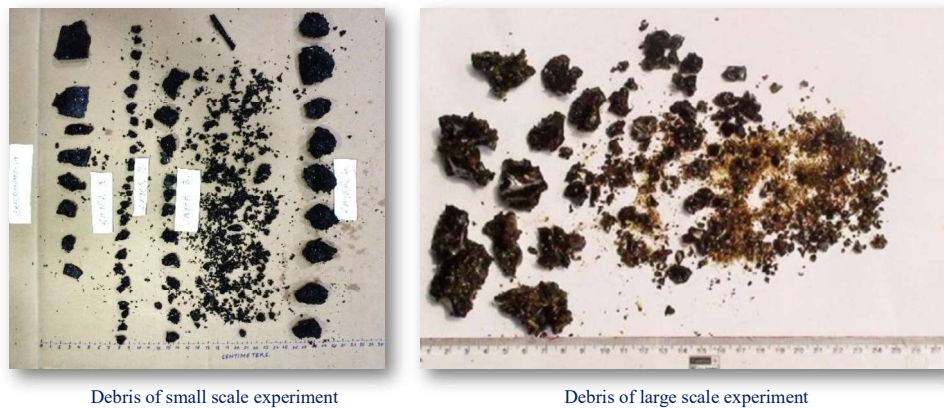


Figure 3: Debris of small scale versus large scale sodium borosilicate glass experiments

- The ratio of the mass flow rates of large scale ( $Q_1$ ) over small scale ( $Q_2$ ) experiments was  $Q_1 \approx 2 \cdot Q_2$ . Quenching time was 93 s for large scale and 61 s for small scale experiments, which is nearly of similar order as that of injected flow rates.
- Hence, it can be concluded that the results of the experiments with small scale experiments can be extrapolated to the experiment with large amount of melt.

### Unresolved Issue 3: Scaling effects – melt compositions

To understand the influence of melt composition on coolability under bottom flooding, experiments were performed using two different melts, one with sodium borosilicate glass and other with  $\text{CaO-B}_2\text{O}_3$ . Both the materials are glassy and have similar thermal diffusivity. In the experiments, the amount of melt, height of the melt pool and the flooding conditions were kept the same.

- The quench-front propagation of two different melt simulants has shown that  $\text{CaO-B}_2\text{O}_3$  took a bit longer steam build-up time before eruption compared to sodium borosilicate glass. This is attributed to the higher strength of  $\text{CaO-B}_2\text{O}_3$  compared to that of glass. Once erupted, the melt gets cooled due to debris formation.

- Debris formed in both the cases consisted of finer particles and porous chunks. The glass debris were more uniform compared to highly rough surfaced debris of CaO-B<sub>2</sub>O<sub>3</sub>. The measured average porosity was 51% and 50% in glass and CaO-B<sub>2</sub>O<sub>3</sub>, respectively.
- The average quenching time was 122s for CaO-B<sub>2</sub>O<sub>3</sub> which is higher compared to 61s in sodium borosilicate glass.

**Unresolved Issue 4: Influence of nozzle diameter and injection pressure on coolability of the molten pool.**

Set of six experiments were performed with nozzle diameter 8, 12 and 18 mm and two different injection pressure (0.35 and 0.75 bar) to study the above effects.

- The quench-front analysis indicates that it took longer time for melt to erupt in case of 8 mm nozzle diameter, which may be attributed to the lower inlet flow rates due to smaller opening area. The eruption occurred earliest in the case with 12 mm diameter. However, the difference in the time of eruption, in case with 12 mm and 18 mm diameters, is insignificant and the possible reason for the same could be that the mass flow rate at the 18 mm nozzle opening was higher, compared to 12 mm nozzle, due to larger cross section. Thus, the build-up time required to convert excess available water into steam, was a bit higher for 18 mm nozzle resulting in higher quenching time.
- The quench-front analysis to understand the effect of inlet water pressure on melt coolability under bottom flooding indicates that the steam build-up time required for the low inlet pressure was higher compared that to higher inlet pressure case. Due to this, melt erupted a bit late in low inlet pressure case resulting in higher melt quenching time. Once erupted, it took nearly the same time to cool the melt.
- Debris morphology was almost the same in all the cases.

- The average quenching times observed for the 8 mm, 12 mm and 18 mm were 116s, 77s and 81s respectively; and the same for 0.35 bar and 0.75 bar inlet pressures were 122s and 77s respectively.

**Unresolved Issue 5: Modelling the phenomenology of melt coolability under bottom flooding and understanding the melt eruption, porosity formation and its variation and cooling behaviour**

It appears from the experiments that steam build-up below the melt is primarily responsible for melt eruption which forms an inverted cone of porous debris as observed in experiments. It was also observed that the porosity within this cone varies radially. On the basis of these findings, a model has been developed from first principle to understand the phenomenology of the melt coolability under bottom flooding. In the model, the average particle size has been used from the experimental measurements as it is very difficult to model debris formation with a distribution of particle sizes. Also, empirical correlation developed for the radial variation in porosity has been plugged into the model. The basic postulates of this model are as follows, and depicted pictorially in figure 4.

- When water is flooded into the melt through nozzles it interacts with water and cools down while forming a thin crust (figure 4 (a)).
- This crust starts growing further upon addition of water (figure 4 (b)).
- Due to heat transfer, steam forms and exerts pressure on crust.
- The crust is now subjected to stresses
  - Steam pressure on one side
  - Hydrostatic head of the melt pool on the other side

- Thermal stresses generated due to temperature gradient across the thickness
- When the total stresses exceed fracture stress, numerous fine cracks occurs on the crust surface due to brittle nature of the material, which acts as the eruption locations (figure 4(c)).
- The principal conical eruption occurs along with numerous secondary eruptions. This inverted cone shaped porous zone is termed as ‘eruption cone’ (figure 4 (d)).

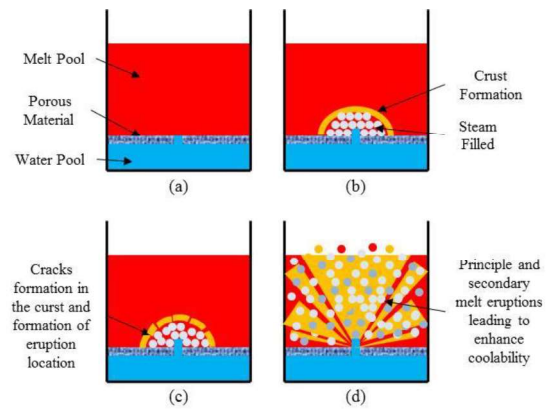


Figure 4: Pictorial depiction of the model postulations

- These eruptions convert melt into debris due to intense shear between up-flowing steam and the melt. The porosity in zone is enhanced and varies spatially.
- Due to high porosity and boiling heat transfer between the melt and the cooling fluids in this eruption cone, the melt coolability is greatly enhanced.

Based on the above postulates, a mathematical model has been developed which considers the heat transfer in the melt pool, steam formation at the bottom of the melt pool, crust formation at the bottom of the melt pool and its fracture. The melt eruption phenomenology is solved by using Bursik and Barsotti models. The porosity formation and its radial variation are modeled using experimentally developed empirical correlation. The interfacial area density is modeled from the experimentally obtained particle sizes and boiling heat transfer from debris to coolant is modeled using Rohsenow model. The governing equations were discretized using finite difference method and solved implicitly using Gauss-Siedel iterative.

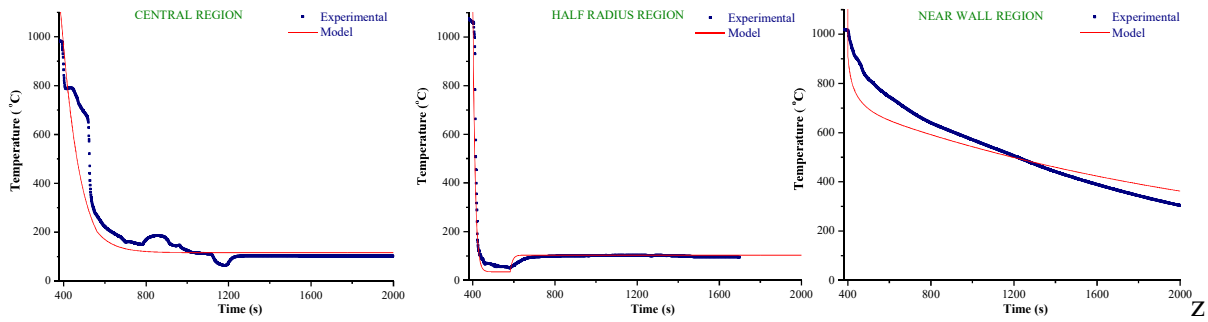


Figure 5: Experimental measurements versus model predictions for melt coolability under bottom flooding with decay heat

Results of the model predictions with experimental measurements are shown in figure 5. The model is able to capture the coolability behaviour of the melt pool with decay heat quite accurately.

## Case II: WET CONDITIONS IN THE CORE CATCHER

If water is already present in the core catcher prior to the melt arrival, it may result into strong fuel coolant interaction (FCI) which may cause a potential steam explosion

In the literature, several experiments have been performed with simulants as well as with prototypic materials to evaluate the resulting pressure rise due to FCI and melt fragmentation behavior. In all these studies, tests have been performed using simulant melts from a few grams to nearly 100 kg which were poured into varying amount of water to study this behaviour. In some cases, steam explosion occurred while in others it did not. However, all these studies are unable to explain the condition for steam explosion. Recently, Moriyama suggested that steam explosion occurs only when the particles formed due to FCI are below 0.1 mm in size.

### Unresolved Issue 6: Is presence of the fine fragments the root cause for steam explosion?

To verify this, several experiments were performed in this study. The melt masses varied from 50 grams to 2500 grams which were poured into a 4.5 litres of water pool to study the fragmentation behaviour of melt and potential pressure spike due to FCI.

The results obtained from the present study show the following

- No pressure spike was observed for melt-to-water ratio less than 0.21, but was observed when this ratio was increased in subsequent experiments as shown in figure 6.
- Debris of sizes ranging from 1 mm to 42 mm porous globular chunks were obtained. Larger melt-to-water ratio leads to the increase in number of agglomerated debris.

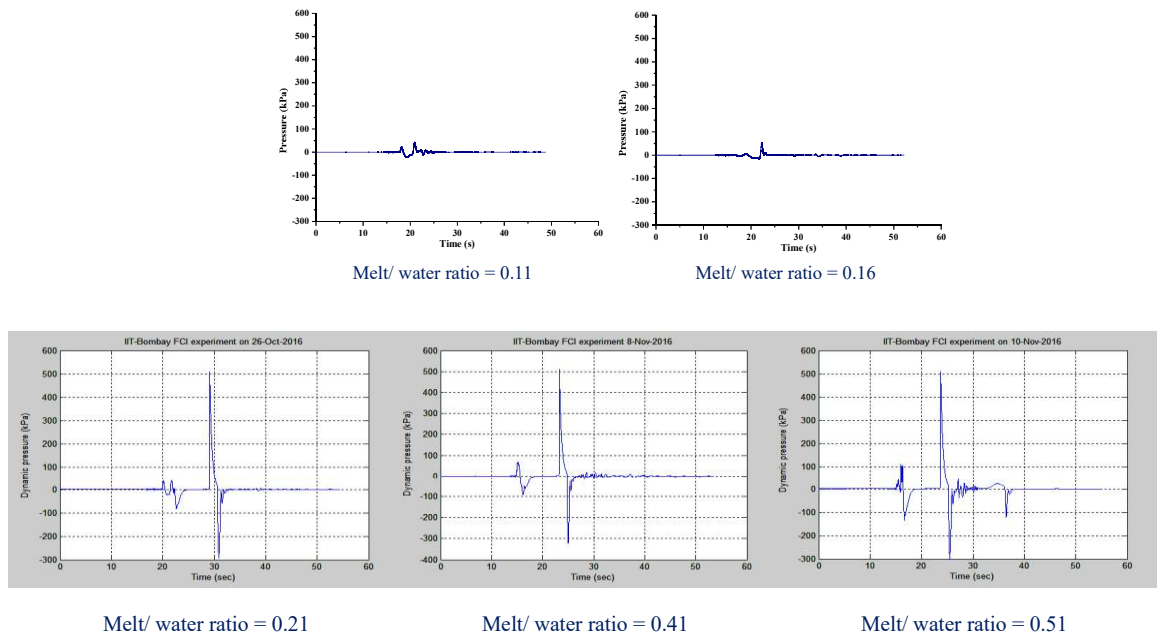


Figure 6: Dynamic pressure peaks observed in present FCI studies

Presence of pressure spike even in the absence of fine fragments, when studied using Moriyama's fine fragmentation theory, found unexplainable. To investigate this, conversion efficiency analysis was performed.

During FCI, thermal energy of melt converts into mechanical energy by developing dynamic pressure peak (due to steam formation). The ratio of this mechanical energy to the thermal energy is called as conversion efficiency.

Table 1: Analysis of various experimental studies performed so far using conversion efficiency theory

Obtaining Pressure Peak From Conversion Ratio													
Expt	Melt	Melt mass	Melt Temperature	Energy IN	Water volume	Water height	Test section Diameter	Area	Conversion efficiency	Mech Energy	Estimated Pressure peak	Explosion	Measured Pressure peak
				$E_{\text{thermal}}$					$\eta$	$E_{\text{pressure}}$			
		kg	K	kJ	l	m	m	m <sup>2</sup>	%	kJ	kPa		kPa
BARC	5	0.925	1409	1982.3	4.5	0.27	0.13	0.11	0.8	1585.8	462		506
	7	1.846	1407	3956.0	4.5	0.27	0.13	0.11	0.8	3164.8	413	Pressure Spike	467
	8	2.285	1399	4896.8	4.5	0.27	0.13	0.11	0.8	3917.4	459		510
KROTOS	9	1.885	1406	1856.7	4.5	0.27	0.13	0.11	0.8	1485.4	447		510
	38	1.522	2665	5040.0	34	1.1	0.2	0.691	0.8	4032.0	930	Yes	1000
	40	1.47	3073	5707.4	34.6	1.1	0.2	0.691	0.8	4565.9	990		1000
	42	1.539	2465	4665.3	34.6	1.1	0.2	0.691	0.8	3732.3	895		1000
	43	1.5	2625	4883.1	34.6	1.1	0.2	0.691	0.8	3906.5	916	Yes	1000
	44	1.5	2673	4983.9	33.2	1.1	0.2	0.691	0.8	3987.1	925		1000
	49	1.47	2688	4915.1	34	1.1	0.2	0.691	0.8	3932.1	919		1000
TROI	1	5	>3373	12524.6		0.67	0.65	1.37	0.8	10019.7	737		1000
	4	4.2	>3373	10520.7		0.67	0.65	1.37	0.8	8416.5	1911		2100
	5	2.9	3373	7264.3		0.67	0.65	1.37	0.8	5811.4	888	Yes	900
	12	8.4	3800	16614.0		0.67	0.65	1.37	0.8	13291.2	849		1000
	13	7.7	2600	10008.9		0.67	0.65	1.37	0.8	8007.2	659*		7000*
14	6.5	3000	9918.1		0.67	0.65	1.37	0.8	7934.5	656		800	

\*Triggered explosion

The conversion efficiencies for all the prior experiments were evaluated and found lying in the range of 0.3-12.7%, while most of them were close to 0.8%. The duration of their peaks were lying in the range of 2-200 milliseconds. The conversion efficiencies for the present tests were also found to be in the range of 0.3 to 0.70%, which is of similar order.

So, using 0.8% as the conversion efficiency and respective durations of pressure spikes, the mechanical energy imparted in the form of dynamic pressure was estimated for all previous experiments as presented in Table 1. It was observed that the estimated peak value is close to that of measured peak value. This explains that the amount of thermal energy converting into mechanical energy during FCI, is more important deciding factor for steam explosion to occur compared to the presence of fine fragments. Thus, Conversion efficiency plays the key role in deciding the steam explosion to occur.

## **CONCLUSIONS**

The present study resolves several scientifically unexplained aspects for coolability of molten corium which are important for the design of core catchers for advanced nuclear reactors with bottom flooding.

- ❑ Influence of decay heat on melt coolability under bottom flooding is insignificant.
- ❑ Experiments conducted in small scale can be safely extrapolated to larger ones
- ❑ The influence of melt composition, when both are of same nature, is found to be of similar coolability behaviour except that the quenching time is different attributed to strength of the material.
- ❑ Effect of Geometrical parameters viz. nozzle diameter and inlet pressure, on melt coolability behaviour is invariably small but they influence the melt quenching time due to change in mass flow rates.

- ❑ The porosity formed during melt coolability under bottom flooding is always found to be more than 50% which is good for debris bed coolability.
- ❑ A new mechanistic model from the first principle has been developed for the melt coolability under bottom flooding. The model explains critical physical phenomena and is found working in concurrence with experimental measurements. It is able to capture the coolability behaviour of the melt pool with and without decay heat.
- ❑ Formation for fine fragments during FCI is not the root cause for steam explosion. Conversion efficiency theory suggests that the amount of thermal energy converting into mechanical energy, in terms of energy, is more important deciding factor for steam explosion to occur.

## List of figures

Figure 1: Global electricity demand and projections .....	30
Figure 2: Schematic of typical nuclear fission reaction.....	31
Figure 3: Dry and wet conditions in the reactor containment.....	35
Figure 4: Schematic of two possible melt-water interaction scenarios in a nuclear reactor....	36
Figure 5: Different melt cooling strategies .....	37
Figure 6: Ex-vessel catcher for the VVER-1000 reactor of the Tyan'van NPP (1) Lower plate (2) vent collector (3) basket with a sacrificial material (4) sectionalized heat exchanger.....	39
Figure 7: EPR core catcher concept.....	39
Figure 8: COMET experimental concept of core catcher using bottom flooding water injection.....	40
Figure 9: Hamazaki's concept of core catcher.....	41
Figure 10: Schematic of Advanced Heavy Water Reactor (AHWR) .....	42
Figure 11: AHWR Core catcher .....	43
Figure 12: AHWR Core catcher located at the basemat within the containment .....	44
Figure 13: Moriyama's map for steam explosion condition .....	55
Figure 14: Schematic of the Large Scale Bottom Flooding Test Facility.....	63
Figure 15: Large Scale Bottom flooding test setup with heaters for decay heat simulation ...	64
Figure 16: Thermocouples arrangement inside the setup for melt pool temperatures measurement .....	65
Figure 17: Actual site photograph of Small Scale Bottom Flooding Test Facility.....	66
Figure 18: Schematic of Small Scale Bottom Flooding Test Facility .....	68
Figure 19: Thermocouples arrangement inside the test section of Small Scale Bottom Flooding Test Facility .....	69
Figure 20: Test section for conducting small melt volume experiments (schematic) .....	70

Figure 21: Test section for large melt volume FCI experiments (schematic).....	71
Figure 22: Measured temperatures at central location.....	75
Figure 23: Measured temperatures at half radius.....	75
Figure 24: Measured temperatures near wall.....	76
Figure 25: Porous mass and debris size in bottom flooding experiment.....	77
Figure 26: Steam flow measurement in without decay heat experiment.....	78
Figure 27: Steam flow measurement in the experiment with decay heat.....	80
Figure 28: Measured temperatures at central location of the test section.....	81
Figure 29: Measured temperatures at Half Radius of the test section.....	82
Figure 30: Measured temperatures near inner wall of the test section.....	82
Figure 31: Porous mass and debris size in bottom flooding with Decay heat experiment.....	84
Figure 32: Temperature vs. Time characteristics curve for melt coolability under bottom flooding.....	85
Figure 33: Average quenching time taken by the melt pool to reach 300°C temperature under bottom flooding with and without decay heat.....	86
Figure 34: Average cooling time taken by the melt pool to reach saturation temperature under bottom flooding with and without decay heat.....	86
Figure 35: Rates of heat removal and decay heat addition during melt quenching.....	87
Figure 36: Temperature contour plots for the bottom flooding without decay heat experiment .....	89
Figure 37: Temperature contour plots for the bottom flooding with decay heat experiment..	90
Figure 38: Post experiment debris just after opening the test section without (a) and with (b) decay heat scenarios, respectively [scale: Test sections' diameter = 300 mm].....	92
Figure 39: Post experiment debris (a) without decay heat {the golden particles visible are micron sized Pele's hairs, and (b) with decay heat scenarios. [Scale: 2 cm = 1 cm actual]....	93

Figure 40: Temperatures profile of small scale experiment using sodium borosilicate glass .	99
Figure 41: Temperatures profile of small scale (upper one) and large scale experiments (lower one), respectively.....	100
Figure 42: Debris of sodium borosilicate glass obtained from (a) Small scale and (b) large scale experiments.....	102
Figure 43: Quench-front propagation in large scale versus small scale experiments.....	103
Figure 44: Temperatures profile of glass (left) and CaO-B <sub>2</sub> O <sub>3</sub> experiments.....	106
Figure 45: Debris of (a) sodium borosilicate glass and (b) CaO-B <sub>2</sub> O <sub>3</sub> experiments. ....	108
Figure 46: Quench-front propagation for CaO-B <sub>2</sub> O <sub>3</sub> versus Sodium borosilicate glass .....	109
Figure 47: Temperature profiles for three different nozzle diameters at 0.75 bar inlet pressure. ....	115
Figure 48: Effect of nozzle diameters on debris sizes for the experiment at 0.75 .....	116
Figure 49: Variation of average quenching time and average porosity with respect to nozzle diameter at inlet water pressure head of 0.75 bar(g).....	117
Figure 50: Quench-front propagation for different nozzle diameters.....	118
Figure 51: Temperature profiles for two inlet pressures at constant nozzle diameter of 12 mm. ....	120
Figure 52: Effect of inlet velocities on debris sizes for the experiments with 12 mm nozzle diameter.....	122
Figure 53: Variation of average quenching time and average porosity with respect to inlet pressure at 12 mm nozzle diameter.....	123
Figure 54: Quench-front propagation for different inlet pressures .....	124
Figure 55: Melt coolability model by Kulkarni and Nayak (2013) .....	127
Figure 56: Variation in porosity along the radius of the porous zone within the test section	128
Figure 57: Melt coolability under bottom flooding with decay heat, the eruption model.....	130

Figure 58: Boundary conditions for melt (upper) and crust layer (lower).....	132
Figure 59: Stresses in the crust. ....	134
Figure 60: Philosophy of boiling heat transfer in the present model.....	138
Figure 61: Modified boundary conditions for solid region.....	140
Figure 62: Modeled vis-à-vis measured temperatures at central location of the test section (with decay heat).....	142
Figure 63: Modeled vis-à-vis measured temperatures at Half Radius of the test section (with decay heat) .....	143
Figure 64: Modeled vis-à-vis measured temperatures near inner wall of the test section (with decay heat) .....	144
Figure 65: Modeled vis-à-vis measured temperatures at central location of the test section (without decay heat).....	145
Figure 66: Modeled vis-à-vis measured temperatures at Half Radius of the test section (without decay heat).....	146
Figure 67: Modeled vis-à-vis measured temperatures near inner wall of the test section (without decay heat).....	146
Figure 68: Steam explosion and its phases of occurrence .....	149
Figure 69: Visuals from high speed shooting of FCI.....	152
Figure 70: Dynamic pressure peak versus time curve for M/W ratio=0.011.....	153
Figure 71: Fine particulate and porous globular debris of small volume experiment (Scale: 1cm of image = 2 cm of actual size) .....	154
Figure 72: Microscopic analysis of debris from small melt volume experiment .....	154
Figure 73: Microscopic analysis of fine particulate of small melt volume experiment (Scale: 1 cm = 8 mm).....	155
Figure 74: Debris particle size distribution of small melt volume experiment.....	155

Figure 75: Dynamic pressure peak versus time curve for M/W ratio=0.11.....	156
Figure 76: Debris obtained from experiment with M/W=0.11 .....	157
Figure 77: Debris particle size distribution of experiment with M/W=0.11 .....	157
Figure 78: Dynamic pressure peak versus time curve for M/W ratio=0.16.....	158
Figure 79: Debris obtained from experiment with M/W=0.16 .....	159
Figure 80: Debris particle size distribution of experiment with M/W=0.16 .....	159
Figure 81: Dynamic pressure peak versus time curve for M/W ratio=0.21.....	160
Figure 82: Debris obtained from experiment with M/W=0.21 .....	161
Figure 83: Dynamic pressure peak versus time curve for M/W ratio=0.41.....	162
Figure 84: Debris obtained from experiment with M/W=0.41 .....	162
Figure 85: Dynamic pressure peak versus time curve for M/W ratio=0.51.....	163
Figure 86: Debris obtained from experiment with M/W=0.51 .....	164
Figure 87: Analysis of present experiments using Moriyama's theory.....	165



## List of tables

Table 1: Different strategies for melt pool coolability.....	49
Table 2: Properties of simulant materials .....	62
Table 3: Accuracy of the measured values .....	66
Table 4: Comparison of small and large scale experiments with glass .....	97
Table 5: Conversion efficiencies for Alumina melt as given in the KROTOS literature .....	166
Table 6: Conversion efficiencies of ZrO <sub>2</sub> and corium melts as given in TROI literature .....	167
Table 7: Conversion efficiencies for the present tests .....	167
Table 8: Analysis of various experimental studies performed so far using conversion efficiency theory .....	168



## List of abbreviations

<b>AHWR</b>	Advanced Heavy Water Reactor
<b>ANL</b>	Argonne National Laboratory
<b>BARC</b>	Bhabha Atomic Research Centre
<b>BWR</b>	Boiling Water Reactor
<b>CCFL</b>	Counter Current Flow Limitation
<b>CDF</b>	Core Damage Frequency
<b>CS</b>	Carbon Steel
<b>DN</b>	Nominal Diameter
<b>DPT</b>	Differential Pressure Transmitter
<b>EPR</b>	European Pressurised Reactor
<b>FBR</b>	Fast Breeder Reactor
<b>FCI</b>	Fuel Coolant Interaction
<b>GW</b>	Giga-watts
<b>JAERI</b>	Japan Atomic Energy Research Institute
<b>kHz</b>	Kilo-Hertz (unit of frequency)
<b>kPa</b>	Kilo-Pascal (unit of pressure)
<b>KTH</b>	KTH Royal Institute of Technology, Sweden
<b>kW</b>	Kilo-Watt (unit of power)
<b>LOCA</b>	Loss Of Coolant Accident
<b>LWR</b>	Light Water Reactor
<b>MCCI</b>	Molten Core Concrete Interaction
<b>mm</b>	Millimetres
<b>MW</b>	Mega-Watt (unit of power)

<b>NEA</b>	Nuclear Energy Agency
<b>NPP</b>	Nuclear Power Plant
<b>OD</b>	Outer Diameter
<b>OECD</b>	Organisation for Economic Co-operation and Development
<b>PCCS</b>	Passive Core Cooling System
<b>PFBR</b>	Prototype Fast Breeder Reactor
<b>PHWR</b>	Pressurised Heavy Water Reactor
<b>RD</b>	Rupture Disc
<b>RPV</b>	Reactor Pressure Vessel
<b>RV</b>	Relieve Valve
<b>SS</b>	Stainless Steel
<b>UK</b>	United Kingdom
<b>USA</b>	United States of America
<b>USSR</b>	Union of Soviet Socialist Republics (now Russia)
<b>VVER</b>	Water-Water Energetic Reactor

## Nomenclature

$d$	diameter (m)
$g$	Acceleration due to gravity ( $\text{m/s}^2$ )
$h$	Heat transfer coefficient ( $\text{W/m}^2 \text{ K}$ )
$h_{\text{bed}}$	Bed height (m)
$h_{\text{fg}}$	Latent heat of vaporization ( $\text{J/kg}$ )
$h_{\text{in}}$	Inlet enthalpy ( $\text{J/kg}$ )
$h_{\text{fs}}$	Liquid saturation enthalpy ( $\text{J/kg}$ )
$k$	Thermal Conductivity ( $\text{W/m K}$ )
$p$	Pressure (Pa)
$q'''$	Volumetric heat generation rate ( $\text{W/m}^3$ )
$r$	Radial distance (m)
$t$	Time (s)
$t_{\text{cr}}$	Crust thickness (m)
$v$	Velocity (m/s)
$z$	Axial direction (m)
$A$	Cross section area ( $\text{m}^2$ )
$A_{\text{ch}}$	Area of openings ( $\text{m}^2$ )
$C_p$	Specific heat capacity at constant pressure ( $\text{J/kg K}$ )
$D_n$	Diameter of nozzle (m)
$E$	Young's modulus ( $\text{N/m}^2$ )
$\hat{E}$	Principal eruption
$L_b$	Length of the opening (m)
$M$	Mass (kg)

$N_n$	Number of inlet nozzles
$P$	Eruption momentum
$T$	Temperature (K)
$V$	Volume ( $m^3$ )
$V_p$	Volume in porous region ( $m^3$ )

### **Greek letters**

$\alpha$	Thermal linear expansion coefficient ( $K^{-1}$ )
$\varepsilon$	Bed porosity
$\gamma$	Density of openings per unit area
$\kappa$	Bed permeability ( $m^2$ )
$\mu$	Dynamic viscosity (Pa s)
$\nu$	Poisson's ratio
$\rho$	Density ( $kg/m^3$ )
$\sigma_b$	Bending stress ( $N/m^2$ )
$\sigma_{max}$	Fracture stress ( $N/m^2$ )
$\sigma_{mc}$	Surface tension between melt and steam (N/m)
$\sigma_{th}$	Thermal stress ( $N/m^2$ )
$\xi$	Critical Taylor wavelength (m)
$\vartheta$	Specific volume of steam ( $m^3/kg$ )
$\psi$	Number of eruption channels
$\Gamma$	Vapour generation rate (kg/s)

### **Subscripts**

$c$	Crust
$erup$	Eruption

in	Inlet
l	Liquid
f	Fluid
m	Melt
nb	Nucleate boiling
r	Radial
s	Solid
st	Steam
sat	Saturation
sub	Subcooled
sup	Superheated
w	Water
v	Vapor
z	Axial



# Chapter

*“There are three principal means of acquiring knowledge... observation of nature, reflection, and experimentation.*

*Observation collects facts; reflection combines them; experimentation verifies the result of that combination”*

— Denis Diderot (5 October 1713 – 31 July 1784)  
French philosopher, art critic and writer



## Chapter 1. INTRODUCTION

### 1.1. Importance of nuclear energy

**E**nergy, the prime constituent of the Universe, is also responsible for the life on Earth. Every form of life, including humans, depends on various forms of energy for the sustainability and progression of our very existence. The ability of using extrasomatic energy has made humans the smartest and given them capability to make life easier and comfortable. Since its inception, humans have discovered different forms of energy and their resources; and have learnt to control them for the sustainable purposes in life. The story began long back with the discovery of fire by the early men millions of years ago. Initially, they were afraid of it but sooner learnt to control and use it for their protection as well as for cooking and other fruitful purposes. Discovery of fire and inventions of numerous methods to use it in modern history and in running machines led mankind to use the true potential of it. Initial source of fire was by burning woods, later by burning fossil fuels like coal, petroleum products and various gases. During the industrial revolution, dependency of humans on machines increased and also the development of medicinal expertise to fight various diseases, agricultural boom to feed the growing population and the increased dependency on electricity for better living further increased the energy demands in all parts of the world. With growing population this demand kept on increasing and led fossil fuels to deplete rapidly, as shown in Figure 1. Depletion of fossil fuels at alarming rate and the emission of greenhouse gases influenced policy makers to look for renewables in their energy mix. Renewables, being scattered source of energy, were unable to replace or become mainstay of electricity production.

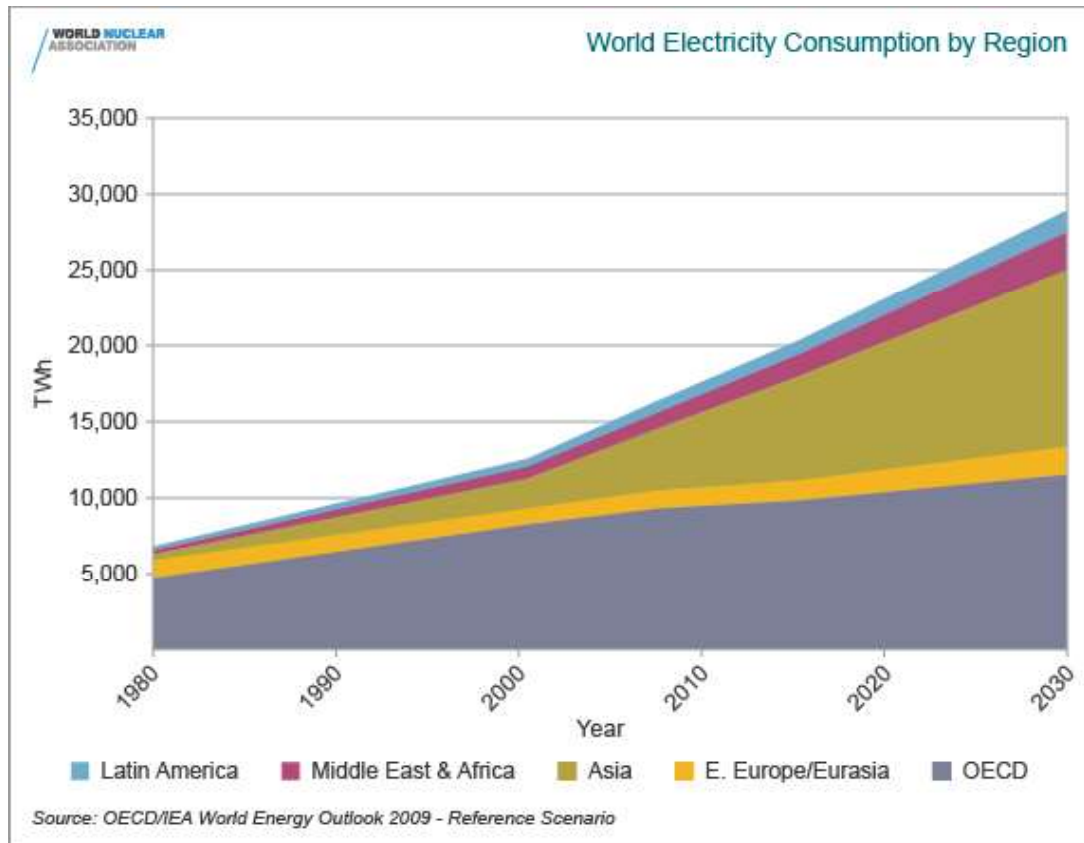


*Figure 1: Global electricity demand and projections*

As the time progressed the quest for betterment of human life led to further research and reassurance of safe along with even more sustainable source of energy. Discovery of radioactivity by the French scientist Henri Becquerel in 1896 and then discovery of nuclear fission by the German scientist Otto Hahn in 1938, incarnated the era of a new energy source called “Nuclear” arrived. Nuclear fission is the process in which a fissile nuclei becomes unstable by absorbing a neutron and subsequently splits into two or more lighter nuclei along with a huge amount of energy liberation, as shown in Figure 2. This nuclear energy can be used for several applications, including electricity generation. Naturally occurring fissile material is Uranium-235 which is found as 0.7% in natural Uranium and rest is Uranium-238. The fertile Uranium-238 in nuclear reactors absorbs neutron to produce another fissile material Plutonium-239. Uranium-233 is one of the isotope of uranium, which is produced by the neutron absorption of

Thorium-232, is very important fissile material for sustainable nuclear energy. These fissile materials are known as ‘fuels’ for the nuclear reactors, in general terms. When substantial amount of fuel was bombarded with neutrons and fission chain reaction sustains, huge amount of energy was liberated. This was the clean and condensed source of energy, which could reduce and even end our dependency on fossils for electricity production; world was looking for.

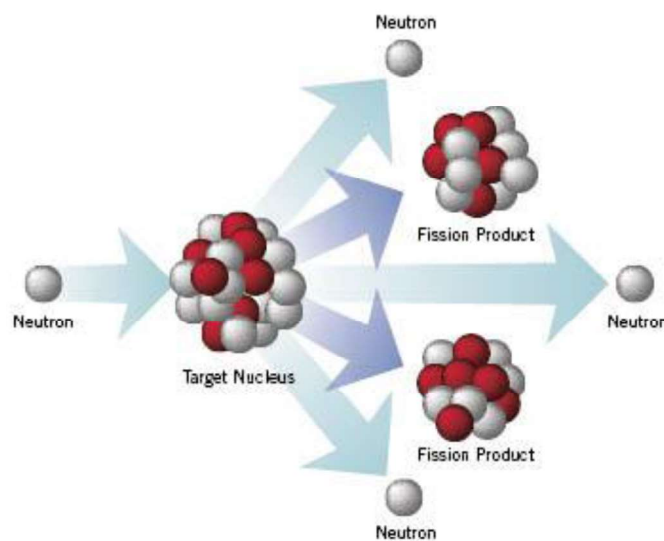


Figure 2: Schematic of typical nuclear fission reaction

Enrico Fermi’s team created the world’s first man-made nuclear reactor to understand sustainable chain reaction and true potential of nuclear energy, known as Chicago Pile-1, which went critical on December 2, 1942. Though, the idea in their mind was of making “dirty bomb” (atomic bomb), this was beginning of extracting the hidden potential of compact and clean form of energy from the constituent elements of matter. On August 6, 1945, atomic bomb nicknamed "Little Boy" was dropped on the city of Hiroshima and three days later, on August 9, other bomb nicknamed "Fat Man" fell on the city of Nagasaki of Japan. These were perhaps the deadliest act and worst impact of such a clean technology on human minds.

The entire world, at that time, has seen the true potential of this technology. The scientific community decided not to waste this technology for devastation, rather use it to make this planet a better place to live. As very well said by the Peter Parker's fatherly figure in the movie Spiderman, "with great power comes great responsibility", and nuclear energy is indeed a great source of power. The designers and researcher across the globe at that time understood the responsibility and dedicated themselves towards unfurling the peaceful use of nuclear technology for the mankind. They began with the electricity production using nuclear fission to reduce the dependence on depleting fossil fuels. On June 27, 1954, the USSR's Obninsk Nuclear Power Plant became the world's first nuclear power plant to generate electricity for a power grid, and produced around 5 Megawatts of electric power. This was the opening of an era of nuclear electricity production. In the following years, major countries like USA, USSR, UK, France and Japan went on producing electricity using nuclear fission. In most of the developed nations, nuclear power became the part of mainstream electricity production. Installed nuclear capacity initially rose relatively quickly, rising from less than 1 GW in 1960 to 100 GW in the late 1970s, and 300 GW in the late 1980s. This was the golden age for the expansion of nuclear power and related technologies. India also heralded the arrival of India's nuclear energy programme with Asia's First Nuclear Reactor "Apsara" at Bhabha Atomic Research Centre (BARC), Trombay on August 4, 1956 built entirely by Indian engineers in a record time of about 15 months. Dr Homi Bhabha himself conceptualised and was the architect of India's three stage nuclear power programme. This long term energy sustainability strategy envisages three stages viz. Stage-I, II and III.

- Stage-I of this strategy deals with the utilization of natural uranium using PHWRs and other LWRs. Reprocessing of the spent fuel from this stage will

produce plutonium be used in stage-II, which will help in attaining closed fuel cycle strategy.

- Stage-II will utilize plutonium obtained from previous stage in fast breeder reactors to produce uranium-233 from thorium. This uranium-233 will be used in stage-III power generation. Prototype Fast Breeder Reactor (PFBR) is one such reactor, under commissioning at Kalpakkam, which will produce the fuel for stage-III using the spent fuel of stage-I.
- Stage-III will be the self-sustaining power generation stage, as it will use the uranium-233 produced in previous stage from India's vast thorium reserves. Advanced Heavy Water Reactor (AHWR) is the prime example of such an innovation.

These three stages will not only produce the clean and environment friendly electricity but also provide us with various spin off technologies for the numerous medical, agricultural and industrial applications.

Everything looks pleasing, then where is the concern? Why everyone in this industry is working towards making reactors even safer?

The answer lies in the brief history of concerns towards nuclear technology.

The journey of concern and fear of radiations were going hand in hand with the inception of nuclear era itself. The inhuman act of using nuclear technology as weapon of mass destruction made people angry and afraid of the term "nuclear" in their lives. The matter of the fact is that, although the electricity generated by nuclear reactors was exactly same as generated by any other conventional source such as coal, gas, etc; society was not able to accept it because of the abhorrent history. With the continual efforts of the various nuclear agencies, nuclear reactor designers and operators towards awareness of the benefits of nuclear technology in human life; general public

started changing mind about this friendly yet powerful source of sustainable energy. Once the society found that it is helping in nation building, they accepted it with demand of utmost safety. The scientist and engineers all around were working to make the reactors as safe as achievable. Optimized strategy of defence in depth and multiple redundant systems are the pillars of such technology. Technological developments and growing experience in reactor operation led to accept nuclear energy as viable source of energy.

This sound and peaceful nuclear energy story got a little prick in the year 1979, a shock in 1986 and a major setback in 2011. These are three major tragic events associated with nuclear industry which made society to reconsider nuclear as the safe source of energy. These events were:

- Three mile island, USA, 1979
- Tchernobyl, Russia, 1986
- Fukushima Daiichi, Japan, 2011

They fall under the category of severe accidents. Severe accidents are regarded as the scenarios where it becomes really challenging to maintain the reactor core in the safe and cool condition. Such a scenario can be initiated by the human error, natural calamity or due to collective errors in operation. An accident can turn into severe accident because of unavailability of various safety and redundant systems. Analyses of the earlier severe accidents have suggested that situation can become even worse if it leads to reactor core melt down. The core melt consists of molten fuel and metallic structural material; and is called as 'Corium'. Corium is highly radioactive molten substance with temperature of the order of 3000 K. It can be relocated to the lower plenum of the reactor pressure vessel, and upon its failure can relocate in lower containment cavity. Concrete ablation upon interaction with corium in this condition

may lead to relocation of corium into the ground. This may lead to environment hazard due to probable ground water contamination. This hypothetical scenario is known as ‘china syndrome’ and it is one of major concern in front of present reactor designers.

## 1.2. Core melt scenario and cooling strategies

Managing corium, as discussed above, is really a great concern while dealing with severe accident scenario. Due to its high temperature, it is difficult to arrest it within the desired location and cool it. Its concern grows when water comes into the picture. There is a potential hazard of vessel breach and reactor pit concrete breach upon interaction of corium in case of dry conditions (water is absence in lower vessel plenum or reactor pit). When melt relocates to the bottom of the reactor cavity it forms the melt pool. In case of wet conditions, when water may be present in the vessel or in the reactor cavity, there is a potential hazard of steam explosion which may damage containment walls. This is so because when melt relocates in this scenario it interacts with water. The dry and wet conditions are shown in Figure 3.

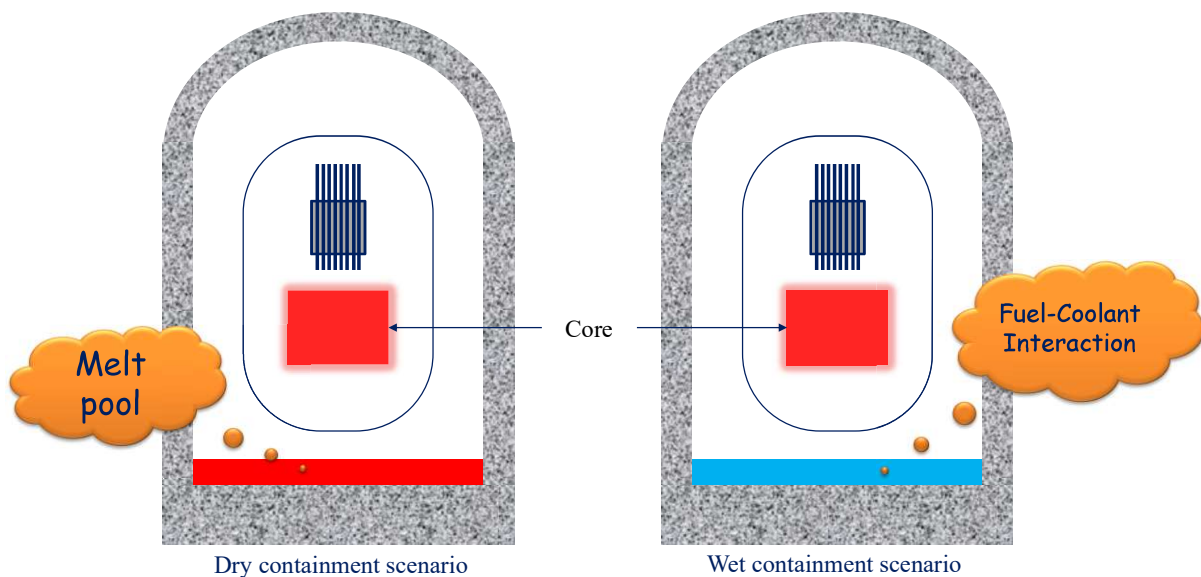


Figure 3: Dry and wet conditions in the reactor containment

Depending on various interactions, scenarios depicted in Figure 4 may occur. The location of interaction defines the name as in-vessel, where the interaction takes place within the reactor vessel; and ex-vessel, where the interaction occurs within the containment but outside the reactor vessel.

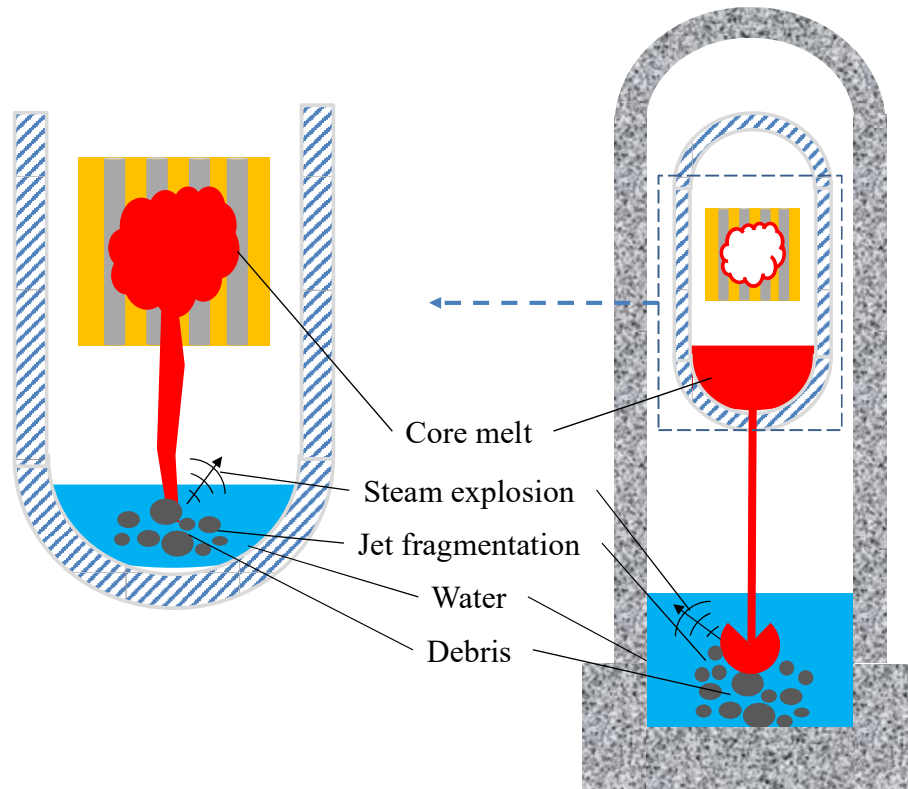


Figure 4: Schematic of two possible melt-water interaction scenarios in a nuclear reactor

Cooling of this corium is utmost important in order to arrest the accident propagation during severe accident in a nuclear reactor. The coolant or water in case of light water reactors, has to come in contact with corium directly or indirectly. Considering this, strategies to cool the melt can be studied by dividing it in following categories as shown in Figure 5.

- Melt coolability using top flooding

This is the simplest possible approach to cool the melt, as shown in Figure 5(a).

The melt pool or melt open surface is flooded with large amount of coolant or

water (for light water reactors). This water keep extracting the heat from the melt and subsequently cools it down.

- Indirect or side cooling of melt

In order to cool the melt by this means, the melt needs to be hold in a vessel (reactor pressure vessel or core catcher vessel). Then water is circulated around the vessel which removes the heat from the vessel boundary and subsequently from the melt, as shown in Figure 5(b). The melt and water doesn't come in contact with each other in this technique.

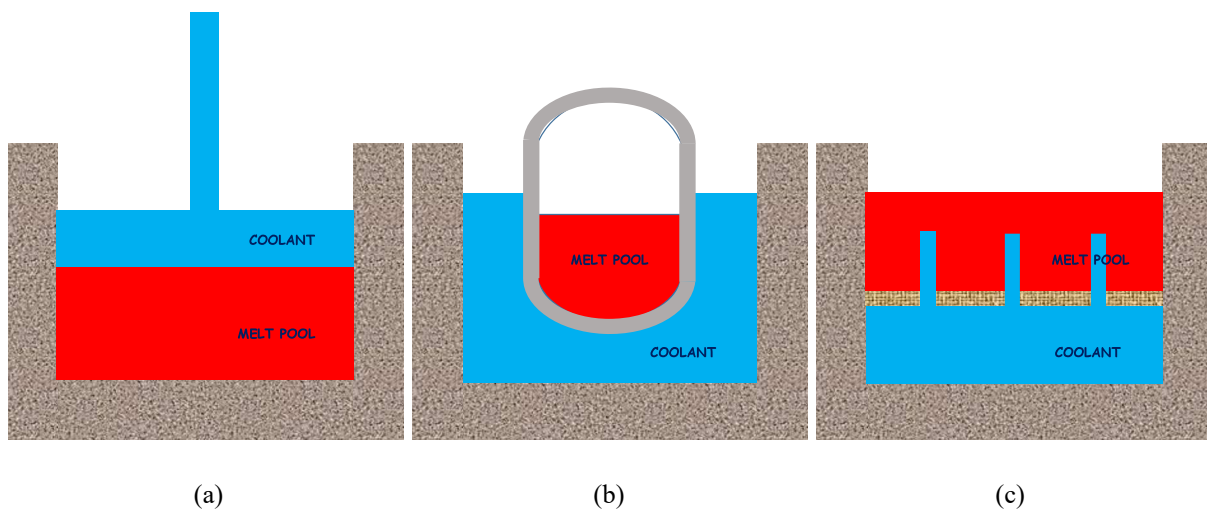


Figure 5: Different melt cooling strategies

- Melt coolability under bottom flooding

The water is injected directly into the melt pool from the bottom of the pool, as shown in Figure 5(c). Water then boils and form steam which helps in creating openings within the melt pool; and thus cooling it down quickly. In this technique, melt solidifies quickly and also breaks in to debris resulting in more water available for cooling per unit surface area.

On the basis of above discussed strategies of cooling the melt, core catchers are designed for advanced nuclear reactors. Core catcher is an arrangement where corium

can be contained and cooled for the long duration in a stabilized state. Considering the type of reactor and severe accident management strategy adopted, different core catchers have been designed and are discussed in the following section.

### 1.3. Different core catcher concepts

In order to address these challenges and to ensure safety of people and environment, a safety system called as “core catcher” has been incorporated in the present and future reactor designs. It is the system which is placed inside the reactor in such a manner that in the severe accidental scenario; it will retain the corium, quench it and then sustain the coolability of the debris formed due to corium water interactions.

The concept of core catcher started as early as in early nineties. The idea to retain the corium melt within the reactor vessel was proposed for the first time by Theofanous[1]. This concept was developed regarding the VVER-440 reactor of the Loviisa NPP in Finland. Due to complex mechanisms of corium cooling inside the vessel and uncertainties in the distribution of the steel and oxide components, and, as a consequence, in the distribution of the heat flux density over the melt-bath boundaries, made it impossible to introduce the concept of the corium melt retention within the vessel of a high capacity reactor. This gave rise to ex-vessel corium catcher concept. Kukhtevich[2] presented the ex-vessel corium catcher for VVER. It consists of a big crucible which is located in the reactor pit beneath the RPV. In case of a RPV failure the corium is collected in the crucible which is cooled externally by flooding of the reactor pit by passive water injection as shown in Figure 6. The crucible is partly filled with sacrificial material (a mixture of sintered iron oxide and alumina) which melts and mixes with the corium, thus reducing the enthalpy in the melt and yielding heat fluxes at the surface of the crucible below the critical heat flux which can be removed by the external cooling.

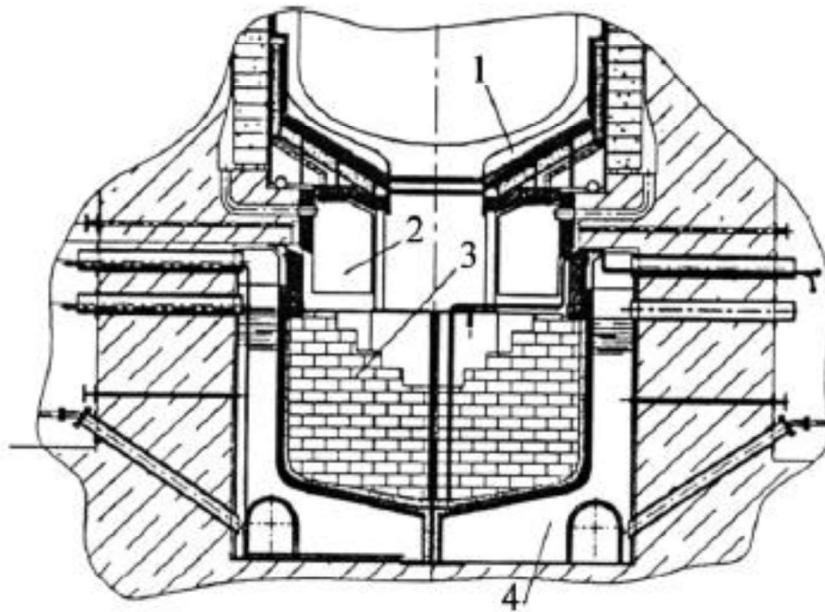


Figure 6: Ex-vessel catcher for the VVER-1000 reactor of the Tyan'van NPP (1) Lower plate (2) vent collector (3) basket with a sacrificial material (4) sectionalized heat exchanger

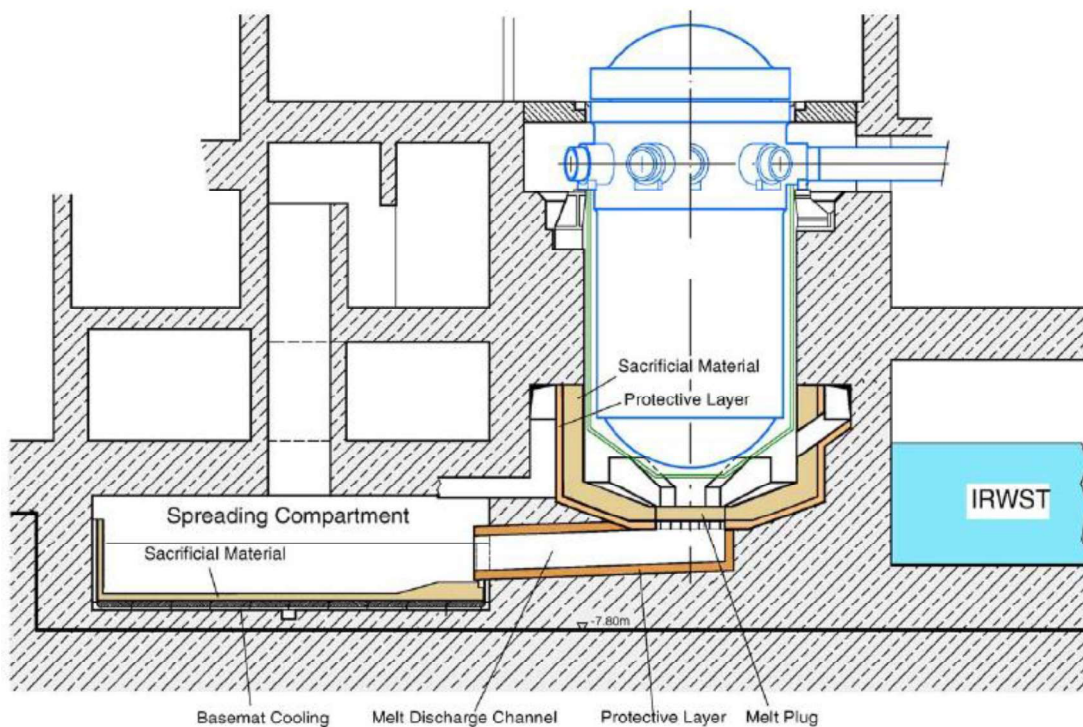


Figure 7: EPR core catcher concept

A different approach to increase the heat transfer surface is used in the current design concept of the European Pressurized Reactor (EPR) as outlined by Fischer[3]. As

shown in Figure 7, the corium melt is collected in the reactor pit, conditioned with sacrificial concrete and subsequently spread onto a large surface (e.g. 170 m<sup>2</sup>) of a special compartment in order to obtain a thin layer that can be cooled by addition of water from the top.

A different core-catcher concept based on the fragmentation of corium and porosity formation has been developed at Forschungs Zentrum Karlsruhe(FZK)[4] and was investigated further within the COMET project[5]–[8]. After erosion of a sacrificial concrete layer, the melt is passively flooded from the bottom by injection of coolant water. The water is forced up through the melt, the resulting evaporation process of the coolant water breaks up the melt and creates a porously solidified structure from which the heat is easily removed. The porous melt is expected to solidify within less than one hour from onset of flooding, and continuous boiling removes the decay heat from the permanently flooded corium bed. It uses an array of plastic tubes, embedded in a horizontal concrete layer which is connected to a water reservoir pressurized by a static overhead. Water is fed into the melt through the plastic tubes after the melt has eroded the sacrificial concrete layer on top as shown in Figure 8.

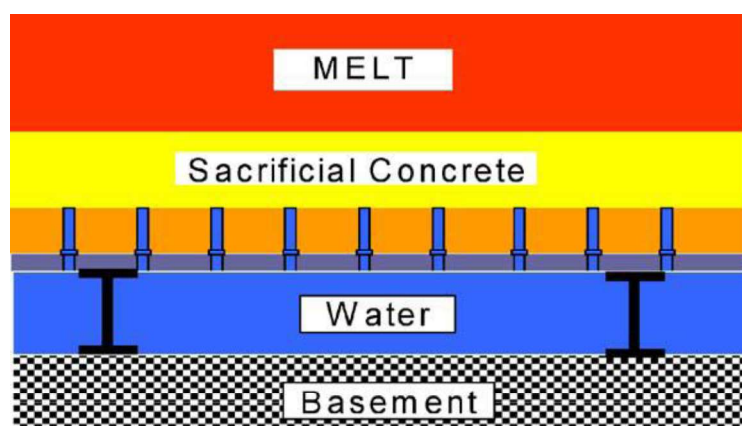


Figure 8: COMET experimental concept of core catcher using bottom flooding water injection

Hamazaki[9] presented a scheme for mitigating severe accidents in a BWR by employing core catcher combined with passive containment cooling system. The core-catcher is installed on the bottom floor of the drywell in the containment to arrest and stabilize the core melt, as shown in Figure 9. The cooling water is supplied from the suppression pool via passive flooders initially, and from PCCS condensate drain lines in the long term. After the core catcher flooding, the core melt on it is effectively cooled by both the overlaying water and the lower cooling channels, and then boiling in the inclined cooling channels which promotes natural circulation. Thereby, molten core concrete interaction (MCCI) is excluded.

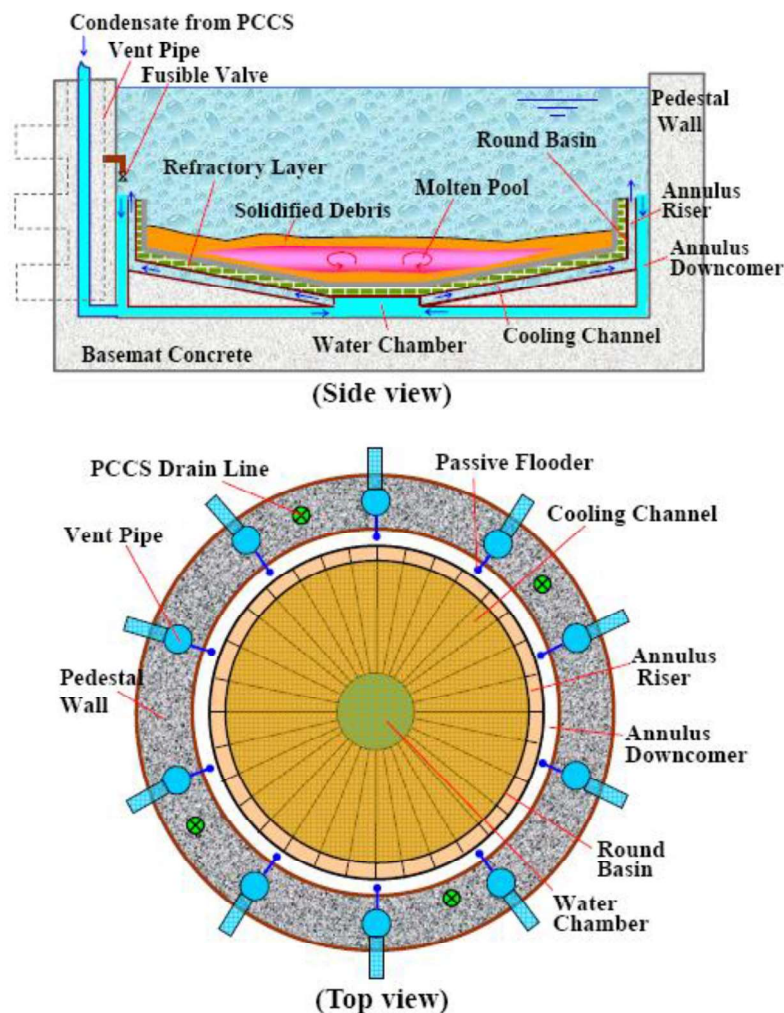


Figure 9: Hamazaki's concept of core catcher

#### 1.4. Advanced Heavy Water Reactor (AHWR) core catcher

The AHWR is a 300 MWe pressure tube type boiling light water cooled, heavy water moderated reactor, as shown in Figure 10. The reactor design is based on well proven water reactor technologies and incorporates a number of passive safety features such as natural circulation core cooling during start-up, power-raising, rated power condition and accidental conditions; direct in-bundle injection of light water coolant during a Loss of Coolant Accident (LOCA) from Advanced Accumulators and Gravity Driven Water Pool by passive means; Core Decay Heat Removal using Isolation Condensers passively without using any active components such as Emergency Condensers which are normally used in conventional BWRs; Passive Containment Cooling System; Passive Containment Isolation System, etc.

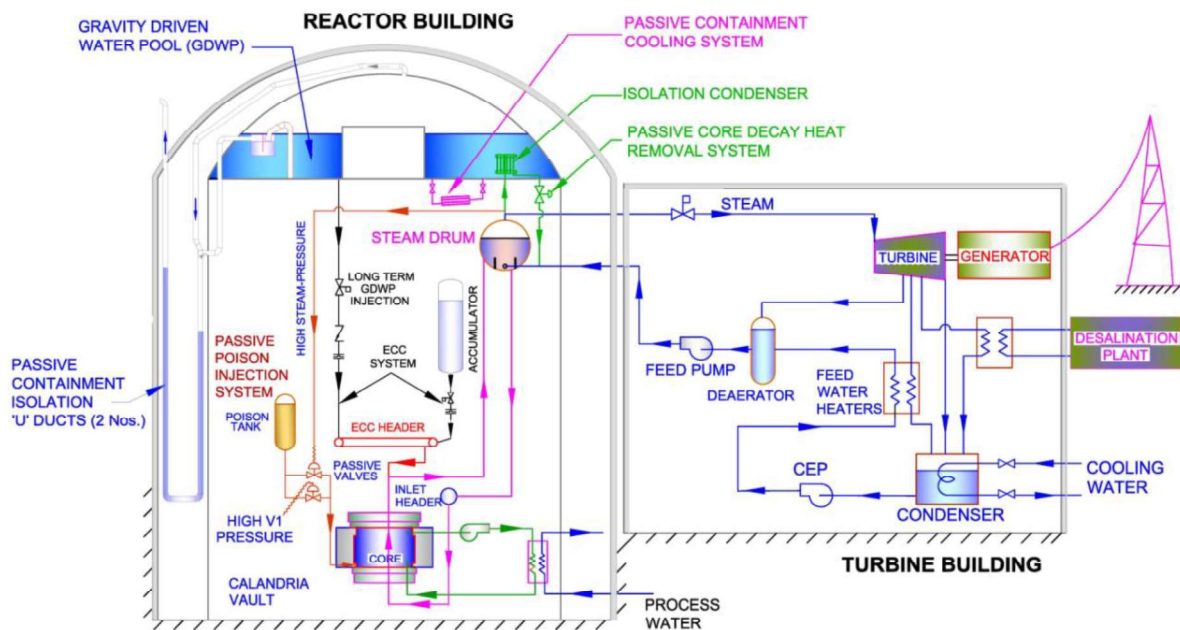


Figure 10: Schematic of Advanced Heavy Water Reactor (AHWR)

In fact, the reactor is designed to remove the core decay heat by passive means for a grace period of seven days during a station blackout situation without significant rise in the clad temperature. With several passive concepts adopted in the reactor design,

the probability of a Core Damage Frequency (CDF) has been estimated to be as low as  $10^{-7}$  per year in this reactor.

However, keeping with current international practice for enhancement in all levels of defence-in-depth, a strategy to build severe accident management scheme in AHWR has been conceived. In case of very low probable accidents involving core melt, the accident will be managed by the core catcher as shown in Figure 11.

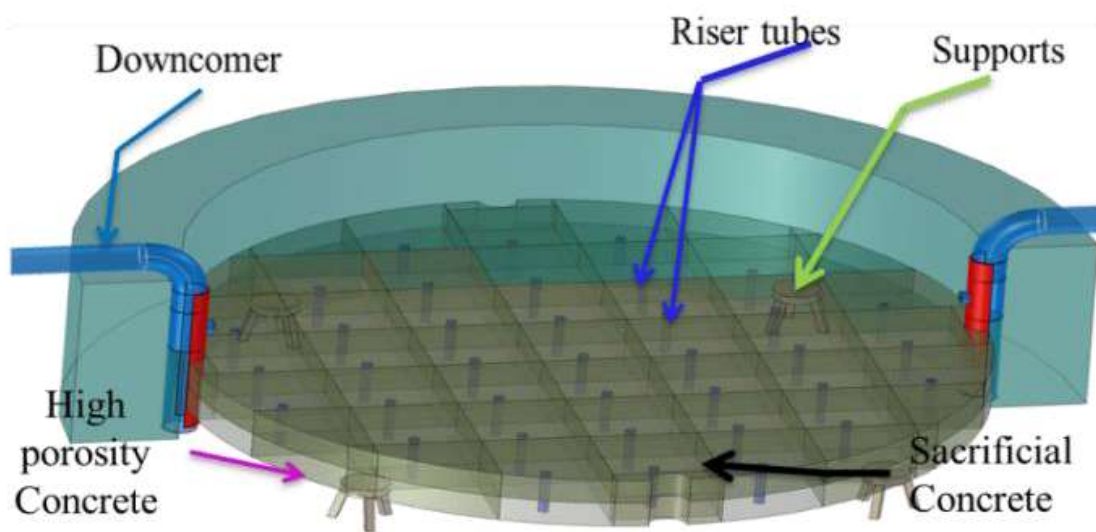


Figure 11: AHWR Core catcher

It is located at the bottom of the reactor pit below the riser tubes so that, in case of core melting, corium should directly fall into the core catcher, as shown in Figure 12. It has adopted the bottom flooding technique to cool the melt pool initially, and then removing the heat by submerging the entire debris bed into the water pool (formed after water reaches the top of the melt pool).

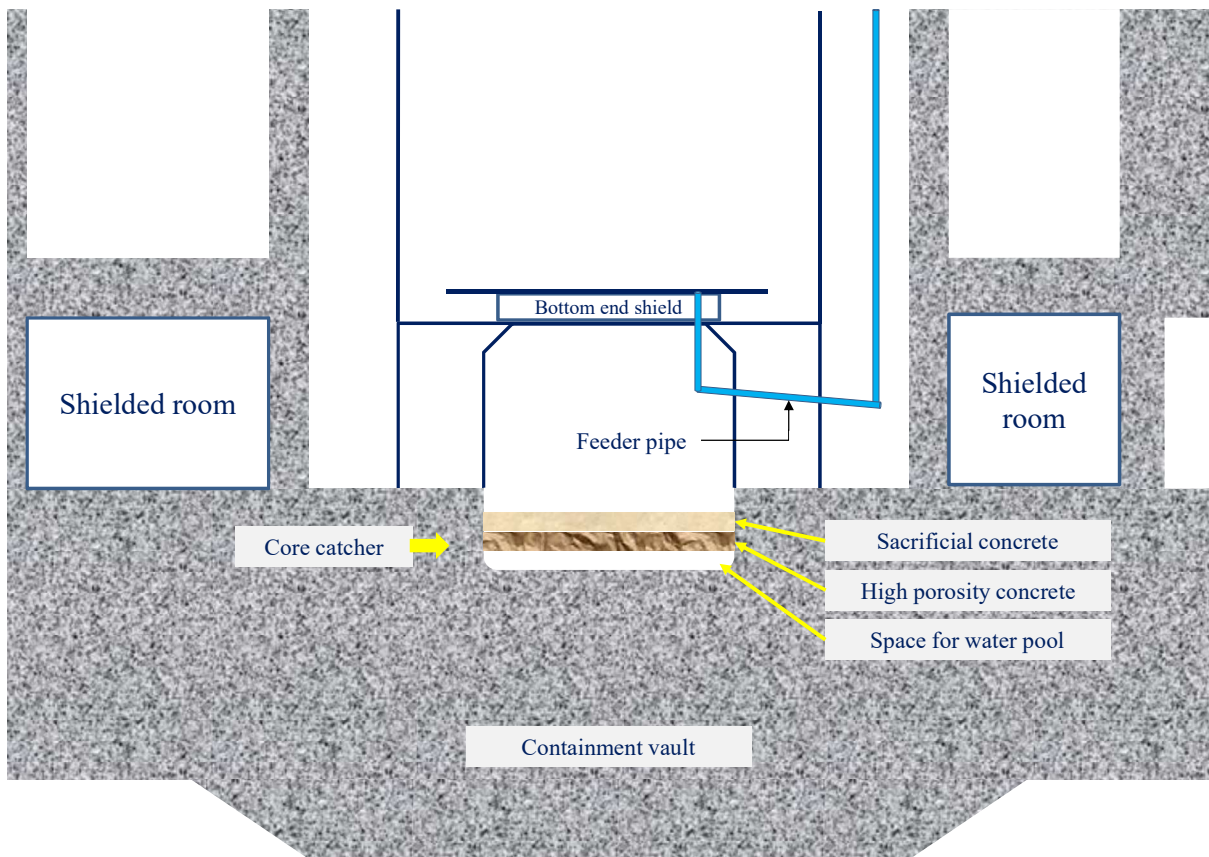


Figure 12: AHWR Core catcher located at the basemat within the containment

Design objective of Core catcher:

- Retention of the melt in the cavity
- Quenching it within 30 minutes
- Stabilize it for substantial period of time

In this kind of core catcher, two scenarios are possible viz. dry conditions and wet conditions in the core catcher located in containment base mat.

**Dry condition:** In this kind of scenario, the corium will relocate to the core catcher and will form a melt pool. This pool needs to be sustained and cooled within the core catcher for substantial period of time.

**Wet condition:** In this scenario, it is assumed that water is present in the core catcher prior to melt arrival. Then, the melt will first interact with water present in the core catcher and may result in volatile interaction.

These two possible scenarios need to be understood well before using the core catcher in actual reactor systems. Limited studies in this regard were found in the open literature and are discussed in the following section.

## 1.5. Dry conditions: Melt pool coolability

### 1.5.1. Top flooding

The most convenient accident management strategy is to cool the melt pool by flooding it from the top. However, the question that arises is to what extent the water can ingress in the corium melt pool to quench and cool it. There are not many studies on the phenomena especially in the ex-vessel situation except for the MACE and the MCCI tests[10] at the Argonne National Laboratory in USA. Viscosity of the corium increases significantly and its melting point is reduced due to its interactions with the structural material as well as the concrete. These can seriously affect the water ingress and hence the coolability of the melt. A literature review suggests that there are a few efforts on modelling of water ingress phenomena. Originally, the motivation behind modeling of water ingress phenomenon did not aim to study the quenching of molten corium pool during a postulated severe accident condition in a LWR. In fact, models were developed for simulation of cracking behaviour of hot rocks in geological reservoirs. In this context, Lister[11] has done pioneering work in modeling the penetration of water into hot rocks by considering the simplest possible one-dimensional model based on the concept of crack front propagation. Björnsson[12] found that penetration of water into hot rock is the primary reason for the intense heat release of the sub-glacial Grimsvötn geothermal area. Jagla and Rojo[13] presented a model to predict the statistical properties of columnar quasi-hexagonal crack patterns, as observed in the columnar jointing

of basaltic lava flows. While Lister's model considered penetration of water into hot but initially solid rock under high pressure condition, recently, Epstein[14] used Lister's models of bulk permeability of cracked rock and developed a model for water penetration into initially molten, heat generating rock like material at low pressure which resembles the water ingress phenomena into molten corium pool.

As said before, there are a few experimental investigations on quenching behaviour and water ingress in top flooded molten pool. In the MACE experimental programme[15], [16]; it was found that a tough crust is formed on the upper surface of the melt pool during top flooding situation, which was found to limit the access of the water over layer to the melt pool below the crust. Post-test examination of the debris of the MACE M3b-test[17] indicated that the crust thickness was about 10 cm, amounting to 1/2 of the initial mass. After 20 minutes of melt/water heat transfer in M3b-test[18], several independent sources of data indicate that the crust had anchored to the test section side walls and the melt separated from the crust. After separation, melt/water heat transfer rate dropped significantly. Test results from COTELS project[19] indicate that water ingress through cracks/defects in core material interacting with concrete can contribute to debris coolability. Water can penetrate into debris at the sidewalls due to erosion at this interface as well as direct penetration of water into channels located in the central regions of the debris. However, the authors did not quantify the relative contributions of water ingress at the sidewall core/concrete interface versus ingress in the central core material region to the overall debris coolability. Melt coolability research was also performed at the Sandia National Laboratory. A series of low temperature

simulant material experiments were conducted by Theofanous et al.[20] at the University of California, Santa Barbara.

### 1.5.2. Side cooling

In indirect cooling techniques, the core melt is often collected in an external vessel containing sacrificial material or contained inside the RPV and the vessel is then cooled externally by water. This scheme is employed by VVER[21], ESBWR[22], AP1000[23] and PHWRs[24]. In the EC-FOREVER program, Sehgal[25] studied the creep behaviour of the lower head of the PWRs. Coolability of an in-vessel melt pool has been investigated experimentally by Henry and Dube[26], [27]. The RASPLAV[28] experiments employed prototypical melt of UO<sub>2</sub>, ZrO<sub>2</sub>, Zr, heated to more than 2200 °C with cooling of the vessel with a jacket full of flowing water. Effectiveness of in-vessel cooling was also studied in ACOPO[29], COPO[30], BALI[31], SIMECO[32] and LIVE[33]. This particular phenomenon is also important in the context of PHWRs where, under severe accidents, the molten core falls at the bottom of the calandria vessel and heat is removed by surrounding vault water through the calandria vessel. The issues in this type of cooling are the formation of crust at the melt–vessel interface which limits the heat removed by the water by natural convection and hence the dryout heat flux.

### 1.5.3. Bottom flooding

In a different kind of cooling strategy of injection of water from the bottom directly into the melt has proved a significant enhancement in coolability. COMET experimental series at FZK and ANL[5], [34]–[37] demonstrated the concept of melt coolability using bottom flooding approach. Simulant materials and corium melts of few kilograms to hundreds of kilograms were used in this

experimental series. The results of this experimental program were able to demonstrate the enhancement in melt coolability even at actual plant scale. DECOBI[38] experimental program at Royal Institute of Technology, Stockholm took further the issue of ex-vessel melt coolability using the bottom flooding approach. A model to understand the coolability phenomena observed in COMET experimental series was developed by Paladino[39], [40]. Later, Widmann[41] studied melt coolability with bottom flooding using nozzles and porous concrete. In the COMET-H series of experiments, about 650 kg of corium was cooled at a decay heat flux of  $450 \text{ kW/m}^2$ . Melt and water interfacial transport phenomena during bottom flooding were experimentally studied by Cho[42]. They postulated that for any melt height, there would be an upper bound to the heat removal rate. Paladino[38] and Widmann[41] attempted modelling of melt coolability under bottom flooding, but their focus was to predict the porosity of the melts formed during bottom injection and its effect on coolability. Foit[36] studied the porosity formation as well as quenching of different melt layers using MEWA code. Lomperski and Farmer[43] carried out experiments on the basis of COMET concept. They used two nozzles to inject water, one filled with a porous concrete and the other composite nozzle which injects both water and non-condensable gas to stabilize the flow and suppress steam explosions. Kulkarni and Nayak[44] presented a simple yet effective model for the fracture of crust formed under bottom flooding scenario while accounting for the thermal stresses acting on the crust.

Kulkarni and Nayak[45] also presented a comparative study of different cooling strategies for melt coolability, as summarized in Table 1. They observed that while cooling with top flooding, it took several hours to cool the melt in the

absence of decay heat as the dominant mode of heat transfer was conduction only. As soon as water came in contact with top melt layer, melt got cooled and formed the crust which hindered further cooling. This crust subjected to thermal stresses got fractured leading to further ingress of water and hence cooling it. This process took long time as melt-water interfacial area is very limited. Also, during water ingress, there is a possibility of counter current flow limitation (CCFL) due to steam flowing upward through the fractured cracks in the crust and water flowing down through same cracks. This may lead to dryout and hence no coolability situation.

Table 1: Different strategies for melt pool coolability

Melt coolability strategy	Conclusive remarks
Top flooding	<ul style="list-style-type: none"> <li>• Took several hours to cool the melt without decay heat</li> <li>• Water ingress occurred only up to few mm depth</li> <li>• Stable solid crust was formed</li> <li>• Limited heat transfer</li> <li>• Insufficient to quench the molten pool in case of severe accidents</li> </ul>
Indirect cooling	<ul style="list-style-type: none"> <li>• Took long time to cool the melt</li> <li>• Crust formed between melt pool and vessel acted as an insulation</li> <li>• Poor heat removal</li> </ul>
Bottom flooding	<ul style="list-style-type: none"> <li>• Steam formation below the melt led to the melt eruption inducing a very high porosity inside the otherwise impervious melt</li> <li>• Quenching of the melt in very short period of time</li> <li>• It took a few minutes to cool the entire melt to room temperature</li> </ul>

In case of side cooling, water cools the melt without interaction and lead to crust formation between melt and vessel. This hinders further heat transfer while acting as an insulation due to its poor thermal conductivity. Also, the melt temperature at the centre of the pool remains high for quite a longer duration and may lead to remelting. Authors also discussed that when water was flooded directly into the melt from bottom, the removal of heat was quicker as compared

to previously discussed techniques. It took fewer minutes to cool the melt compared to several hours took by other techniques.

#### 1.5.4. Unresolved issues in dry core catcher scenario with bottom flooding

##### **1.5.4.1. Influence of decay heat on melt coolability under bottom flooding**

In spite of the above studies, the literature lacks the fundamental understanding of the effect of decay heat on melt coolability under bottom flooding.

##### **1.5.4.2. Scalability of melt coolability tests under bottom flooding**

There are international and regulatory concerns with regard to scalability of experimental results to actual reactor system applications. Since experiments are conducted at smaller scales compared to actual scale of the system, extrapolation of their results are always concerns especially with regard to following aspects.

###### **1.5.4.2.1. Influence of melt volume**

The actual core catcher will deal with tonnes of corium while experiments are performed with smaller amounts. What will be the influence of melt volume on melt coolability under bottom flooding?

###### **1.5.4.2.2. Influence of melt composition**

The corium composition is always subjected to various factors like the type of fuel, type of structural material, extent of damage, burn-up, etc. In view of this, most of the tests have been conducted with different melt simulants. Thus, influence of melt

composition on melt coolability under bottom flooding needs to be understood.

#### **1.5.4.3. Effect of geometrical parameters**

There are concerns with regard to effects injection velocity on efficacy of melt coolability with bottom flooding. Injection velocity can be altered by the geometrical parameters like nozzle diameter and inlet pressure of water. This concern enhances because, it is extremely difficult to conduct and repeat experiments with prototypic materials and prototypic conditions.

#### **1.5.4.4. Lack of models for melt coolability under bottom flooding**

It was found that there is a lack of models in the literature which can give insights about the phenomenology and can predict the melt coolability under bottom flooding to a better extent. This is mainly because of the lack of experimental data available in the open literature, complexities involved like multiphase multi-component coupled system and the lack of understanding of actual process.

### **1.6. Wet conditions: Fuel coolant interaction**

#### **1.6.1. Current status and literature review**

Steam explosion is one of the volatile phenomena which is a concern during cooling of molten materials during fuel coolant interaction (FCI). The introduction of a hot, molten liquid into a volatile coolant, under certain circumstances, the energy transfer rate can be so rapid and coherent that an explosion results. This can lead to the formation of shock waves and/or the production of missiles at later times, during the expansion of coolant vapor that may endanger surrounding structures. Such explosions can present a hazard in

any industry where there is the potential for the contact between a hot liquid at a temperature well above saturation temperature of a cold volatile liquid.

The occurrence of steam explosions in nature goes back to the earliest days of this Earth. No doubt as man began to work with metals he found that the contact of molten metal with water posed a significant hazard. In the fourteenth century the hazard of metals casting is recounted in the Canon's Yeoman's tale in "The Canterbury Tales" by Geoffrey Chaucer[46], written about 1386 and translated into modern English by Nevill Coghill.

In case of severe nuclear reactor accidents, the corium, while interacting with water, may cause an energetic explosion. Such phenomena can occur inside the reactor vessel during flooding of a degraded core or when molten corium falls into the lower head filled with water. Similar phenomena may occur outside the reactor vessel when molten corium is ejected into a flooded reactor cavity or into the flooded containment after the vessel failure. There is then a risk of release of radioactive fission products into the environment, which is the reason that these phenomena have been widely analysed during nuclear safety studies. A steam explosion is a complex, highly nonlinear, coupled multi-component, multi-phase, multi-space-scale and multi-time-scale phenomenon encountered in nuclear safety. This thermal interaction process largely depends on the hydrodynamic behaviour, such as core melt jet breakup, droplet fragmentation, stability of vapour film, which can be characterized as interface instability phenomena.

Steam explosion has been studied intensively for a few decades mainly with a focus as the premixing phase of energetic steam explosions[47]–[51]. They suggest that the melt undergoes a coarse and fine fragmentation during the

interaction of melt with water. They observed steam explosions with alumina but not with corium due to difference in fragmentation behaviour. Those works provided a comprehensive data base for the debris formation and its size distribution. A series of experiments were carried out at various laboratories across the globe as reviewed by Corradini[52], [53]and Berthoud[54]. Cho et al[55] studied the effect of metallic melt on steam explosion behaviour. Similar program called MISTEE (Micro-Interactions in Steam Explosion Experiments) was carried out at KTH, Stockholm. The objective of the steam explosion study at KTH was to develop a basic understanding of micro-interactions in steam explosion, with a hope to identify mechanisms which may limit the explosivity of molten corium in a prototypic severe accident scenario with FCI. Experiments in FARO[47], [49], [56], [56]–[58], [58]–[60], KROTOS[48], [48], [58], [58], [61], [62], [62]–[64], [64]–[68], [68]–[71] and TROI[59], [72]–[76], [76], [77], [77]–[88] suggested that physical properties of corium ( $\text{UO}_2\text{-ZrO}_2$  as a binary oxidic material) may have been responsible for its low explosivity. The evidence is however far from being conclusive, so that extrapolation of the observed behaviour to reactor scenarios is not possible without an in-depth understanding. In the ALPHA program[89], [90] initiated at JAERI (Japan Atomic Energy Research Institute) in Japan; they focussed their study to investigate better strategy for safe corium cooling. The ALPHA program suggested that void fraction during premixing plays an important role in deciding the occurrence of steam explosion. They also observed that steam explosion was not observed with saturated water. Their conclusive remark was that the explosive interaction in stratified configuration was less energetic compared to that in melt drop configuration. The PREMIX (FZK, Germany)

experiments have been performed to study the premixing of sizable amounts of very hot oxidic melts with water when being released as a jet in a reasonably characterized way and with full optical access. PREMIX involves the full physics of the mixing process including jet break-up and melt drop fragmentation using Alumina melt. KROTOS tests[68] were carried out on molten alumina and prototypic melts. These tests brought out that, no spontaneous explosion is possible in case of corium and a trigger was needed. Also, the effect of coolant temperature was highlighted. The recent study by Kudinov et al.[91]–[95] provided additional information. They performed a series of experiments with a focus on the fractions of particulate debris and the agglomerations on the pool bottom as well as the debris size distribution during FCI.

### **1.6.2. Unresolved issues in wet core catcher scenario**

However, all these studies are unable to explain the conditions for steam explosion. Moriyama[96] suggested that steam explosion occurs when the fine fragments i.e. the particles of the order of 0.1 mm in size or below formed during fragmentation and constitute about 10-50% of debris mass, considering the history of melt fragmentation in the prior experiments, as shown in Figure 13.

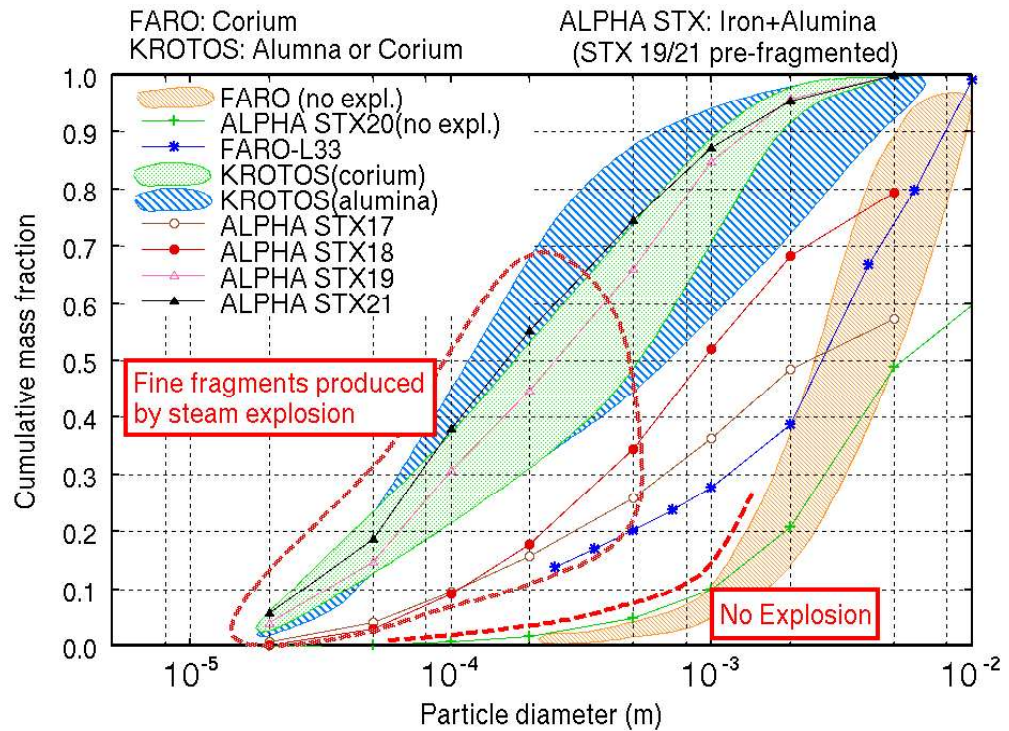


Figure 13: Moriyama's map for steam explosion condition

On the contrary, energetic interaction occurred in the experiments even in the absence of fine fragments. This raises a question, is the fine fragmentation a root cause of steam explosion? What is the cause of energetic interactions occurred in the absence of fine fragments? Does the conversion efficiency play any role in deciding whether steam explosion will occur or not?

### 1.7. Objective of thesis

The main objective of this thesis is to address these above stated unresolved issues. All these unresolved issues are scientifically unknown and they have a key role to play in understanding the detailed phenomenology and various mechanism of melt coolability. The findings of these issues will help in design of core catcher for advanced nuclear reactors.

### 1.8. Strategy to address these unresolved issues

To address these issues, dedicated experimental programme for melt coolability under dry conditions and under wet conditions were performed.

To understand the melt coolability under bottom flooding to cool the melt pool formed during dry core catcher conditions, a series of experiments were conducted to study the influences decay heat, melt volumes, melt compositions, nozzle diameters and inlet water velocities on it. Transient melt pool temperatures and porosity were measured. The test facilities equipped with furnaces, test section assemblies and required instruments for the measurements of temperature history, inlet water flows and steam outlet flows were used to conduct these experiments. The measurements obtained from these experiments were analysed to conclude various inferences.

A new mathematical model has been developed from first principle to understand the phenomenology of the melt coolability under bottom flooding which considers the heat transfer in the melt pool, steam formation at the bottom of the melt pool, crust formation at the bottom of the melt pool and its fracture, melt eruption, porosity formation and its radial variation using experimentally developed empirical correlation, interfacial area density depending on experimentally obtained particle sizes and boiling heat transfer from debris to coolant. The model is able to capture the coolability behaviour of the melt pool with and without decay heat quite accurately. The developed new model was validated using the above discussed experimental measurements.

Similarly, a series of experiments were conducted to understand the effect of fine fragmentation on steam explosion which may occur during wet conditions in a core catcher. Dedicated facilities for small and large masses equipped with fast and dynamic pressure transducers were designed and erected.

### 1.9. Outline of the thesis

All unresolved issues discussed in this chapter have been addressed in the following chapters of this thesis.

**Chapter 1** discusses the introduction of the thesis providing the necessity for research on this topic and establishing the background for this work. It also includes the insights brought out of the literature and states the unresolved issues which will be addressed in the subsequent chapters of this thesis. In the end, the chapter has been summarised.

**Chapter 2** presents the details of all experimental facilities and simulant materials used for various experiments to address unresolved issues. The first part of the chapter discusses the details of simulant materials used for various experiments along with their properties and specifications. The chapter also includes the details of large scale bottom flooding test facility in which melt coolability experiments with and without decay heat were conducted. Its design and instrumentation details have been discussed. Along with that, small scale bottom flooding test facility design and instrumentation details have also been addressed. In this facility, all the scalability related experiments have been conducted. It was specifically designed to conduct experiments by changing several parameters like type of melt, nozzle diameter and inlet water flow rates which was possible due to its modular design concept. Another dedicated FCI test facility, to perform melt-water interaction experiments using different melt volumes, have been discussed in this chapter. Two different kind of facilities were used viz. small scale with viewing window and large scale for varying masses. Their instrumentation and necessary design information have been provided for ready reference. A summary of the chapter is present in the end.

**Chapter 3** sequentially discusses the influence of decay heat on melt coolability under bottom flooding. To address that two experiments were performed viz. without decay

heat and with decay heat, with sodium borosilicate glass melt of about 20 litres. The temperatures measurements of the experiment without decay heat have been presented first, and then the measurements with decay heat experiment. Both the results have been compared to understand the influence of decay heat on melt coolability under bottom flooding. Their temperature contours and debris profiles have also been compared and discussed. In the last part, inferences has been discussed as a closure of the chapter.

**Chapter 4** give us the insights on scalability of melt coolability under bottom flooding. This chapter is basically divided into three sections which deals with the effect of melt volumes, effect of type of melts and the effect of various geometrical parameters on coolability. In the first section, results of the experiments with 3 litres and 20 litres of melt volumes have been discussed and compared to understand the effects of different melt volumes performed with same material (CaO-B<sub>2</sub>O<sub>3</sub>). In the second part, experiments conducted with two types of simulant melts viz. sodium borosilicate glass and CaO-B<sub>2</sub>O<sub>3</sub> have been discussed and compared to study their effects on melt coolability.

**Chapter 5** presents the discussion on effects of nozzle diameter and injection pressure on melt coolability under bottom flooding. Results of all the experiments performed with three different nozzle diameters i.e. 8 mm, 12 mm and 18 mm; and with two injection pressures i.e. 0.35 bar(g) and 0.75 bar(g), have been discussed. The temperatures contours of all these results have also been compared to get the insights and their influence on melt coolability under bottom flooding. The same have been summarised in the end of the chapter.

**Chapter 6** provides the details on development of a new mechanistic model to understand melt coolability under bottom flooding in presence of decay heat. In detail

description of model, its applicability, assumptions made and the postulations have been presented. In the later part, the mathematical model has been structured along with the necessary boundary conditions. The procedure to solve the equations in order to obtain temperatures profile of the melt pool has also been mentioned. The predicted temperatures for with and without decay heat scenarios have been presented and have also been validated using their respective experimental data. Highlights and inferences have been summarised in the end.

**Chapter 7** brought out the insights of the experiments conducted to understand whether presence of fine fragments during melt-water interaction, which may occur in wet conditions of a core catcher, is the root cause for steam explosion. It provides the systematic study of melt-water interaction conducted using varying mass of simulant melt from about 50 g to about 2500 g. Dynamic pressure measured in all these experiments have been presented and the role of conversion efficiency has been discussed in detail along with the analysis. The chapter has been summarised in the end with the inferences obtained from this study.

**Chapter 8** concludes the entire study and presents the key insights of the thesis.

**References** included in the thesis have been arranged in the last part of the thesis.

#### 1.10. [Summary](#)

This chapter provides wide introduction and motivation of this research work. It began with the discussion on the necessity of nuclear power and the concerns associated with the severe accidents. It further discusses about various core catcher concepts in order to manage severe accidents in different types of nuclear reactors. The AHWR core catcher is then mentioned in detail as it is the one to utilise this research directly. Followed by this is the literature review on melt coolability in dry core catcher conditions. Various cooling techniques, viz. top flooding, side cooling and bottom

flooding, have been reviewed. Along with this, fuel-coolant interactions have also been thoroughly reviewed to better understand the concerns during wet core catcher scenario. Subsequently, the unresolved issues and the objective of the thesis were brought out and the strategy to address them has been discussed. The outline of the thesis has also been presented in the last section of this chapter, and the chapter has been summarized in the end.



# Chapter

*“Experimental observations are only  
experience carefully planned in advance, and  
designed to form a secure basis of new  
knowledge”*

— *Sir Ronald Aylmer Fisher (17 February 1890 – 29 July 1962)*  
*British statistician and geneticist*



## **Chapter 2. EXPERIMENTAL FACILITIES**

### **2.1. Introduction**

Experimental approach, to understand the phenomenology and to address the unresolved issues towards melt pool coolability and melt-water interaction, is the mainstay of present research work. In the beginning of this work the scarcity of experimental measurements was felt in the literature. The proprietary nature and strategic importance of such experimental data also contributed to unavailability of such measurements in the literature. Thus, following experiments served prime importance in the present research work. In order to perform such experiments, state-of-the-art experimental facilities to deal with specific scientific issue were designed and erected. Details of these facilities are discussed in the following section.

### **2.2. Simulant materials**

The most important component needed to perform the melt coolability experiments was ‘the melt’. Conducting experiments using actual corium or prototypic melt (melt consisting of actual fuel and structural material prepared for corium studies) possess certain difficulties like radioactivity associated with it, unavailability of such melts, melting challenges and of course, the cost per experiment is considerably high. Thus, it was decided to use simulant materials instead. In an actual scenario, when corium interacts with sacrificial concrete, it behaves as amorphous glass due to presence of metal oxides and silicates. Thus, oxides with such properties and whose transient heat transfer behaviour was similar to corium were chosen as the melt for the experiments. As we all know, transient thermal behaviour between melt and coolant is strongly dependent on thermal diffusivity of the material, hence, the simulants having thermal diffusivity close to corium value were selected. Sodium borosilicate glass and the non-eutectic mixture of CaO-B<sub>2</sub>O<sub>3</sub> (in ratio of 30:70 respectively by weight) were used as

the simulants, which have been established and tested at KTH, Sweden[38]; and have also been used by many researchers in the past. Table 2 summarizes the properties of both simulants used and their comparison with the corium properties; as mentioned by Paladino et al.[38], and Kulkarni and Nayak[45].

Table 2: Properties of simulant materials

Simulants	CaO-B <sub>2</sub> O <sub>3</sub>	Glass	Corium
Composition	30:70 by weight (Non-eutectic)	Sodium Borosilicate	UO <sub>2</sub> + ZrO <sub>3</sub> mixture (80:20 by weight)
Melting point	977 °C	600-804 °C	2527 °C
Liquidus temperature	1027 °C	890 °C	2577 °C
Specific heat (C <sub>p</sub> )	1530 J kg <sup>-1</sup> K <sup>-1</sup>	750 J kg <sup>-1</sup> K <sup>-1</sup>	410 J kg <sup>-1</sup> K <sup>-1</sup>
Thermal diffusivity (α)	5.45 x 10 <sup>-7</sup> m <sup>2</sup> s <sup>-1</sup>	6.67 x 10 <sup>-7</sup> m <sup>2</sup> s <sup>-1</sup>	7.45 x 10 <sup>-7</sup> m <sup>2</sup> s <sup>-1</sup>

### 2.3. Large scale bottom flooding test facility

In order to study and understand the melt coolability under bottom flooding technique at actual reactor system, it was decided to build an engineering scale facility. It consisted of a cold crucible induction furnace as a melt generator. To account for relatively poor electrical conductivity of ceramics (simulant materials), induction melting requires high frequency for efficient heating. For this, a 200 kHz, 350 kW induction furnace was chosen.

#### 2.3.1. Design details

The schematic of the Large Scale Bottom Flooding Test Facility is shown in Figure 14. The test section consists of a 300 mm OD carbon steel pipe with 600 mm height. The capacity of test section is about 25 litres corresponding to melt height of 500 mm. The upper part of the test section has the capacity to contain a water pool up to 700 mm height.

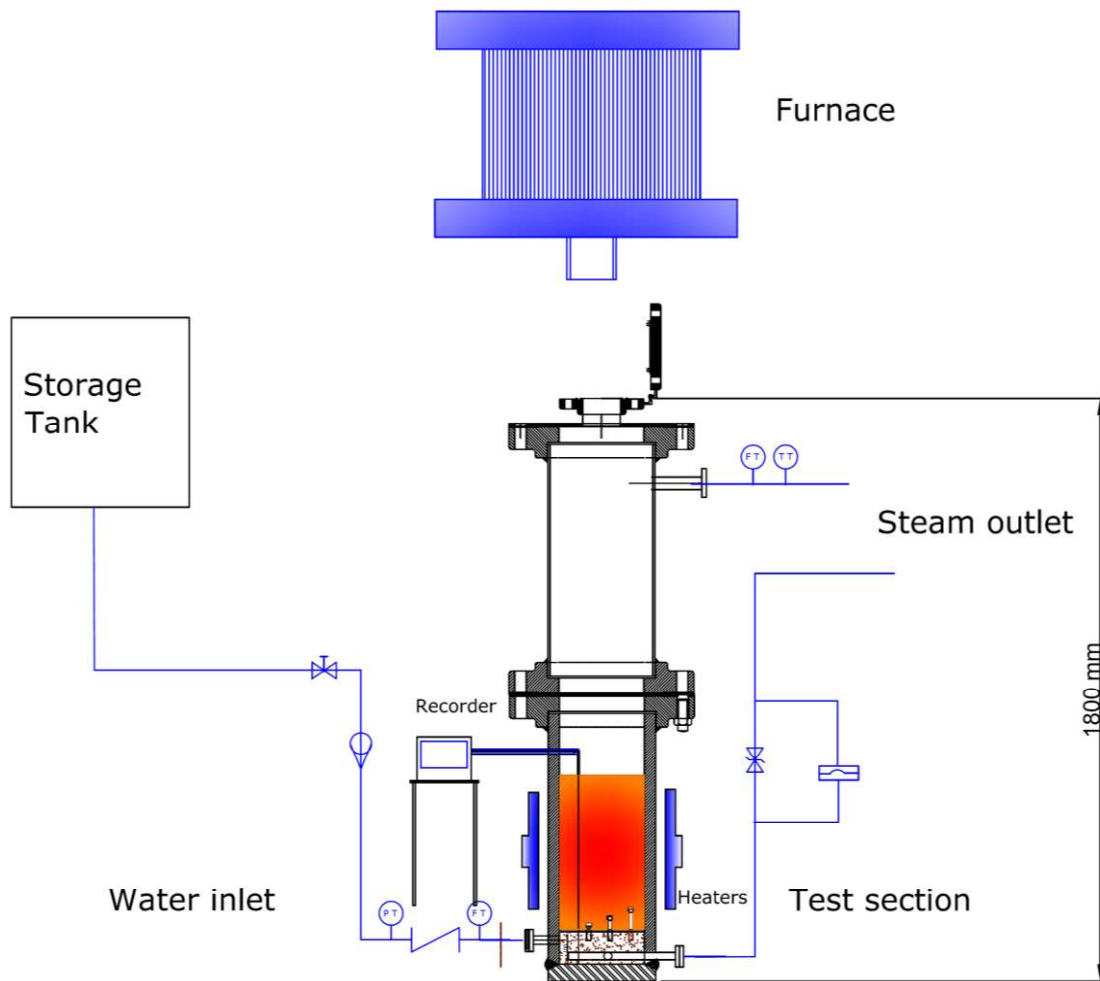
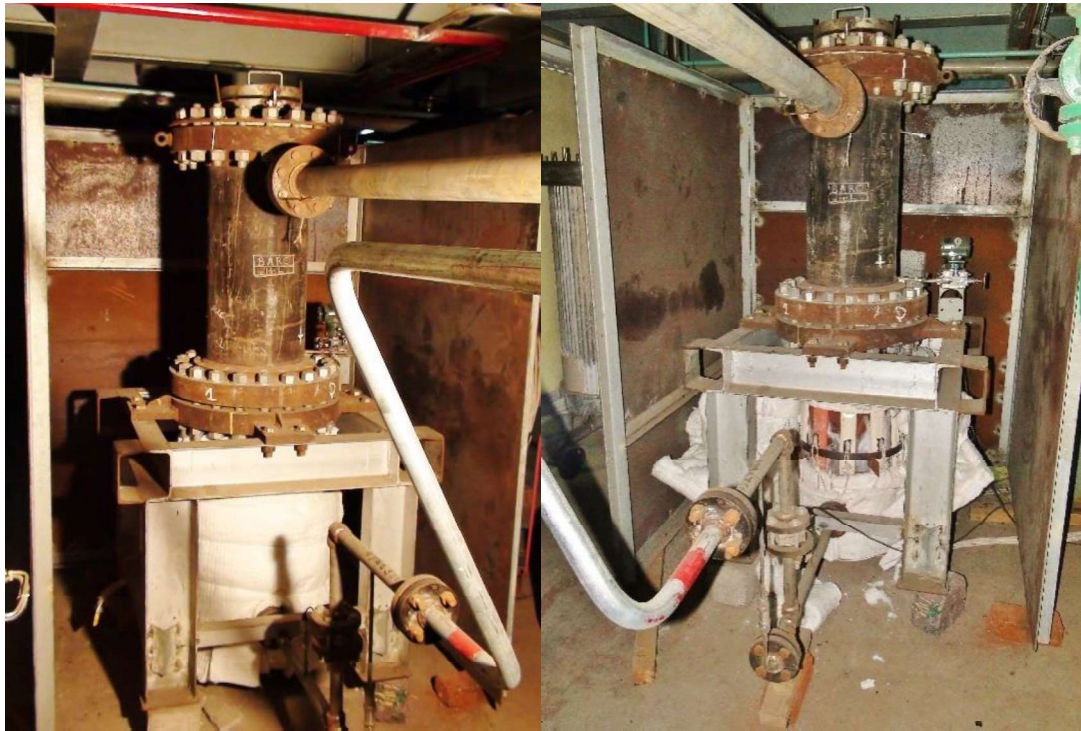


Figure 14: Schematic of the Large Scale Bottom Flooding Test Facility

At the bottom, a water distributor was provided to inject water to the melt pool. On the top of it, a plate having six nozzles of different heights was placed. Each nozzle was a 12 mm diameter SS tube. Water was fed through an overhead tank under gravity flow. The tank was placed at a height of nearly 15 m from the test section. An additional safety steam line was provided at the bottom to relieve the overpressure. Total 24 K-type thermocouples were used to map the temperatures profile of the melt pool. In addition, inlet water temperatures and temperature of outgoing steam were also measured by thermocouples in the

upper part of test section. The test section was insulated in lower part using ceramic wool as shown in Figure 15.



*Figure 15: Large Scale Bottom flooding test setup with heaters for decay heat simulation*

### 2.3.2. Instrumentation

The aim of these experiments is to generate sufficient data to understand the phenomenology behind the melt coolability under bottom flooding and use this data further for validation of mathematical model. Hence, adequate process instrumentation was provided in the facility, which includes:

- Temperature measurements: Temperature inside the melt pool was measured at 8 axial and 3 radial locations using 24 K-type thermocouples as shown in Figure 16.
- Flow rates: DPTs located at inlet and outlet line was used to measure water inlet and outgoing steam flow rate.

- Level transmitter: DPT fitted on the upper part of the test section was used to measure the water level inside the test section.
- Pressure measurements: The pressure gauge was used to monitor the gauge pressure at water inlet. The pressure history inside the test section was measured and recorded using the pressure transducer.
- Data acquisition system: All these measurements are recorded by a 48-channel hybrid multivariable recorder with a time span of 1s, which was installed at an appropriate distance from the test section.

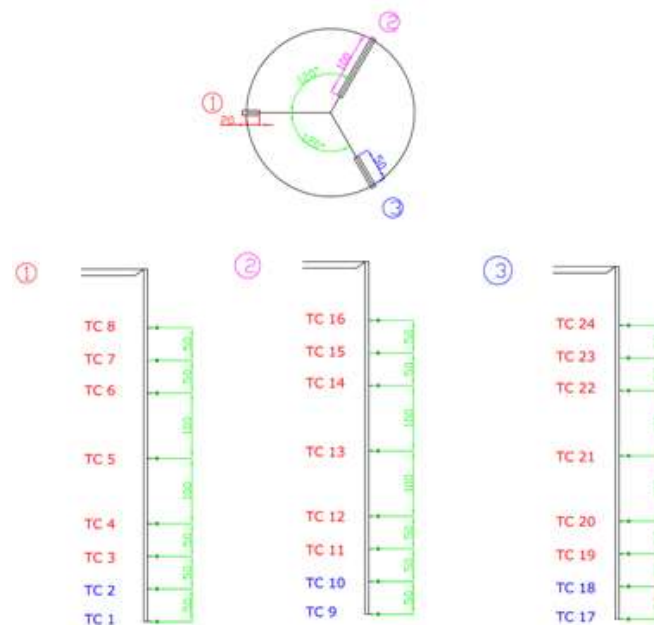


Figure 16: Thermocouples arrangement inside the setup for melt pool temperatures measurement

In all experiments conducted, the parameters measured and the instruments used for these measurements have been discussed in Table 3. It also discusses the uncertainty in the measured results.

Table 3: Accuracy of the measured values

Parameter	Instrument	Accuracy	Range
Temperature	'K' type thermocouples	$\pm 0.75\%$ of the measured values	0-1200 °C
Pressure	Pressure transducer	$\pm 0.35\%$ of the measured values	0-100 bar
Differential pressure	Differential pressure transmitters	$\pm 0.2\%$ of the measured values	0-1500 mmWC
Water level	Differential pressure transmitters	$\pm 0.2\%$ of the measured values	0-1000 mmWC



Figure 17: Actual site photograph of Small Scale Bottom Flooding Test Facility

## 2.4. Small scale bottom flooding test facility

In a large scale facility it is difficult to perform the parametric studies to understand the effects of nozzle diameter, inlet water velocities, melt eruption, etc. on the coolability of molten pool with bottom flooding. Thus, a series of small scale experiments were performed in a dedicated facility specially designed for studying the effects of various parameters on melt coolability under bottom flooding. Figure 17 shows the actual site photograph of the experimental facility. The facility included a resistive heating type furnace of power rating 6 kW, 415V and 32A using three phase power supply; housed within the closed area at upper floor of the facility. On the lower floor, the test section along with the expansion section was housed within the closed area. Outside of this closed two floored facility; the data acquisition system, furnace control system and the water inlet arrangement were placed at a safe distance. Nearby, an overhead tank was placed at a variable height of 7.5 m (maximum) above the ground. Steam outlet and safety relief outlet were directed outside of the building.

### 2.4.1. Design details

Figure 18 shows the schematic of the facility. The facility consists of a furnace for melting the simulants, a funnel arrangement to direct the melt into the test section, the test section to receive and cool the melt, input-output piping and various measuring instruments. The test section consisted of two parts viz. lower part to hold the melt and upper to allow steam to expand. The upper part of this test section is made of a DN 150 Sch 160 carbon steel pipe of 500 mm height. For the outlet of steam, a DN 40 line has been provided. This part was welded with a SS slide lock arrangement on top for closing the test section after the melt pouring. The lower part of the test section in which melt was used to be poured is similar to the upper part except for the internal arrangement of

nozzle to flood the water from bottom. Water used to be injected into the test section through a DN 15 CS water supply line, provided at the bottom of the test section. A relief line of DN 15 Sch 80 CS has been provided which is connected to two diverse parallel lines, one fitted with rupture disc (RD) and another with a relief valve (RV), as shown in Figure 18.

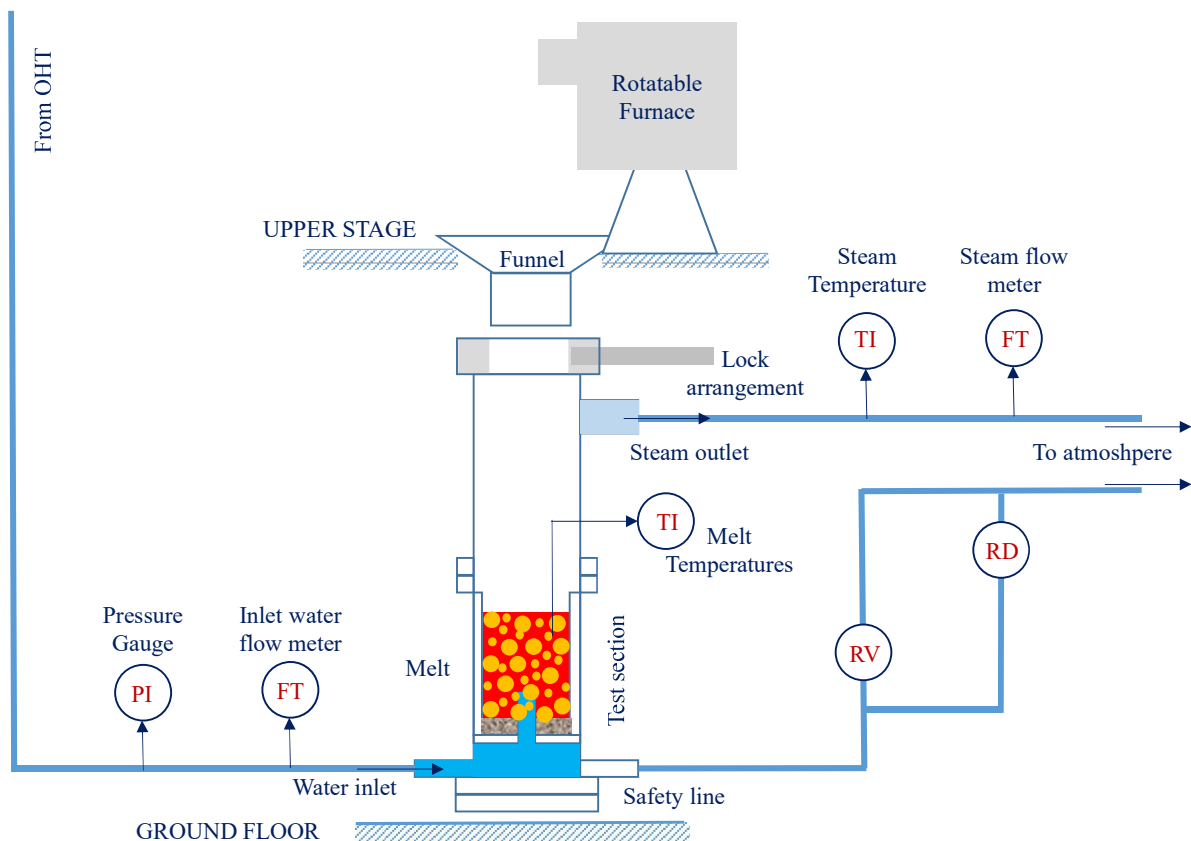


Figure 18: Schematic of Small Scale Bottom Flooding Test Facility

#### 2.4.2. Instrumentation

Adequate process instrumentation has been provided in the facility. The instrumentation for the experiment includes the below mentioned and the accuracy of the measurements are mentioned in Table 3.

- Temperature measurements: Temperatures inside the melt pool were measured at different locations using 18 K-type thermocouples. They were

arranged radially at central, half radius and near wall locations at 120° to each other, covering 300 mm melt bed by axially placed at 6 locations, each at 50 mm height to another; as shown in Figure 19.

- Flow rates: DPTs located at inlet and outlet line were used to measure water inlet and outgoing steam flow rate.
- Level transmitter: DPT fitted on the test section was used to measure the water level inside the test section.
- Pressure measurements: The pressure gauge was used to monitor the gauge pressure at the water inlet.

Data acquisition system: All these measurements are recorded by a 48-channel hybrid multivariable recorder with a time span of 1s.

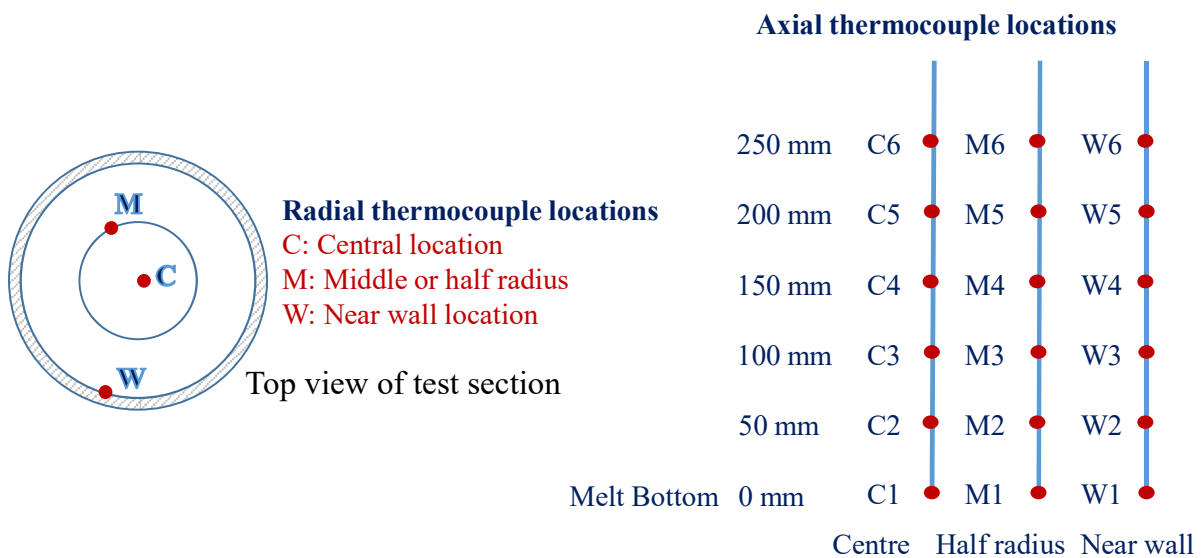


Figure 19: Thermocouples arrangement inside the test section of Small Scale Bottom

Flooding Test Facility

## 2.5. FCI test facility

### 2.5.1. Design details

Experiments were performed in two different set-ups for the small and large amount of the melt volumes.

The first set-up consisted of a small induction melt generator attached to the test section. CaO-B<sub>2</sub>O<sub>3</sub> mixture was melted in the induction furnace and was poured into the test section using specially designed fast acting valve arrangements. The test section was a steel vessel with transparent observation window. The test section was of 6 litres water capacity (150mm x 150mm x 300mm) as shown in Figure 20. It was instrumented with a piezoelectric dynamic pressure transducer (Make: PCB, model – 101A05, S/N 6449) to record the dynamic pressure within the water pool. To measure the temperatures of water pool, k-type thermocouples were used.

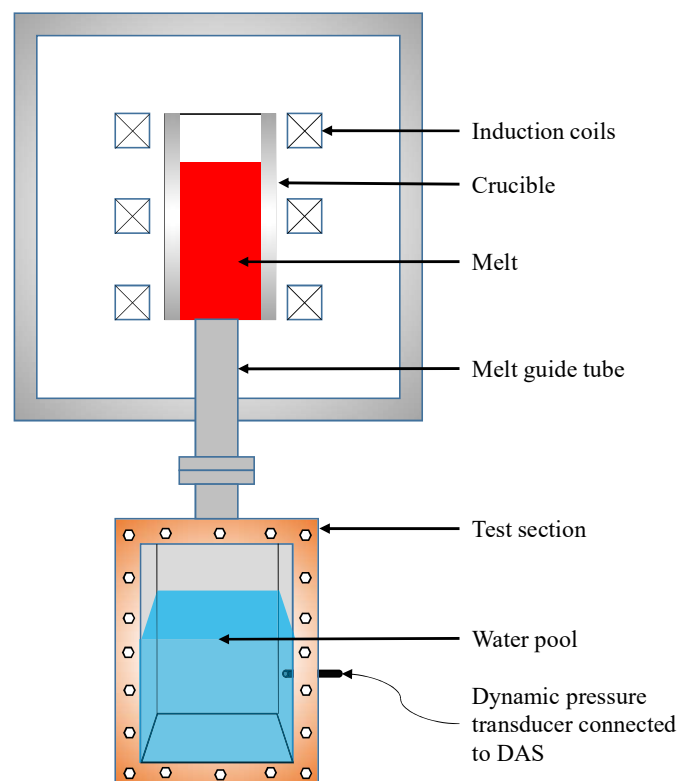


Figure 20: Test section for conducting small melt volume experiments (schematic)

The second set-up for large melt volumes consisted of the furnace and the test section of 12 litres water capacity. The melt was generated in the furnace and poured into the test section. The test section was a steel vessel of 130 mm diameter and 500 mm height as shown in Figure 21. It was instrumented with a piezoelectric pressure transducer to record the dynamic pressure and with k-type thermocouples to measure the temperatures within the water pool.

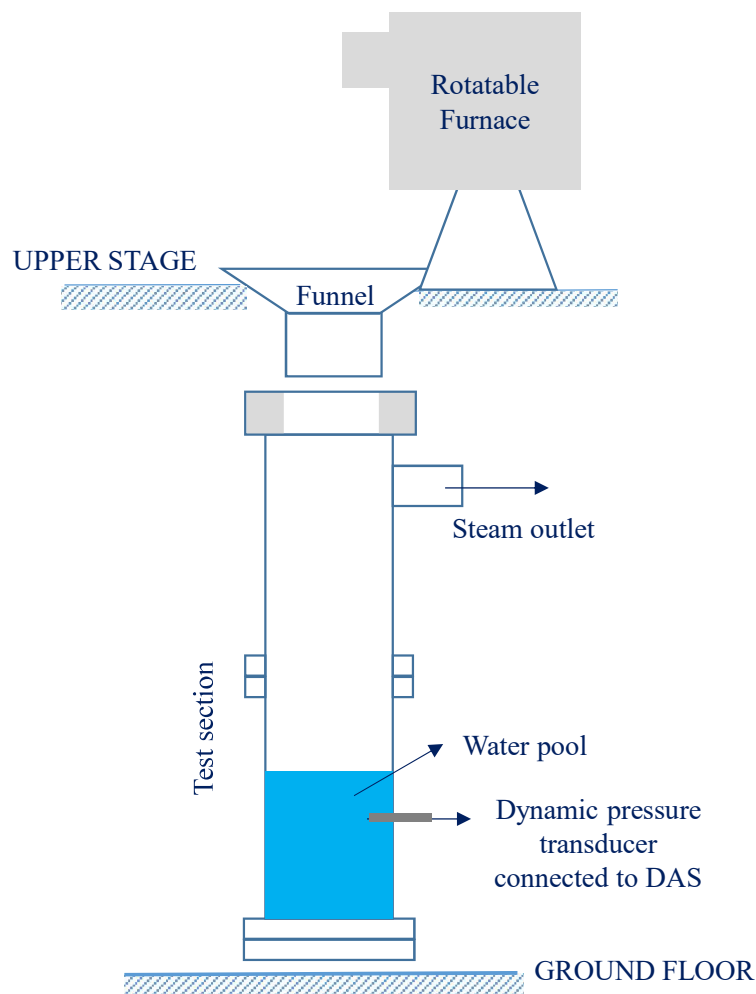


Figure 21: Test section for large melt volume FCI experiments (schematic)

## 2.6. Summary

Dedicated experimental programme to address each unresolved issues as discussed in chapter one, has been developed and experiments are planned in these state-of-the-art engineering scale facilities. To perform these experiments, simulants materials

(Sodium borosilicate glass and CaO-B<sub>2</sub>O<sub>3</sub>) were used which have thermal properties similar to that of corium.

- a) To study the influence of decay heat on melt coolability under bottom flooding, the experiments were performed with 25 litres of melt in a test section of 500 mm height and 300 mm diameter. The temperatures profile were recorded using 24 k-type thermocouples arranged in three radial and eight axial locations.
- b) To study the scalability and influence of geometrical parameters on melt coolability under bottom flooding, small scale test facility was used. It has the test section of 500 mm height and 130 mm diameter. The temperatures profile was mapped using 18 k-type thermocouples arranged in three radial and six axial locations.
- c) Fuel-coolant interaction was studied in two separate test sections of capacities 6 litres and 12 litres and both fitted with piezoelectric dynamic pressure transducers to measure dynamic pressure spike.

Results and insights obtained from these experiments have been discussed in the following chapter.



# Chapter

*“Observation is a passive science,  
experimentation an active science”*

— *Claude Bernard (12 July 1813 – 10 February 1878)*  
*French physiologist and historian*



## **Chapter 3. INFLUENCE OF DECAY HEAT ON MELT COOLABILITY UNDER BOTTOM FLOODING**

### **3.1. Introduction**

In spite of the various studies, the literature lacks the fundamental understanding of the effect of decay heat on melt coolability. This section presents experimental study on influence of decay heat on melt coolability under bottom flooding. Two experiments, i.e. one without decay heat and another with decay heat, were conducted in Large Scale Bottom Flooding Test Facility as discussed in chapter two. About 20 litres of borosilicate glass melt at initial temperature of nearly 1200°C was used as melt simulant in both the cases. To simulate the decay heat, 10 radiative heaters were used to directly heat the melt pool from outside. In both the cases, water was injected into the melt pool by using nozzles located at the bottom of the melt pool. The temperatures profile in both the cases were measured and recorded. Post-test debris were examined for their sizes and porosities formed during the experiment. The results of the experiment with decay heat were then compared with the experiment without decay heat, to understand the influence of decay heat on melt coolability under bottom flooding.

### **3.2. Experiment without decay heat**

#### **3.2.1. Test facility**

This experiment was performed in the large scale test facility as discussed in section 2.3 of chapter 2. The test section consists of a 300 mm OD carbon steel pipe with 600 mm height. The capacity of test section is about 25 litres corresponding to melt height of 500 mm. The upper part of the test section has the capacity to contain a water pool up to 700 mm height. About 20 litres of

Sodium borosilicate melt at 1200°C was poured into the test section of 500 mm height and 300 mm diameter as shown in Figure 14.

### 3.2.2. Operating procedure

Sodium borosilicate glass was first melted in a cold crucible induction furnace. On account of relatively poor electrical conductivity, induction melting of glass requires high frequency for efficient heating. For this, a 200 kHz, 350 kW induction furnace was chosen. The glass was melted and the melt temperature was raised up to 1200 °C. The experimental setup was placed below the furnace and the melt was delivered in the test section by opening a solenoid valve below the furnace. After pouring was completed, the top flange of the test section was remotely closed which had an automatic locking arrangement. After the flange was closed, water was flooded from overhead tank by opening the inlet valve. Water through the nozzles was injected directly into the melt. Water supply was stopped when the level in the upper part of the test section showed 100% mark. The transient temperature history inside the melt was recorded till the entire melt reached room temperature.

### 3.2.3. Results and discussion

After the water supply was started, within a few seconds, a large amount of steam was seen coming out of the discharge line. Within few minutes, most of the thermocouples showed saturation temperature indicating complete quenching. Water supply was stopped when the level in the upper part of the test section showed 100% mark. Figure 22 shows the temperatures in the central region, Figure 23 shows the temperatures in the half radius region and Figure 24 shows temperatures near wall region. It took some more time to cool the melt

near wall region as compared to that in the central region. The average melt quenching time in this experiments was found to be 93s.

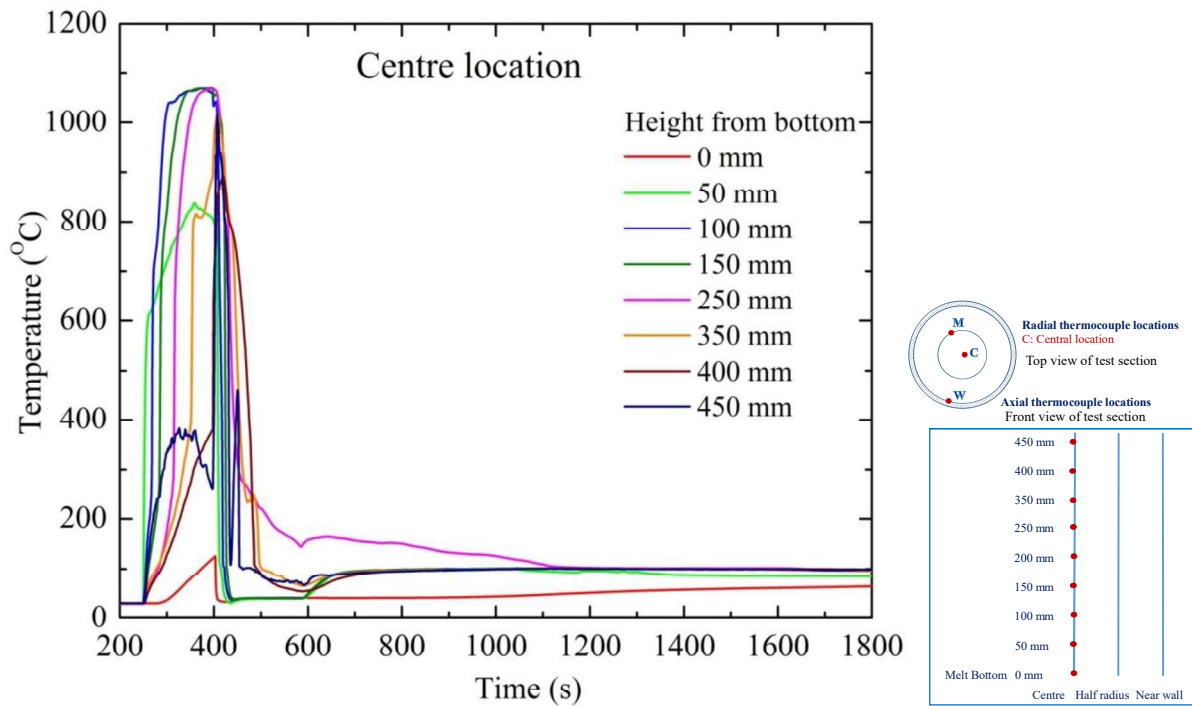


Figure 22: Measured temperatures at central location

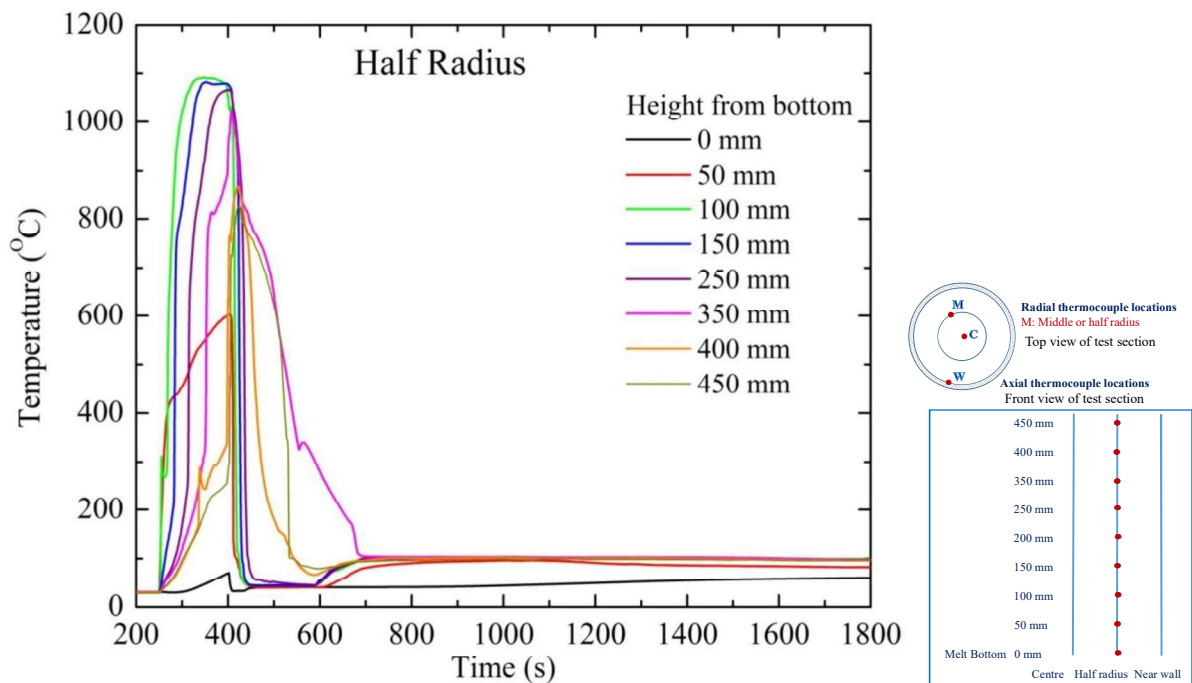


Figure 23: Measured temperatures at half radius

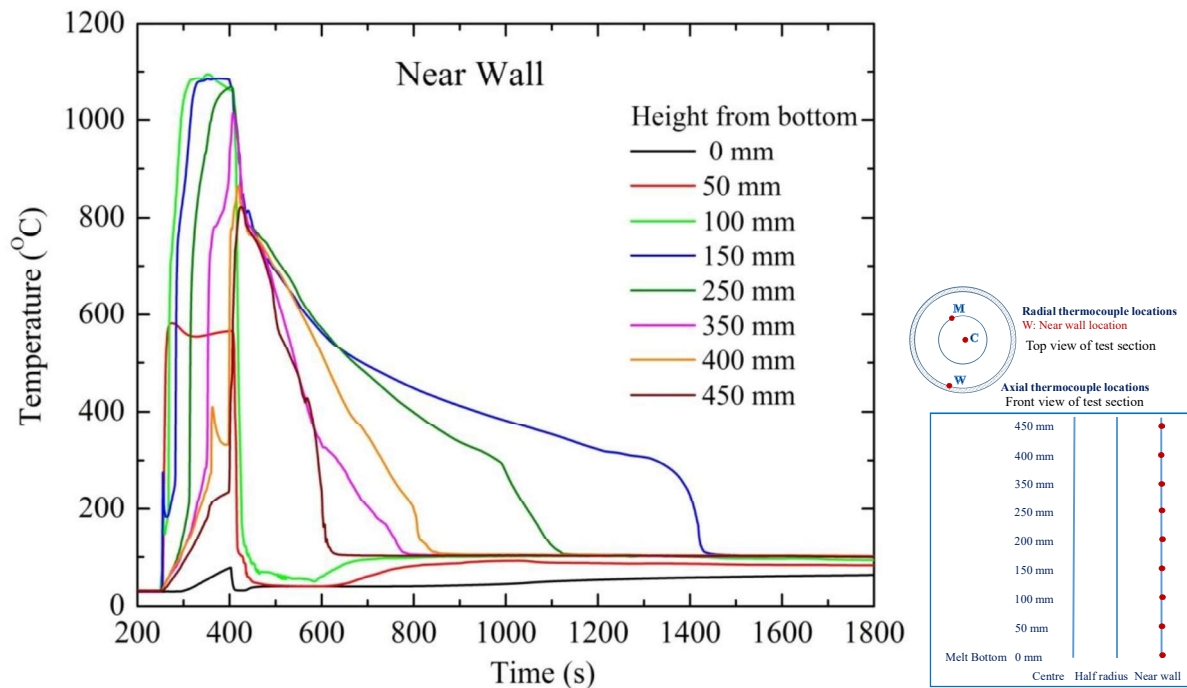


Figure 24: Measured temperatures near wall

After the experiment was completed, the section was opened. It was observed that, the melt was converted into a large porous mass as shown in Figure 25, which rose to double its initial height. The porous mass had crumbled into debris at one location. The debris consisted of particle sizes ranging from very fine particles to 10 mm size chunks. Numerous Pele's hairs were observed with thickness ranged from a few microns to a millimetre (marked with arrows on Figure 25). They covered entire top surface of the debris and can be seen golden in colour. The measured average porosity was 51%.

The experiment showed that,

- With bottom flooding, the steam formation (as shown in Figure 26) and water backpressure below the melt causes steam eruption through the melt which induces porosity inside the otherwise impervious melt. Fine particles formed during the experiment increased the interfacial heat transfer area by many folds.



Figure 25: Porous mass and debris size in bottom flooding experiment

- Subsequently, the heat transfer between melt and water was so rapid and nearly instantaneous. It took only a few minutes to quench the melt to room temperature which otherwise took several hours as compared to top flooding experiments[97].
- Figure 22 shows the rapid melt quenching in the central melt region possibly due to an eruption. The measurement at 0 mm is less than 200°C because the thermocouple was placed below the melt within the porous bed. Being an eruption site, entire melt within this region got quenched within a few minutes.
- Figure 23 shows the measurements at half radius inside the test section. The measurements at heights 400, 450 and 350 mm respectively took a little longer time to get cooled compared to lower locations.

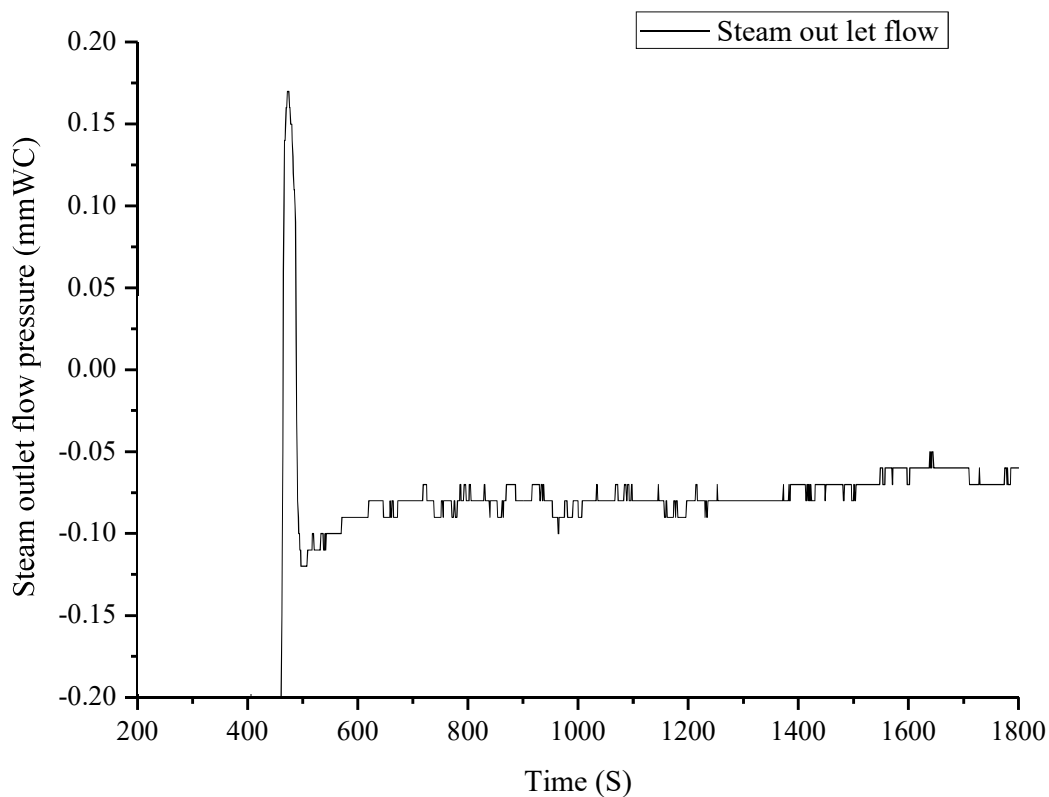


Figure 26: Steam flow measurement in without decay heat experiment

- Figure 24 shows the measurements near the inner wall of the test section during the experiment. Measurements at heights 450, 350, 400, 250 and 150 mm respectively have shown delayed cooling rate (in ascending order) as compared to the lower ones. This also indicates that the middle region took longer time as compared to lower and upper part of the melt. This may be due to the formation of packed debris bed after the eruption at central location which delayed the further cooling of debris.

### 3.3. Experiment with decay heat

#### 3.3.1. Test facility

This experiment was also conducted in the same large scale test facility as discussed in section 2.3 of chapter 2. Similar to previous experiment without decay heat, about 20 litres of Sodium borosilicate melt at 1200°C was poured into the test section of 500 mm height and 300 mm diameter as shown in Figure 14. To simulate decay heat 10 radiative heaters of 2kW each were used and put outside the test section periphery as shown in Figure 15. These heaters imparted 20kW power to simulate the decay heat of 0.5 MW/m<sup>3</sup>, which is equivalent to the decay heat considered in the actual reactor scenario when corium reaches into the core catcher.

#### 3.3.2. Operating procedure

The lower part of the test section was preheated to 550 °C by using the radiative heaters before the melt was poured and kept 'ON' during the melt quenching. Sodium borosilicate glass was first melted in the same furnace and the melt temperature was raised to 1200 °C. The experimental setup was placed below the furnace and the melt was delivered in the test section by opening a solenoid valve below the furnace. After pouring was completed, the top flange of the test

section was remotely closed which had an automatic locking arrangement. After the flange was closed, water was flooded from overhead tank by opening the inlet valve. The heaters were kept ‘ON’ throughout the experiment. Water was injected directly into the melt through the nozzles of 12 mm in diameter, which were located inside the melt. In this case, it was observed that the melt was quenched within a few minutes. Water supply and heating were continued till the temperatures inside the test section reached saturation temperature. The transient temperature history inside the melt pool was recorded till all temperatures achieved saturation level.

### 3.3.3. Results and discussion

Once water supply was fed from the bottom, a lot of steam (as shown in Figure 27) was observed coming out of the steam outlet similar to that without decay heat simulation.

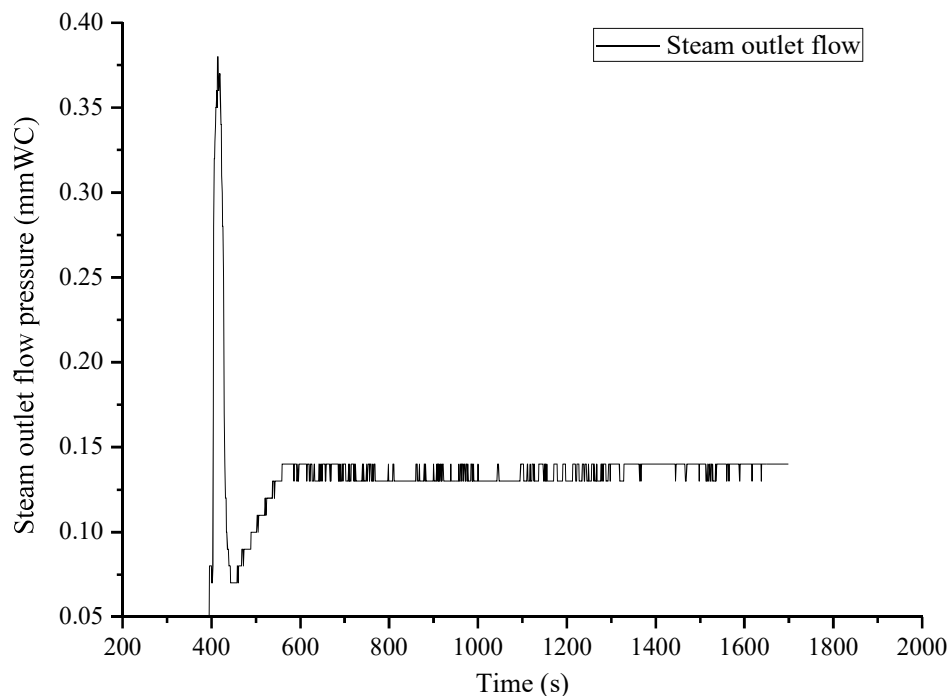


Figure 27: Steam flow measurement in the experiment with decay heat

Within a few minutes, most of the temperature measurements inside the melt pool reached saturation temperature indicating complete quenching. Figure 28 shows the temperatures in the central region. All thermocouples show that the overall quenching in this region took place within a few minutes. The measurements at different melt heights showed that the bottom portion was cooled later as compared to other regions. Figure 29 shows temperatures at the half radius location. In this case, the mid-height region was found to have delayed cooling as compared to top and bottom region.

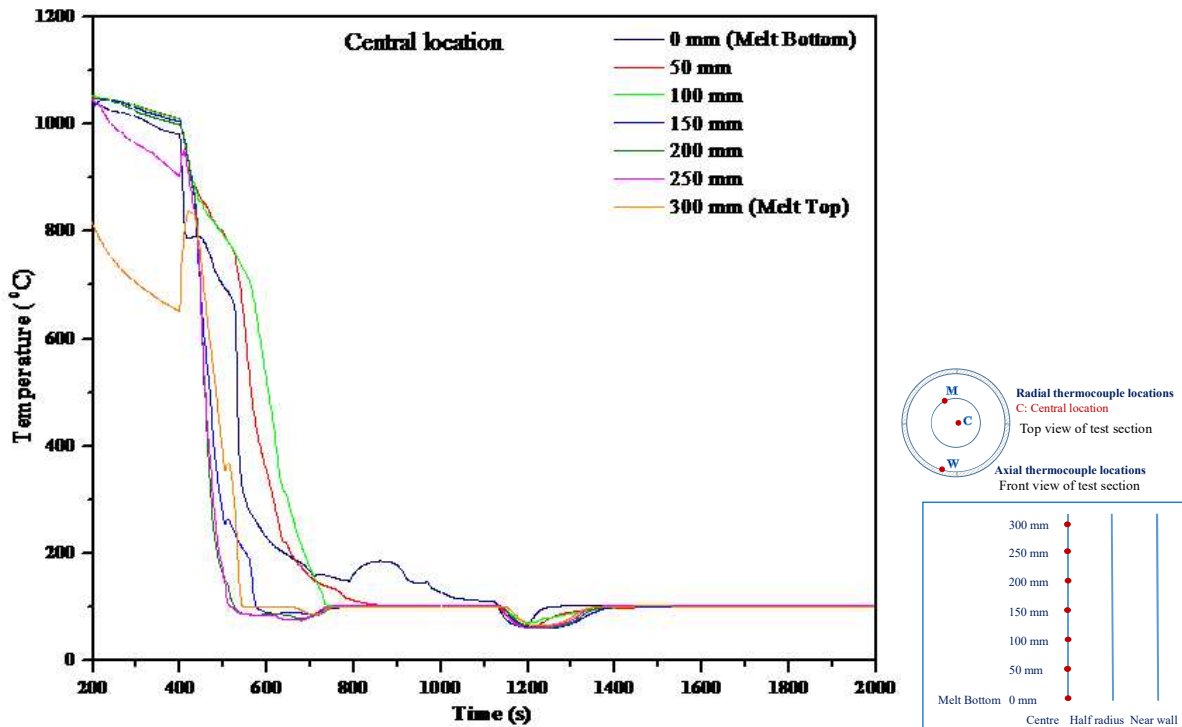


Figure 28: Measured temperatures at central location of the test section

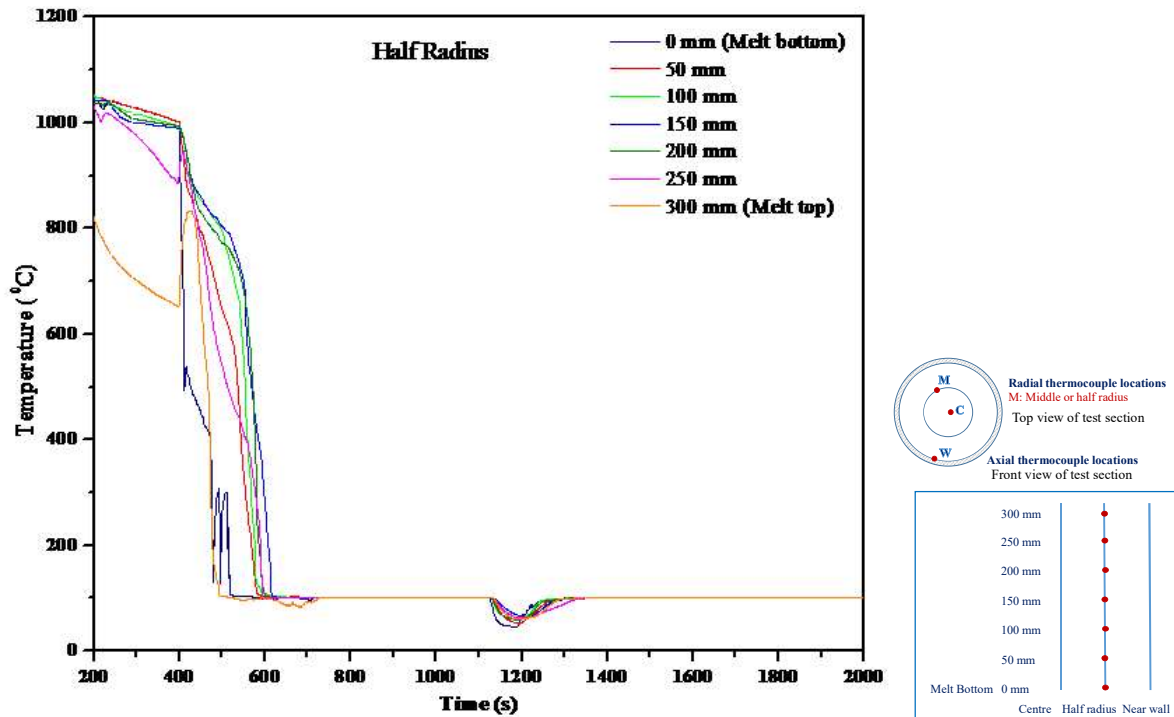


Figure 29: Measured temperatures at Half Radius of the test section

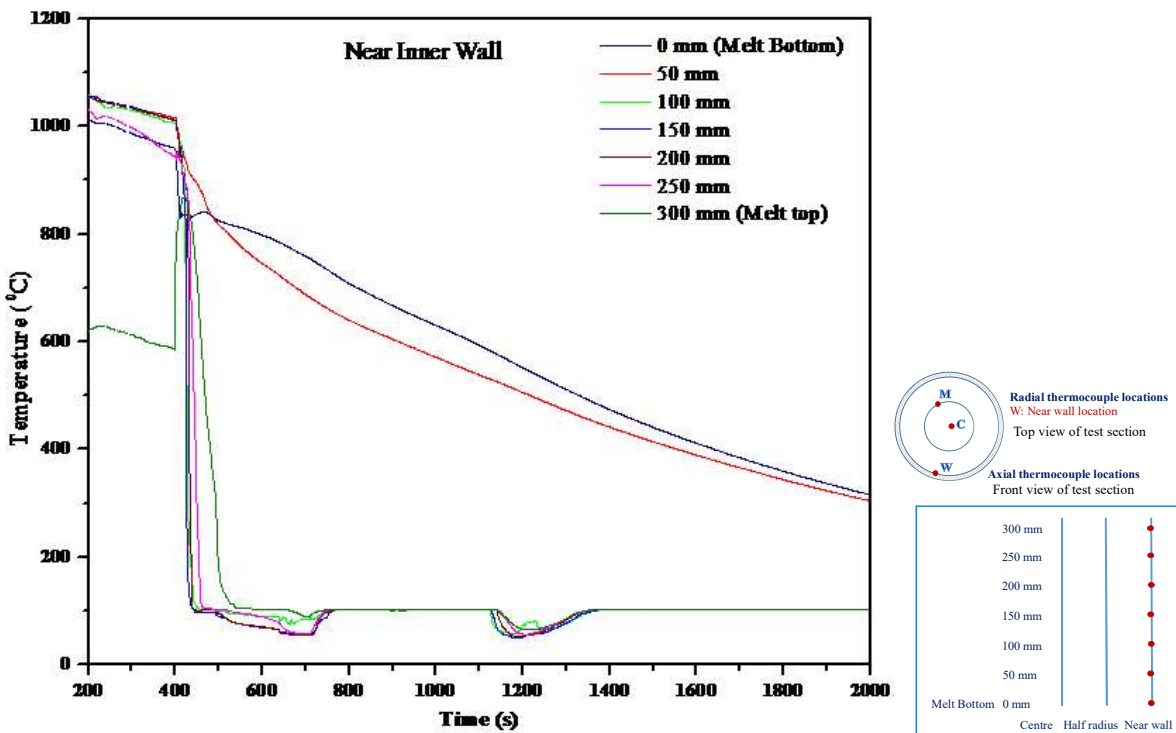
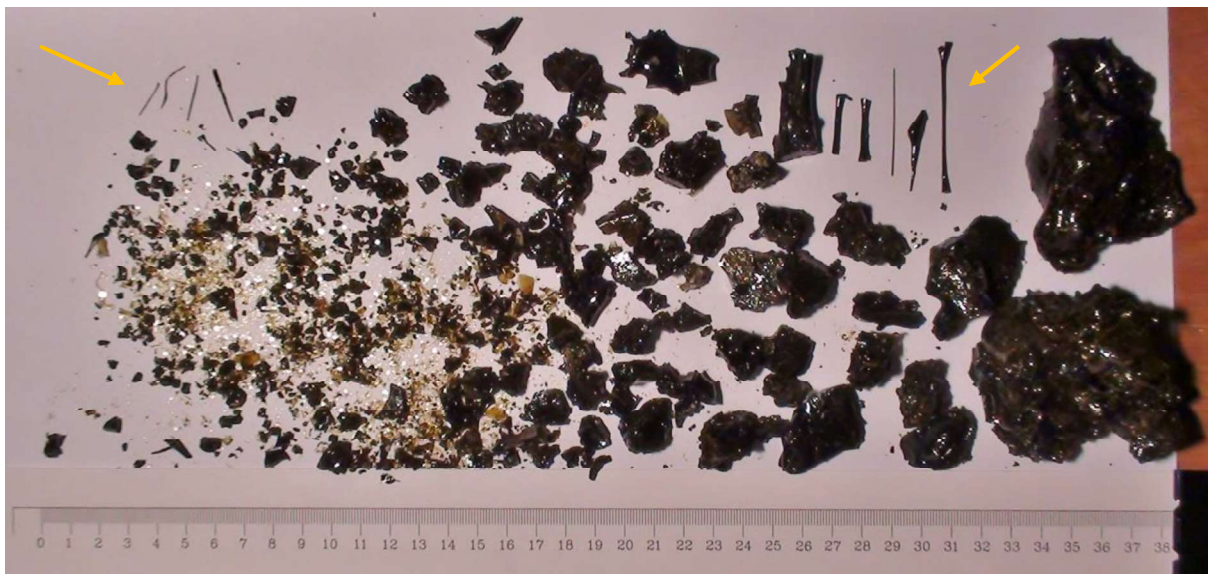


Figure 30: Measured temperatures near inner wall of the test section

Figure 30 shows temperatures near inner wall of the test section. Except for the two thermocouples, which were below the nozzle opening, all thermocouples

showed a rapid melt quenching. These two measurements imply that they were outside the eruption zone, and hence cooled by top flooding only; thus delayed cooling was observed. Also, since decay heat was imparted to it from the sides of test section walls, this solidified melt took such a long time to get cooled as the effective heat transfer mode was conduction only. In this case, the melt got delayed cooling at the bottom as compared to other regions. The average melt quenching time in this experiments was found to be 96s, which is of similar order as it was in the earlier case without decay heat.

After the experiment was completed, the section was opened. It was observed that, the melt was converted into a large porous mass as shown Figure 31, which was similar to earlier case. However, in this case, the debris formed during the experiment consists of particles of size ranging from 0.5 to 50 mm sized porous chunks as shown in Figure 31. The hairs like strands known as “Pele’s hair”[98] (marked with yellow arrows in Figure 31) were also obtained of diameters ranging from few microns to 3 mm. Although, these particles were so fragile that their recovery from the debris was itself challenging. Still, many of them were recovered. Existence of such particles shows the high shear interaction between steam and melt. The measured average porosity was 67%. The overall temperature profile shows that melt erupted on the insertion of water from bottom, forming the highly porous path for water and steam to pass through. The quenching was, thus, rapid and nearly instantaneous except for the location where melt stuck below the nozzle openings. The entire melt reached to the saturation temperature within 15-20 minutes.



*Figure 31: Porous mass and debris size in bottom flooding with Decay heat experiment*

### 3.4. Comparative analysis

Considering water insertion time as the initial time (shown in Figure 32), the quenching time and debris cooling time under bottom flooding for both with and without decay heat were calculated.

### Melt coolability under bottom flooding Temperature vs time characteristic curve

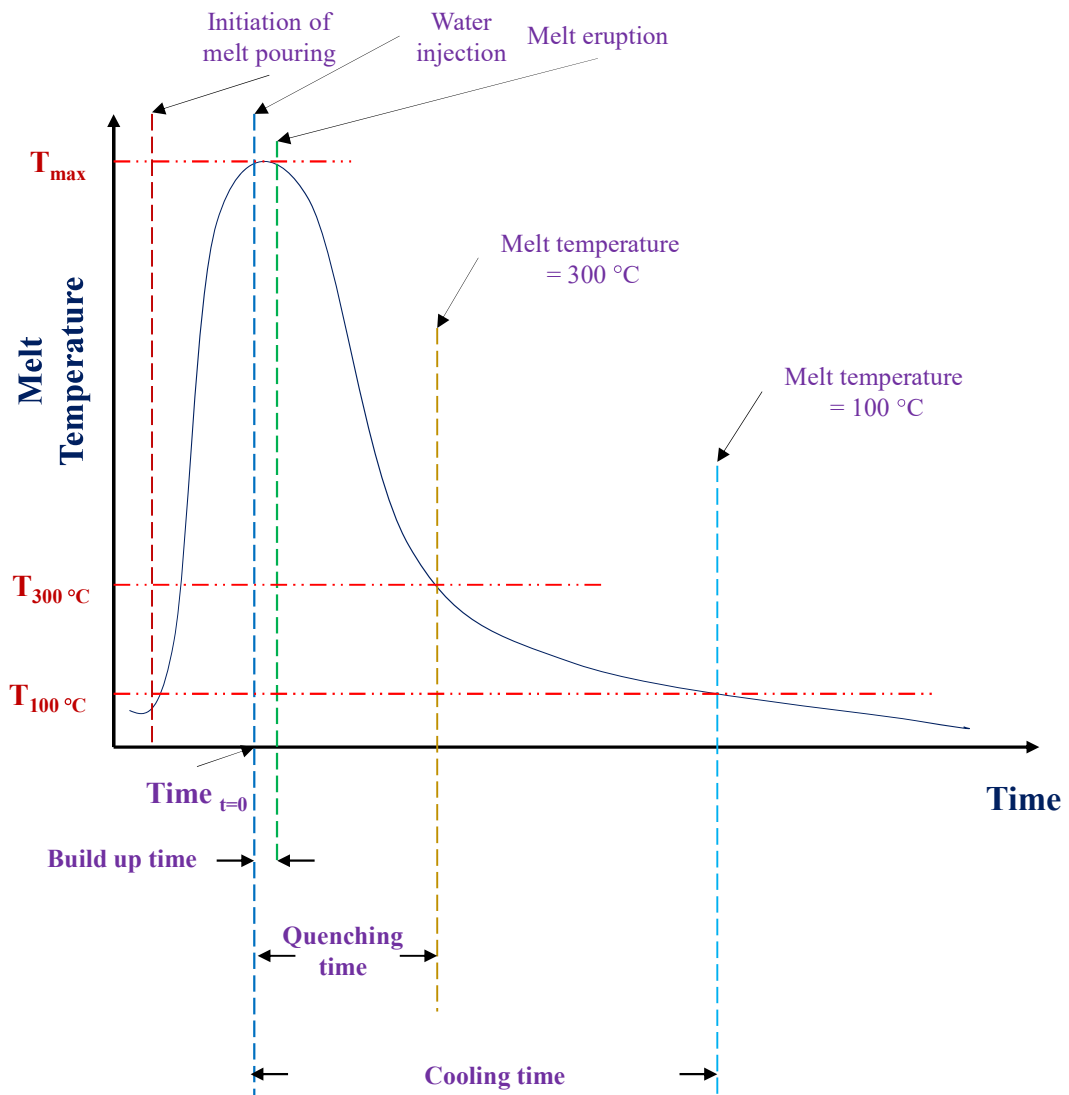


Figure 32: Temperature vs. Time characteristics curve for melt coolability under bottom flooding

The quenching time taken by the melt pool to reach 300°C under bottom flooding for both with and without decay heat scenarios is found to be nearly similar, as shown in Figure 33.

Once quenching is done, only porous debris are left to be cooled. The cooling time taken by the debris to reach saturation temperature under bottom flooding was found to be more with decay heat as compared to without decay heat, as shown in Figure 34.

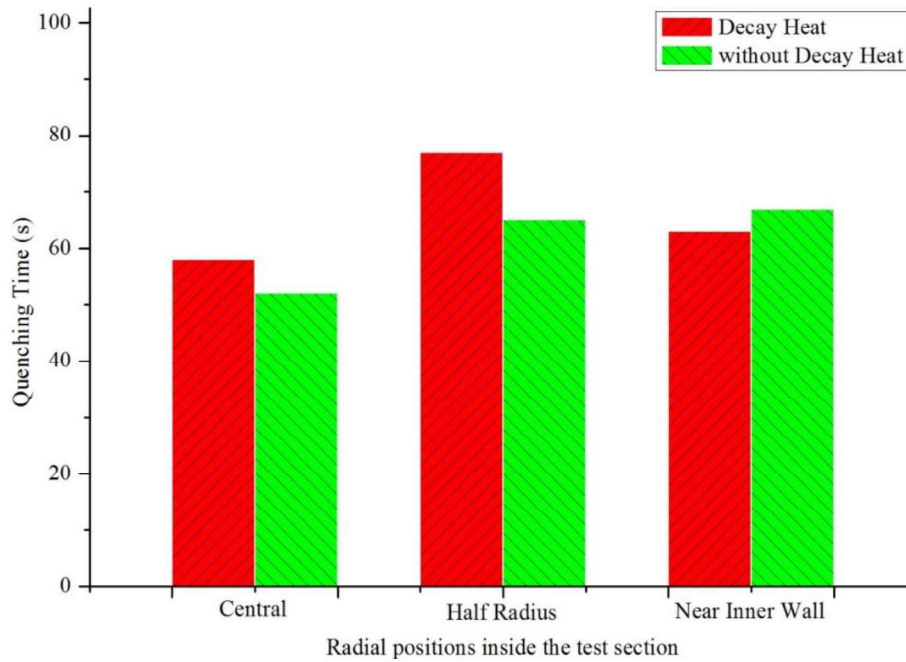


Figure 33: Average quenching time taken by the melt pool to reach 300°C temperature under bottom flooding with and without decay heat

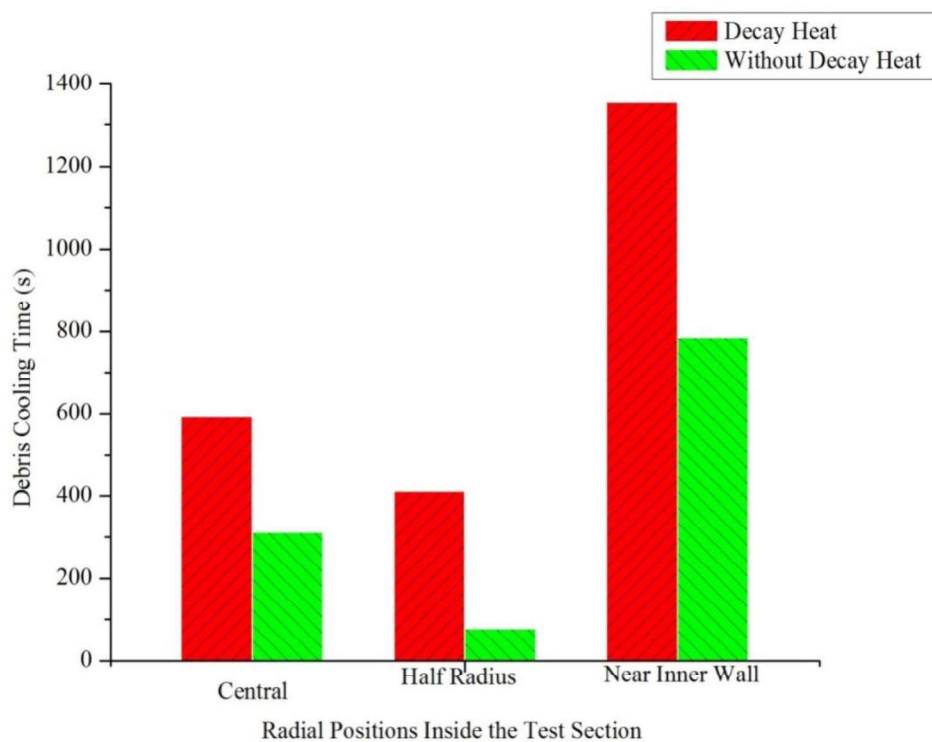


Figure 34: Average cooling time taken by the melt pool to reach saturation temperature under bottom flooding with and without decay heat

The trend of quenching in both the experiments is almost similar. This behaviour certainly implies that the quenching of melt takes place due to rapid heat transfer because of the porous debris formed due to melt eruption.

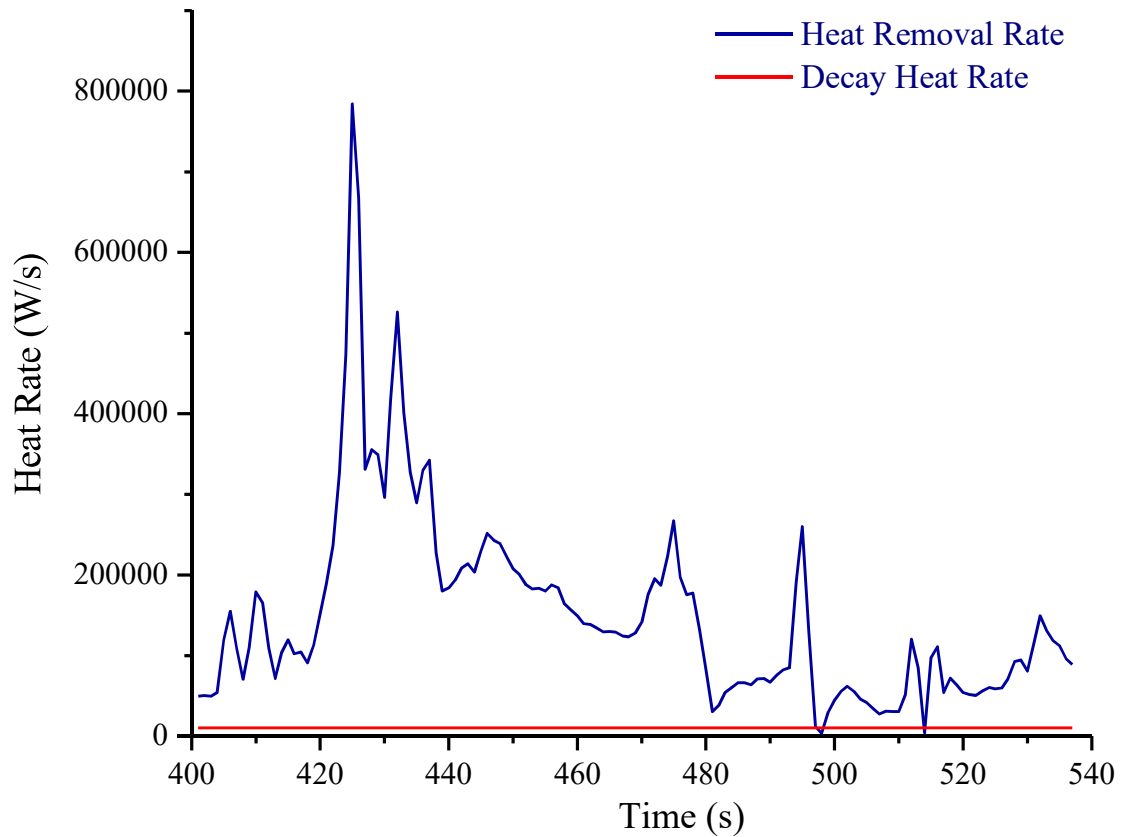


Figure 35: Rates of heat removal and decay heat addition during melt quenching

This can be further explained as, during melt eruption debris formed which in turn substantially increases the interfacial area. Due to high interfacial area, more water is available per unit of debris surface. Since there is a high temperature difference between debris temperature and the available water temperature, the boiling of water occurs and thus formed steam takes away the heat within a few minutes. This process is taking place simultaneously among all debris-water system formed during the melt eruption. Hence, the rate of decay heat imparted is significantly less than the rate of heat removal as shown in Figure 35. The initial large peak shows the melt eruption, which removes significant amount of heat while converting melt into debris.

Thus, these experiments show that decay heat has a role in delaying the cooling of debris formed but insignificant effect on quenching of the melt pool.

#### 3.4.1. Quench-front Analysis

##### a) Experiment without decay heat

The temperature contours for without decay heat, were plotted by taking melt height on y-axis and test section radius on x-axis as shown in Figure 36. Time  $t=0s$  was defined when the melt pouring was completed and melt pool was ready for water insertion. At  $t=33s$ , the water was inserted from the bottom which can be seen in the figure. At  $t=36s$  and  $t=48s$ , the melt front appears to move progressively as indicated by quenching. At  $t=62s$ , the melt eruption appears to have started as indicated by sudden quenching in a localised position. Due to the opening and the porosity created within the melt, the debris got cooled within a few minutes. At  $t=651s$ , almost entire melt was cooled. Without decay heat, a perfect quench front was observed during the melt eruption and cooling.

##### b) Experiment with decay heat

Similar temperature contours were also plotted with decay heat as shown in Figure 37. At  $t=0s$ , melt pouring was completed. The melt was in molten state due to decay heat supplied to it. At  $t=243s$ , the water was inserted from the bottom. At  $t=253s$ , the melt eruption appears to have started at half radius indicated by rapid quenching. At  $t=263s$  and  $t=283s$ , progression of cooling of the melt can easily be observed. This further followed by the cooling of debris due porosity formed within the melt. At  $t=1993s$ , almost entire melt was cooled. In this scenario, no perfect quench front was observed during the melt eruption and cooling.

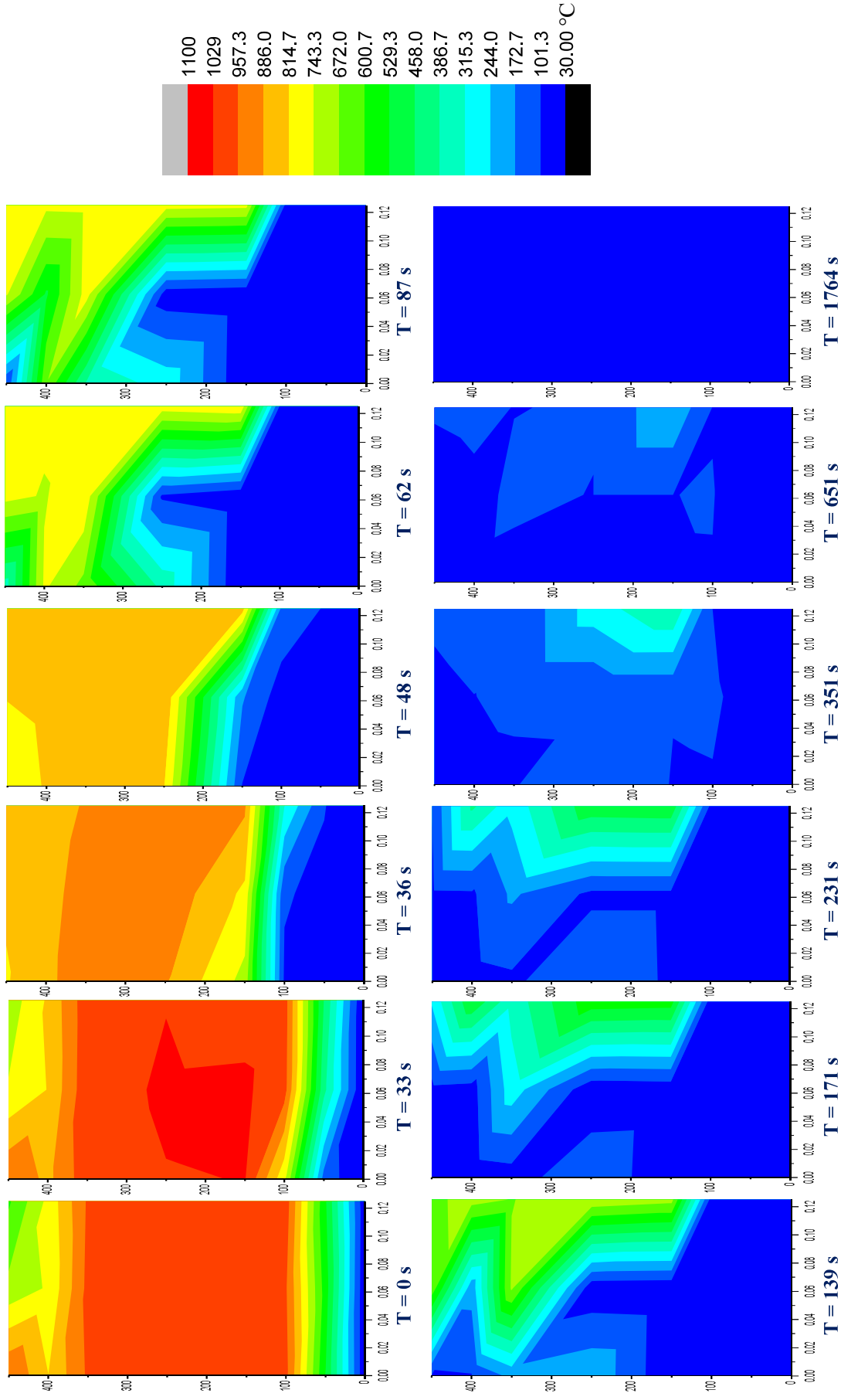


Figure 36: Temperature contour plots for the bottom flooding without decay heat experiment

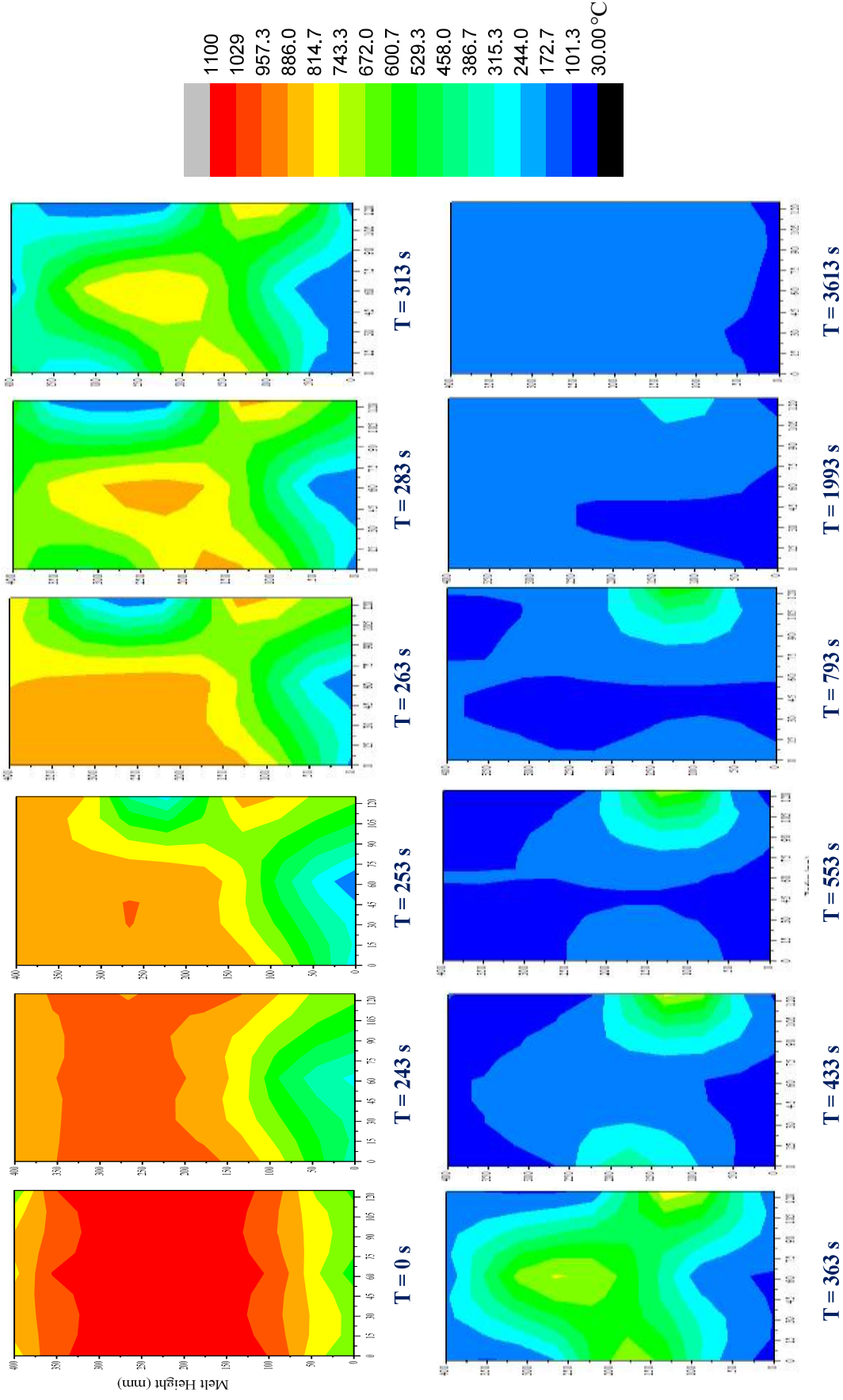


Figure 37: Temperature contour plots for the bottom flooding with decay heat experiment

This resulted in intermingling of coolant within the melt and such a rapid and conjugate heat transfer took place.

#### 3.4.2. Debris comparison

Figure 38 and Figure 39 show the post experiment debris formed without and with decay heat scenarios. The visual analysis of the debris shows that fine debris formed without decay heat leading to more packing and hence less porosity compared to decay heat case. Also, the Pele's hair particles (marked with arrows) were much large in number and were of micron range. Such a fine hairs like structure proves the strength of eruption was higher without decay heat. The larger particles sizes with decay heat are also due to the same fact.

#### 3.5. Summary

To understand the influence of decay heat on coolability of molten corium under bottom flooding, experiments were performed, without decay heat and with decay heat, using Sodium borosilicate glass under similar initial conditions. To simulate the decay heat radiative heaters were used to heat the molten pool.

Both the experiments have shown that the quenching of melt occurred nearly at the same time. Thus it can be concluded that decay heat has insignificant effect on melt quenching under bottom flooding conditions. However, cooling of debris to reach saturation temperature took longer time in presence of decay heat compared to stored heat case.

The quench-front analyses in both the cases showed that the due to steam pressurisation below the melt, melt erupts to form inverted conical like porous zone. This was evident in both the cases.

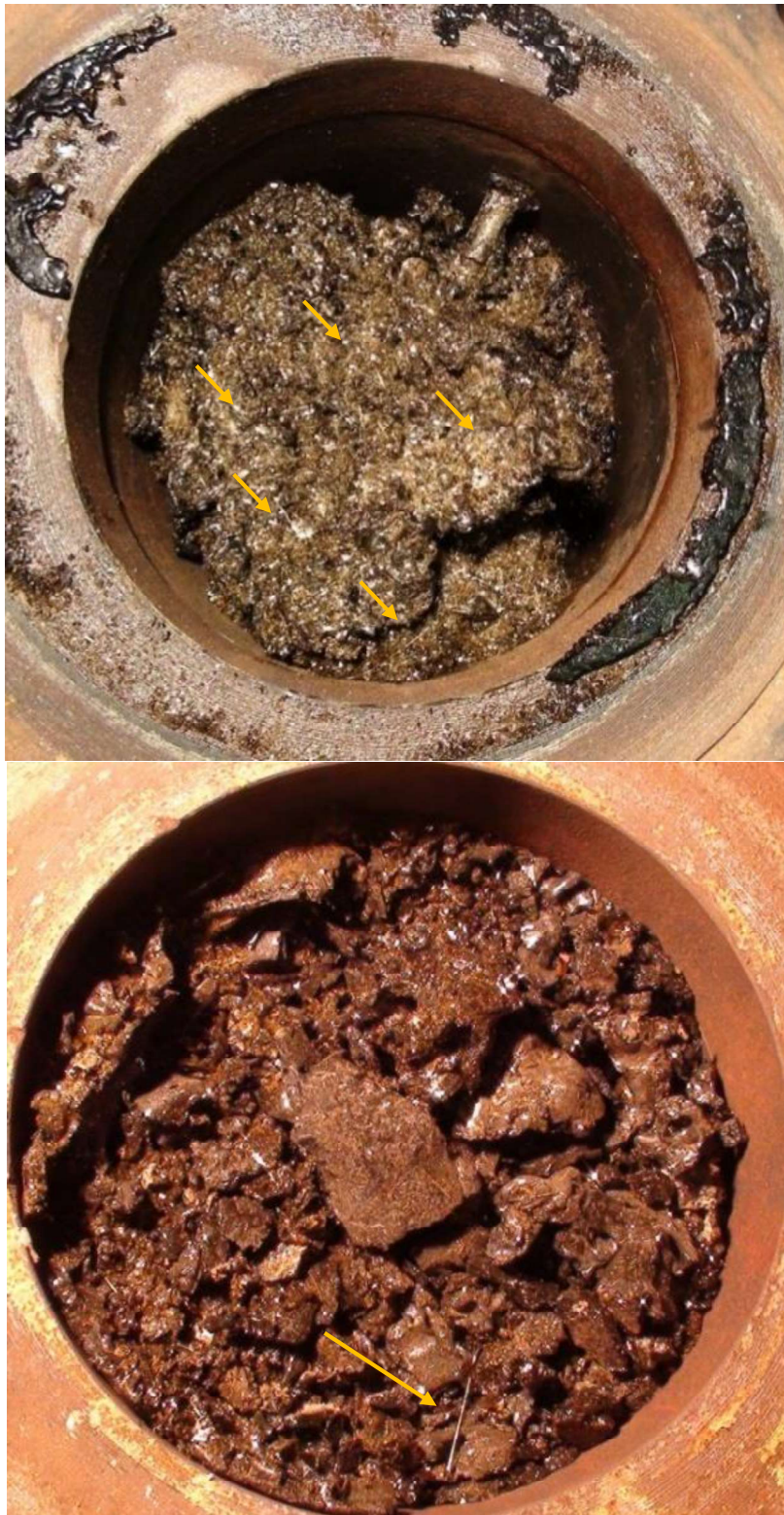


Figure 38: Post experiment debris just after opening the test section without (a) and with (b) decay heat scenarios, respectively [scale: Test sections' diameter = 300 mm]



(a)



(b)

Figure 39: Post experiment debris (a) without decay heat {the golden particles visible are micron sized Pele's hairs, and (b) with decay heat scenarios. [Scale: 2 cm = 1 cm actual]

The entire melt was converted into fine and large sized porous debris which enhanced the coolability. The debris formed had sizes ranging from 0.5 to 50 mm sized porous chunks including “Pele’s hair” particles. Presence of these fine strands of debris confirms the eruption with high shear between melt and resulted steam. The average porosity was 51% in without decay heat case, while a bit bigger in decay heat case as measured to be 67%.

Thus, it can be concluded that the quenching characteristics of molten pool does not depend on decay heat, although stabilization of debris temperatures at saturation take a bit longer duration as compared to stored heat scenarios. The bottom flooding technique for melt coolability is the most efficient technique even under actual decay heat scenario.



# Chapter

*“Nothing has such power to broaden the mind  
as the ability to investigate systematically and  
truly all that comes under thy observation in  
life”*

— *Marcus Aurelius (26 April 121 – 17 March 180 AD)*

*Roman emperor*



## **Chapter 4. SCALABILITY OF MELT COOLABILITY**

### **EXPERIMENTS UNDER BOTTOM FLOODING**

#### **4.1. Introduction**

Study of corium coolability during severe accident scenario becomes difficult due to the fact that performing experiments with prototypic melt in actual conditions is itself a concern, because of radioactive nature of the fuel, difficulty in high temperature melting and of course handling of such melts. Thus, experiments are conducted on smaller scales and with simulant materials which have similar heat transfer properties as that of corium. Then arises another concern of scalability of these experiments to actual reactor scenario due to use of smaller amount of melt (few kg) compared to several tonnes in reactors, differences in melt composition, geometric factors etc. For example, in the present case, the issue was whether the results of the experiment conducted with 20 litres of melt will be applicable to other melt volumes? Whether the coolability characteristics of the simulant materials like Sodium borosilicate glass and CaO-B<sub>2</sub>O<sub>3</sub> will be the same? To investigate this a series of tests were conducted in this chapter at smaller scales and with different simulants, and their results were compared. Two possible scenarios have been considered to study the scalability of melt coolability under bottom flooding experiments.

##### a) The influence of melt volume

The experiments were conducted with two melt volumes viz. 20 litres and 3 litres to understand their effect on melt coolability. These tests were conducted using same melt of sodium borosilicate glass poured at 1200°C in both the cases in different dedicated test sections. The melt height in both the cases was also kept constant at 300 mm. The results of this experiment will help us in understanding that the results of engineering scale of experiments with few tens

and hundreds of kilograms of melt can be extrapolated to actual reactor scenario dealing with tonnes of melt.

b) The influence of melt composition

Corium consists of molten fuel and structural material. During core melt accidents, the corium composition depends on type of fuel and its composition, and burn-up, structural materials, clad materials, etc. Similarly, there are several simulant materials which have thermal properties compared to corium and are used for melt coolability studies, have different composition. To study this, experiments were performed using two different simulants i.e. Sodium borosilicate glass and  $\text{CaO-B}_2\text{O}_3$  in same test section. The melt volumes, melt heights and melt temperatures were kept the same in both the experiments. The results of these experiments will help us in understanding the possibility of extrapolating the results of simulant materials to corium systems.

#### 4.2. Influence of melt volume

To understand the influence of melt volume on melt coolability under bottom flooding, experiments were performed with two different melt volumes while keeping the melt type, melt temperature and melt height same in both the experiments. Both of these experiments were conducted without decay heat as it has been observed in chapter 3 that decay heat does not influence the melt coolability under bottom flooding. The experiment discussed in chapter 3 was conducted in an engineering scale test using 20 litres of sodium borosilicate glass. To understand the effect of melt volume, small scale experiment was conducted with 3 litres of melt and compared. Table 4 below shows the various parameters of both the experiments. The melt temperature and melt height was kept more or less same in both the tests.

Table 4: Comparison of small and large scale experiments with glass

	Small scale	Large scale
<b>Simulant</b>	Sodium borosilicate glass	
<b>Amount of melt</b>	3 litres	20 litres
<b>Melt temperature</b>	~1200 °C	~1200 °C
<b>Melt height</b>	300 mm	300 mm

#### 4.2.1. Details of the test sections

The large scale experiment was performed in the large scale test facility as discussed in [section 2.3](#) of chapter 2. About 20 litres of Sodium borosilicate melt at 1200°C was poured into the test section of 500 mm height and 300 mm diameter as shown in Figure 14.

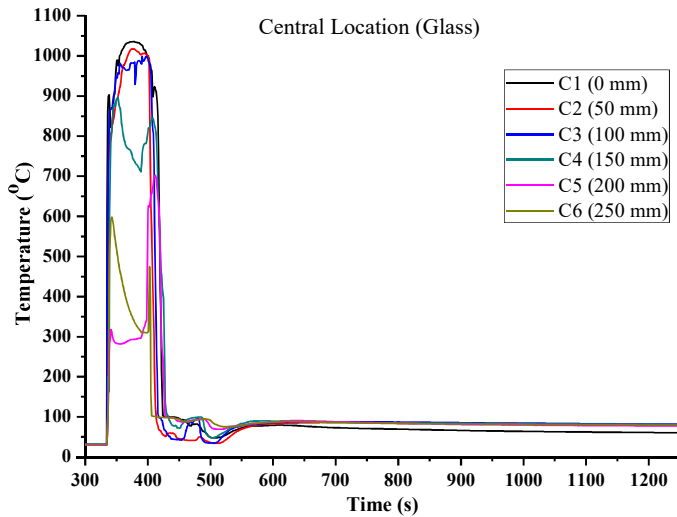
The small scale experiment was performed in the small scale test facility as discussed in [section 2.4](#) of chapter 2. The test section consisted of two parts viz. lower part to hold the melt and upper to allow steam to expand (Figure 18) similar to the large scale facility. The upper part of this test section is made of a DN 150 carbon steel pipe of 500 mm height. For the outlet of steam, a DN 40 line has been provided. This part was welded with a SS slide lock arrangement on top for closing the test section after the melt pouring. The lower part of the test section in which melt was used to be poured is similar to the upper part except for the internal arrangement of nozzle to flood the water from bottom. Water used to be injected into the test section through a DN 15 CS water supply line, provided at the bottom of the test section.

#### 4.2.2. Experiments conducted

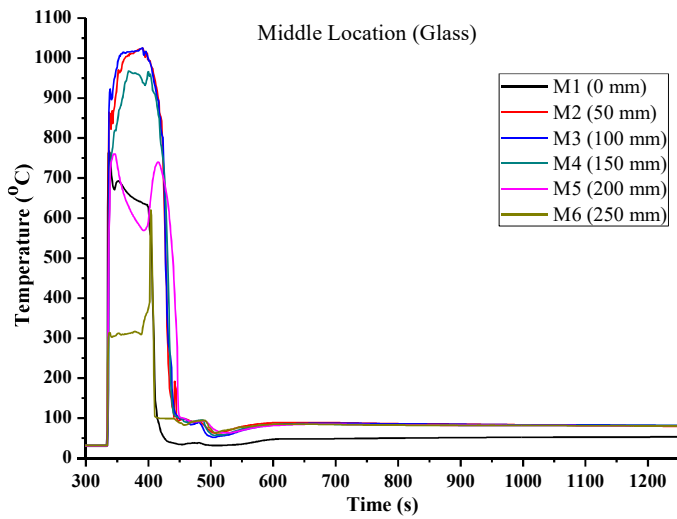
In large scale experiment, when water was inserted into the melt from bottom, it was found that the melt got quenched quickly within a few minutes in all the regions. This has been discussed in detail in [section 3.2](#) of chapter 3.

The small scale experiment was repeated with same borosilicate glass melt in the small test section as discussed above. Sodium borosilicate glass was first melted in the furnace. The glass was melted and the melt temperature was raised up to 1200 °C before pouring. The experimental setup was placed below the furnace and the melt was delivered in the test section by rotating the furnace. After pouring was completed, the slide lock was remotely closed. Subsequently, water was flooded from overhead tank by opening the inlet valve. Water through a 12 mm nozzle was injected directly into the melt. Water supply was stopped when the level in the upper part of the test section showed 100% mark. The transient temperature history inside the melt was recorded till the entire melt reached room temperature.

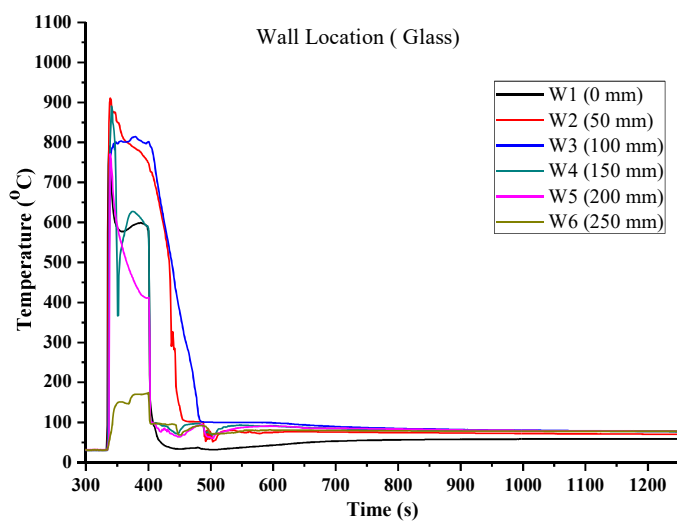
It was observed that the melt got quenched within a few minutes like in large scale case as shown in Figure 40. The temperatures in all regions, viz. centre [Figure 40(a)], half radius [Figure 40(b)] and near wall [Figure 40(c)], got cooled nearly in same time.



(a)



(b)



(c)

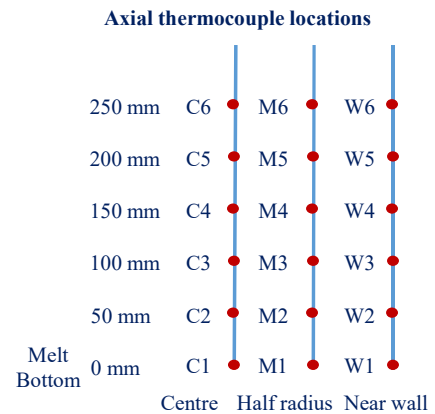
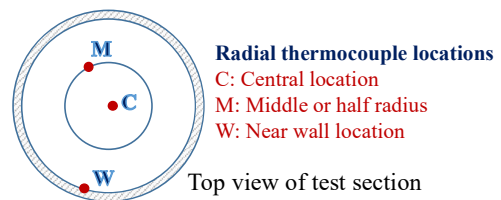


Figure 40: Temperatures profile of small scale experiment using sodium borosilicate glass

4.2.3. Comparative analysis

It can be observed from Figure 41 that the cooling characteristic of the glass remained the same in both the experiments.

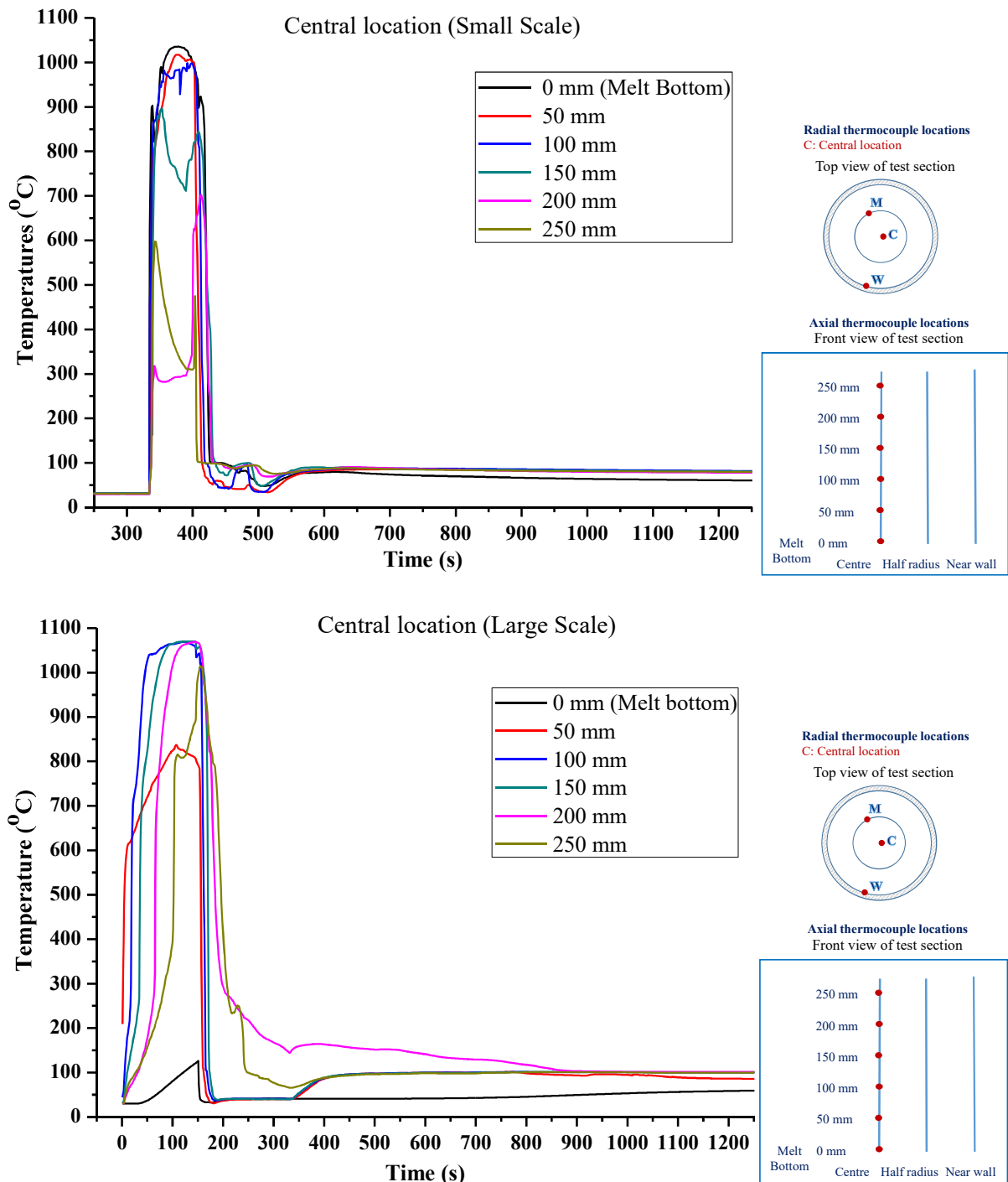
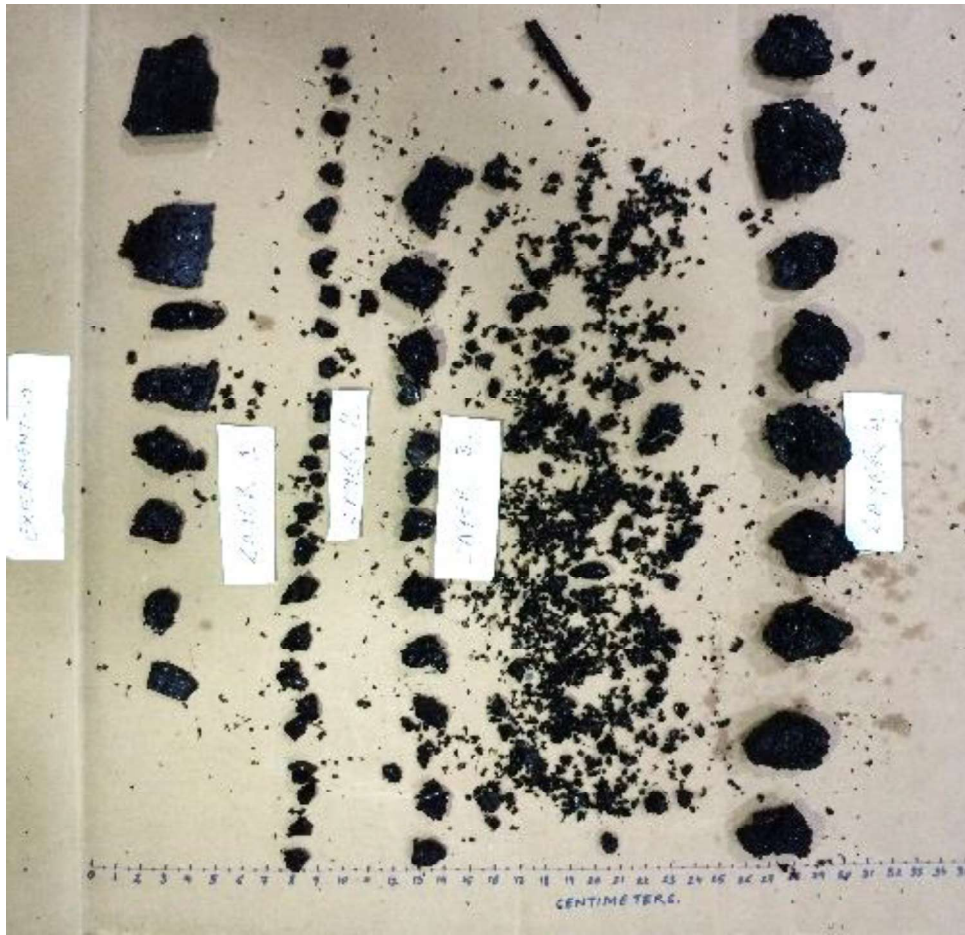


Figure 41: Temperatures profile of small scale (upper one) and large scale experiments (lower one), respectively.

The temperatures within the melt came down to 100°C within a few minutes in both the cases. The average quenching time was 61s and 93s in small scale and large scale experiments respectively, which of similar order.

In the large scale experiment, the cooling of melt took place due to the opening of the nozzle which was located at the half radius in the test section, while it was at the centre in case of small scale experiment. Due to this the eruption occurred at the half radius region of the test section and not covering the maximum possible cone volume. So the melt which was outside this eruption cone took a bit longer time to get cooled. Hence, the time taken by the large scale experiment is higher compared to small scale experiments.

Figure 42 shows the debris characteristics in both the experiments. The average porosity measured in both the experiments were found to be 51%. Debris in both the experiments were consisting of very fine particles, numerous Pele's hairs and porous chunks of sizes ranging from a few millimetres to 50 millimetres. Thus, it can be easily stated that the phenomenological behaviour of both the experiments remained same irrespective of different scale of experiments. This also proves the effectiveness of bottom flooding technique at both the scales.



(a)



(b)

Figure 42: Debris of sodium borosilicate glass obtained from (a) Small scale and (b) large scale experiments.

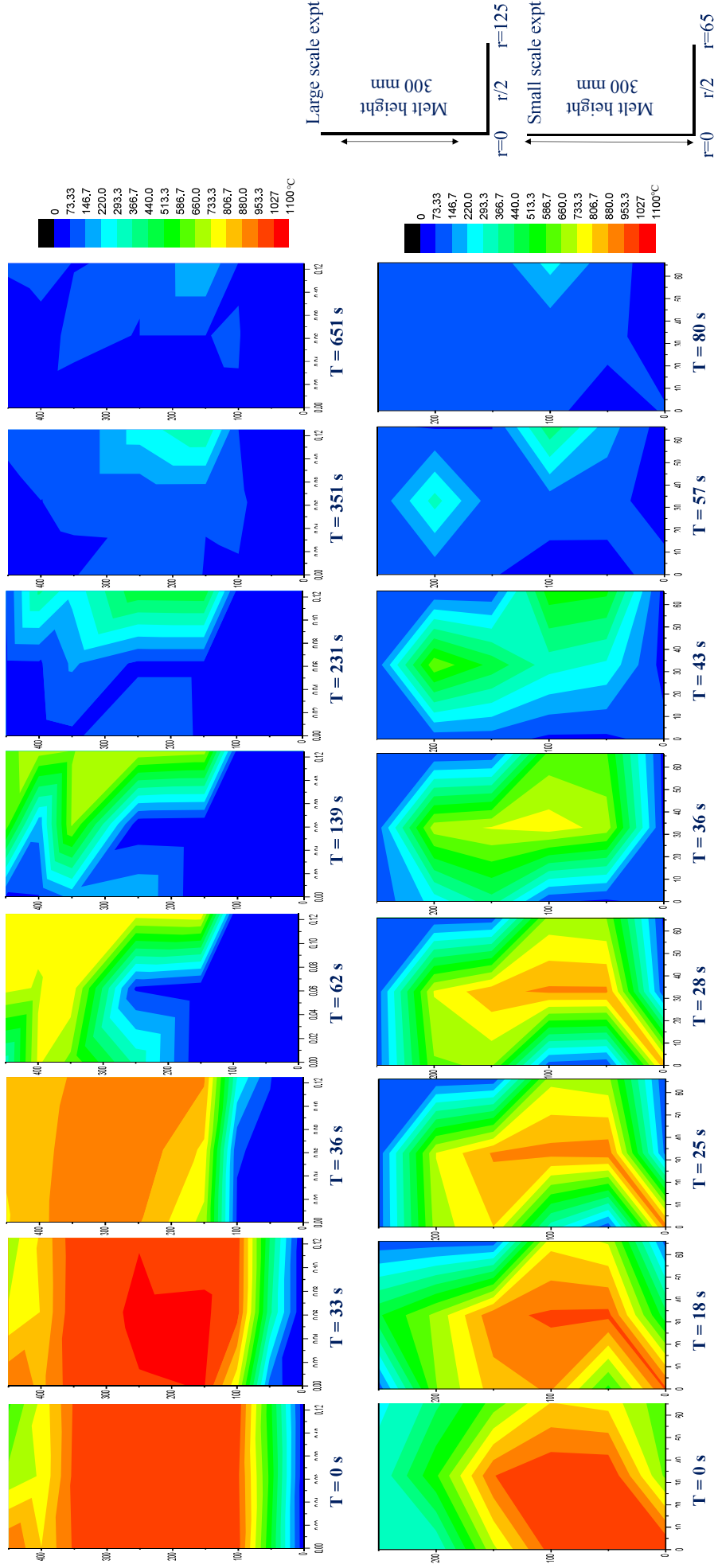


Figure 43: Quench-front propagation in large scale versus small scale experiments

#### 4.2.3.1. Quench-front Analysis

Results show that melt erupted in both scales of experiments almost at the same time and once melt erupted, it converted the melt into porous debris and hence they got cooled. Figure 43 shows the quench-front propagation in both the experiments which are quite similar to each other.

In case of large scale experiment, water was inserted at  $T=33s$  and the quench-front propagation can be seen at  $T=36s$ . At  $T=62s$ , the melt eruption is evident at the centre of the test section as seen from the contour. Then onwards it cooled as the quench-front propagates further. Similarly, in case of large scale experiment, the water was inserted at  $T=18s$ . At  $T=25s$ , the eruption opening can be seen. From  $T=28s$  onwards, eruption quench-front propagation leading to complete coolability can be easily observed.

It was found that, in both the cases, once melt erupts forming the porous zone the quenching of melt occurs quickly within a few minutes.

### 4.3. Influence of melt composition

#### 4.3.1. Details of the test section

The experiment with two different simulants i.e. sodium borosilicate glass and  $CaO-B_2O_3$  were conducted in same test section of 500 mm height and 130 mm diameter as shown in Figure 18, which is discussed in detail in [section 2.4](#) of chapter 2. In both the experiments, about 5 kg of melt was used nearly at the same temperature close to  $1200^{\circ}C$ . The melt height was also kept constant in both the cases.

### 4.3.2. Experiments conducted

One experiment was conducted using 5 kg of sodium borosilicate glass at 1165°C and with a melt height of 300 mm. It was found that all temperatures come down to saturation within a few minutes as discussed in section 4.2.2 of this chapter.

This experiment was then repeated using 5 kg of CaO-B<sub>2</sub>O<sub>3</sub> melt at 1160°C and with a melt height of 300 mm. It was observed that the quenching took longer time at centre location compared to other regions as shown in Figure 44(b). On the other hand, the near wall region got cooled very quickly compared to other regions, as seen in Figure 44(d); and the half radius region cooled in between as can be seen in Figure 44(f). This is so because the melt eruption occurred near the wall and hence it got cooled faster than other regions.

The results of both the experiments have been compared in the next section to understand the influence of melt composition on melt coolability under bottom flooding.

### 4.3.3. Comparative analysis

The small scale experiment conducted with CaO-B<sub>2</sub>O<sub>3</sub> was compared with small scale experiment of glass to study the effect of melt composition on coolability behaviour.

Table 4: Comparison of Glass vs. CaO-B<sub>2</sub>O<sub>3</sub> experiments

Simulants	Glass	CaO-B <sub>2</sub> O <sub>3</sub>
Amount of melt	~5 kg	~5 kg
Melt temperature	1165 °C	1160 °C
Melt height	300 mm	300 mm

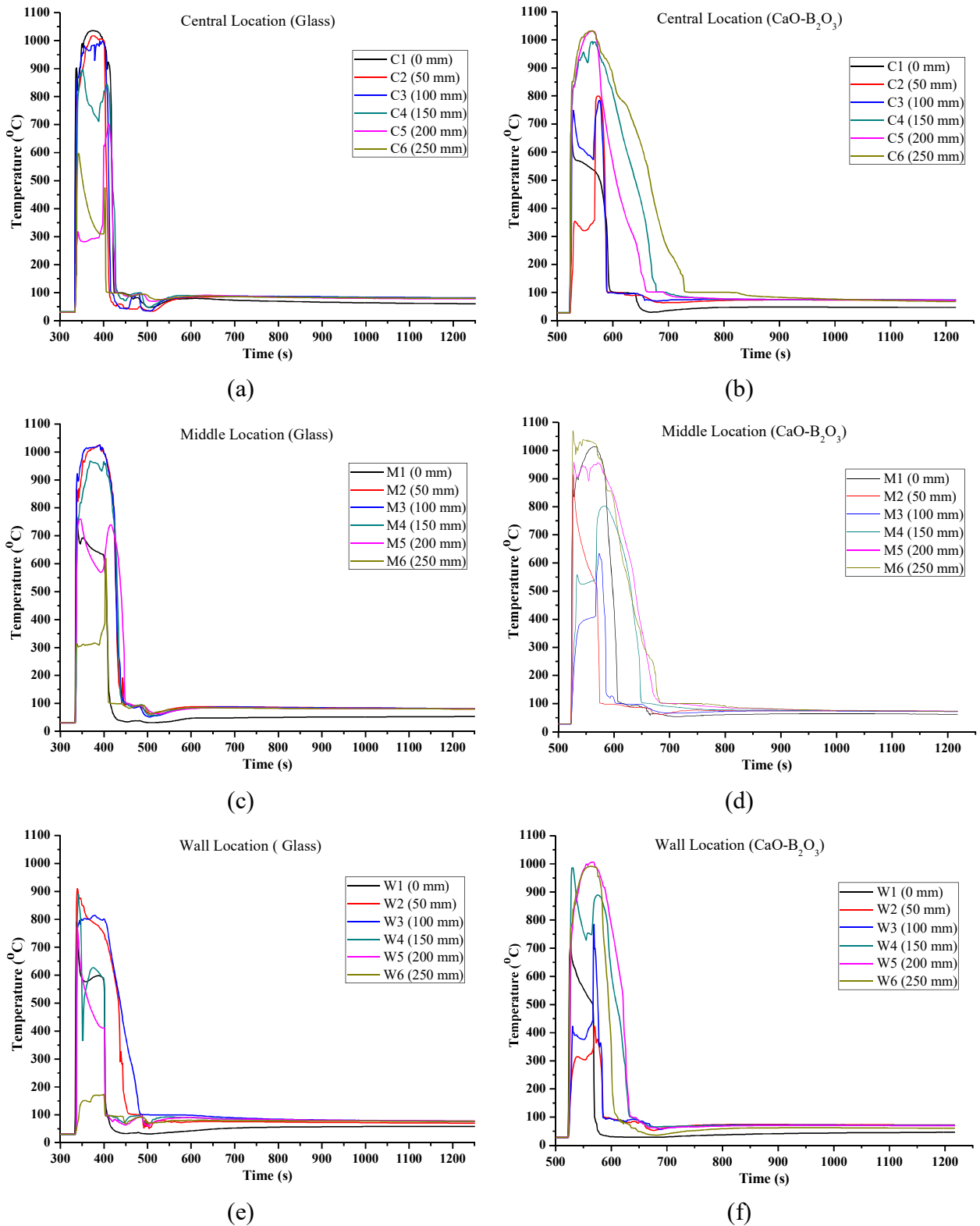


Figure 44: Temperatures profile of glass (left) and CaO-B<sub>2</sub>O<sub>3</sub> experiments

The cooling characteristics of glass and CaO-B<sub>2</sub>O<sub>3</sub> are shown in Figure 44.

Figure 44(a), Figure 44(c) and Figure 44(e) shows the temperature profile of

glass at central, middle and near wall locations respectively. It is clearly visible that all the temperatures took nearly the same time to come down to saturation temperature. On the other hand, the temperature profile of CaO-B<sub>2</sub>O<sub>3</sub> as shown in Figure 44(b), Figure 44 (d) and Figure 44(f) at central, middle and near wall locations respectively; indicates that the time taken was little more than the glass case. The time taken by the CaO-B<sub>2</sub>O<sub>3</sub> is higher possible due to the more strength of the material. Glass being more brittle compared to CaO-B<sub>2</sub>O<sub>3</sub> leads to quicker debris formation. Overall, the temperatures within the melt came down to 100°C within a few minutes. The average quenching time was 61s and 122s in glass and CaO-B<sub>2</sub>O<sub>3</sub> experiments respectively.

Figure 45 shows the debris characteristics of glass and CaO-B<sub>2</sub>O<sub>3</sub> simulants. The average porosity measured for glass and CaO-B<sub>2</sub>O<sub>3</sub> melt were found to be 51% and 50% respectively. Figure 45(a) shows the debris from glass melt consisted of very fine particles, numerous Pele's hairs and porous chunks of sizes ranging from a few millimetres to 30 millimetres. However, debris from CaO-B<sub>2</sub>O<sub>3</sub> melt had fewer fine particles compared to that of glass as shown in Figure 45(b). Debris of the sizes 5-10 mm were most prominent. They were highly rough on their surface. The so formed surface was due to the trapping of water on their surface and subsequently breaking due to conversion of water into steam and bubble bursting. Then, there were large chunks ranging from 10-50 mm in size. They were porous structures formed during the eruption and contained the internal cavities to make the water and steam flow through them. The upper layer consisted of chips like structures stating that the melt was compressed to the sides of the test section while erupting. Also, the thickness of Pele's hair was more compared to that of glass, which tells that the relative shear

between melt and surrounding steam was less in CaO-B<sub>2</sub>O<sub>3</sub> case. The debris of glass were more fragile compared to the of CaO-B<sub>2</sub>O<sub>3</sub> melt. Though, there are such differences existed in the structures of debris, still the entire melt was cooled within a few minutes and the porosity measured was of similar order. Thus, it can be easily stated that the phenomenological behaviour of both the experiments remained same irrespective of different melt composition.

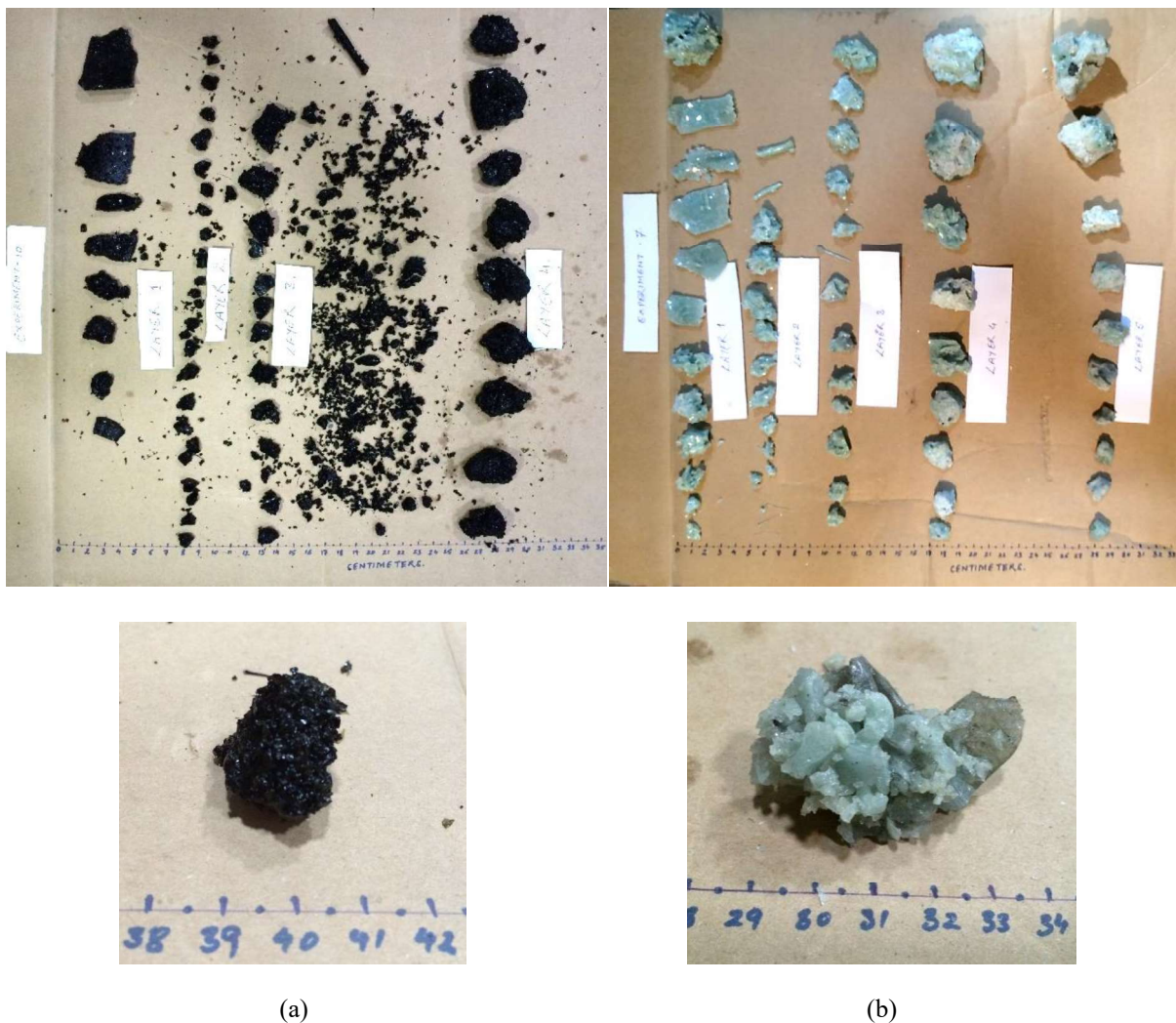


Figure 45: Debris of (a) sodium borosilicate glass and (b) CaO-B<sub>2</sub>O<sub>3</sub> experiments.

#### 4.3.3.1. Quench-front Analysis

The quench-front propagation of two different melt simulants is shown in Figure 46. In case of CaO-B<sub>2</sub>O<sub>3</sub>, the water was injected at T=15s.

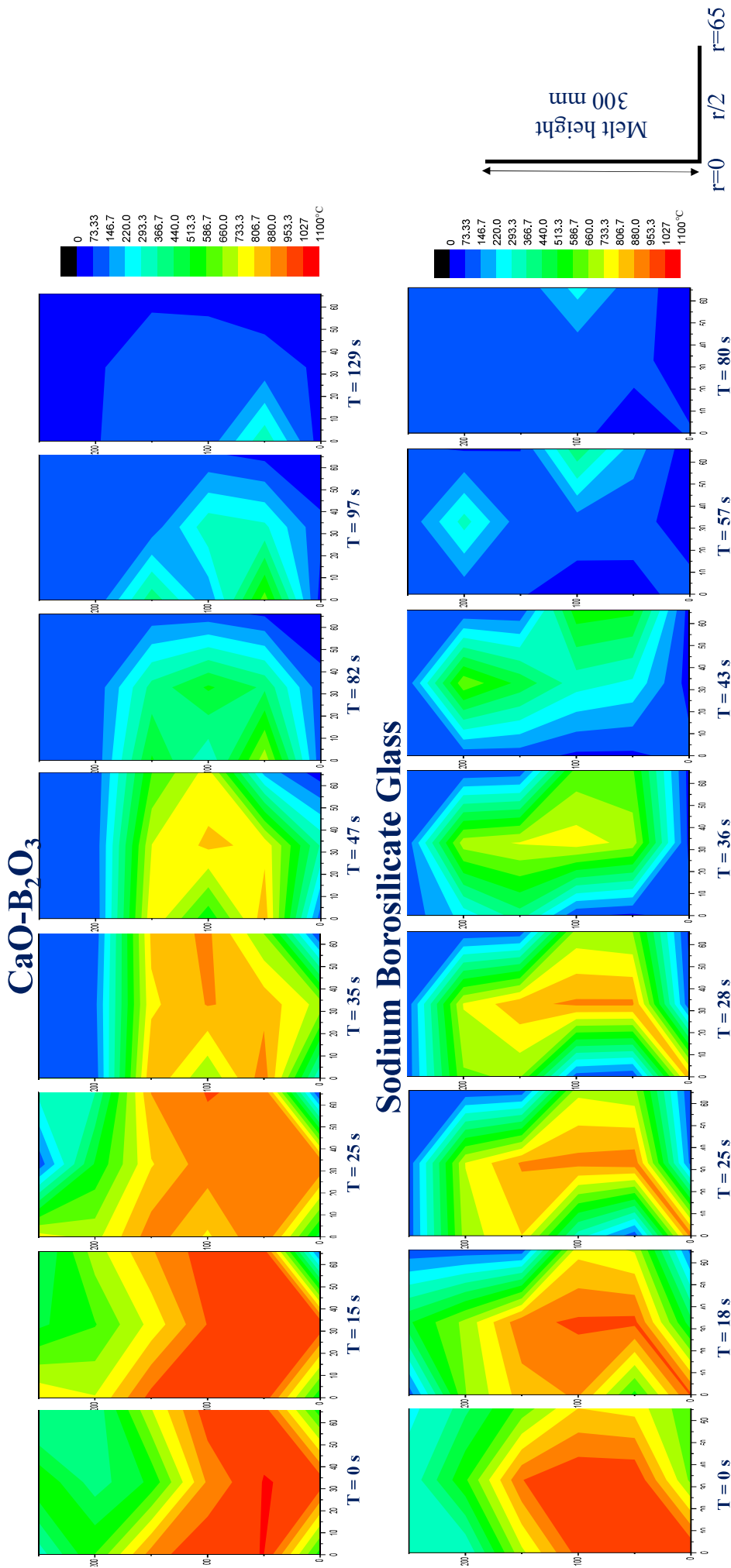


Figure 46: Quench-front propagation for CaO-B<sub>2</sub>O<sub>3</sub> versus Sodium borosilicate glass

It can be seen that the CaO-B<sub>2</sub>O<sub>3</sub> took a bit longer steam build-up time before eruption compared to sodium borosilicate glass. This is attributed to the higher strength of CaO-B<sub>2</sub>O<sub>3</sub> compared to that of glass. At T=47s, the eruption quench-front can be observed. Also, the eruption in this case occurred near the wall leading to faster cooling near to wall region compared to other regions. Once erupted, the melt got cooled due to debris formation.

In case of sodium borosilicate glass, being brittle in nature, the steam build-up time before eruption was found to be less. And hence it got cooled faster compared to CaO-B<sub>2</sub>O<sub>3</sub>.

#### 4.4. Summary

To understand the scalability of melt coolability experiments with respect to melt volume and melt composition, an experimental study has been presented in this chapter. The following insights are obtained from this investigation.

- Experiments performed with borosilicate glass with two different melt volumes suggest that the melt coolability behaviour under bottom flooding remains more or less same independent of melt volume. The debris particles sizes and morphology were also found to be the same in both the cases.
- To investigate the effect of melt composition on melt coolability, two different melt simulants were used i.e. sodium borosilicate glass and CaO-B<sub>2</sub>O<sub>3</sub>. The initial condition of the melt and water injection were kept same in both the cases. It was observed that the quenching time was higher for CaO-B<sub>2</sub>O<sub>3</sub> compared to borosilicate glass. This is because glass being brittle converts easily into debris compared to CaO-B<sub>2</sub>O<sub>3</sub> having higher strength. Once the melt eruption occurs, the quenching time is found to be almost the same.

- The average porosities measured were found to be in the range of 50-60% for all the cases, which is sufficiently large for cooling any debris bed.

It can thus be concluded that the results from the scaled experiments can be safely extrapolated to large scale experiments, as well as to reactor conditions.

# 5

# Chapter

*“See now the power of truth; the same experiment which at first glance seemed to show one thing, when more carefully examined, assures us of the contrary”*

— Galileo Galilei (15 February 1564 – 8 January 1642)  
*Italian polymath*



## **Chapter 5. EFFECT OF NOZZLE DIAMETER AND INJECTION PRESSURE ON MELT COOLABILITY WITH BOTTOM FLOODING**

### **5.1. Introduction**

In the last chapter we have seen that during the injection of water from bottom of the melt pool into the melt, the water gets converted to steam and thus pressurises the melt from bottom; subsequently leading to melt eruption. The phenomenology of melt eruption and coolability can be affected by geometrical parameters like the diameter of the nozzle injecting water into the melt pool and the injection pressure. To investigate this aspect, experiments were conducted to perform parametric studies in order to understand the effect of nozzle diameter and injection pressure on melt coolability under bottom flooding.

#### **a) The influence of nozzle diameter**

The experiments were conducted with three nozzle diameters viz. 8 mm, 12 mm and 18 mm to understand their effect on melt coolability. These tests were conducted using same melt of CaO-B<sub>2</sub>O<sub>3</sub> poured at around 1200°C in all the cases in same test sections. The melt height in all the cases was also kept constant at about 300 mm.

#### **b) The influence of inlet injection pressure**

To study this, experiments were performed at two different injection pressures i.e. 0.35 bar(g) and 0.75 bar(g) in same test section and in similar initial conditions. The melt volumes, melt heights and melt temperatures were kept the same in both the experiments.

## 5.2. Influence of nozzle diameters

### 5.2.1. Details of the test sections

These experiments were performed in the small scale test facility as it is difficult to perform parametric study and repetitive experiments in large scale facility. Details of small scale test facility have been discussed in [section 2.4](#) of chapter 2. As said before, the test section consisted of two parts viz. lower part to hold the melt and upper to allow steam to expand (Figure 18). The lower part of the test section was detachable from the entire set-up and had replaceable nozzle arrangement to flood the water from bottom. To conduct experiments with three different nozzle diameters; three of these lower parts each fitted with nozzle of diameters 8 mm, 12 mm and 18 mm, were used. Water used to be injected into the test section through a DN 15 CS water supply line, provided at the bottom of the test section.

### 5.2.2. Experiments conducted

The experiments were conducted with three nozzle diameters, viz. 8 mm, 12 mm and 18 mm, to study its effect on melt coolability. To perform all these experiments,  $\text{CaO-B}_2\text{O}_3$  was used to be melted in the furnace and poured at around 1200 °C into the test set-up kept below. After pouring was completed, the slide lock was remotely closed. Subsequently, water was flooded from overhead tank by opening the inlet valve. Water through a nozzle of specific diameter in each case, was injected directly into the melt. Water supply was stopped when the level in the upper part of the test section showed 100% mark. The transient temperature history inside the melt was recorded till the entire melt reached room temperature.

### 5.2.3. Comparative analysis

The temperatures history of all these experiments show similar trend in melt cooling as shown in Figure 47. It was observed that the average quenching time viz. 116s, 77s and 81s respectively for nozzle diameters of 8, 12 and 18 were nearly of similar order. In case of 8 mm nozzle diameter, the quenching time was higher compared to other two cases. This can be attributed to the lower inlet flow rates due to smaller diameter. Figure 47(a), Figure 47(b) and Figure 47(c) show the temperatures profile for experiment with 8 mm nozzle at central, middle and near wall locations respectively. It can also be observed that the temperatures at the central and wall locations came down nearly at the same time; while at the middle location, the temperatures at 50 and 100 mm took a bit longer duration probably due to formation of local chunks of solidified melt. But this situation was for quite a small duration.

Figure 47(d), Figure 47(e) and Figure 47(f) show the temperature profile for experiment with 12 mm nozzle at central, middle and near wall locations respectively. It can be seen that the temperatures at the central and middle locations came down nearly the same time; while near the wall, the temperatures at 50 and 100 mm took a bit longer time similar to that observed in 8 mm nozzle case. Figure 47(g), Figure 47(h) and Figure 47(i) show the temperatures profile for experiment with 18 mm nozzle at central, middle and near wall locations respectively. The overall results are similar to that observed for 8 mm and 12 mm nozzle cases.

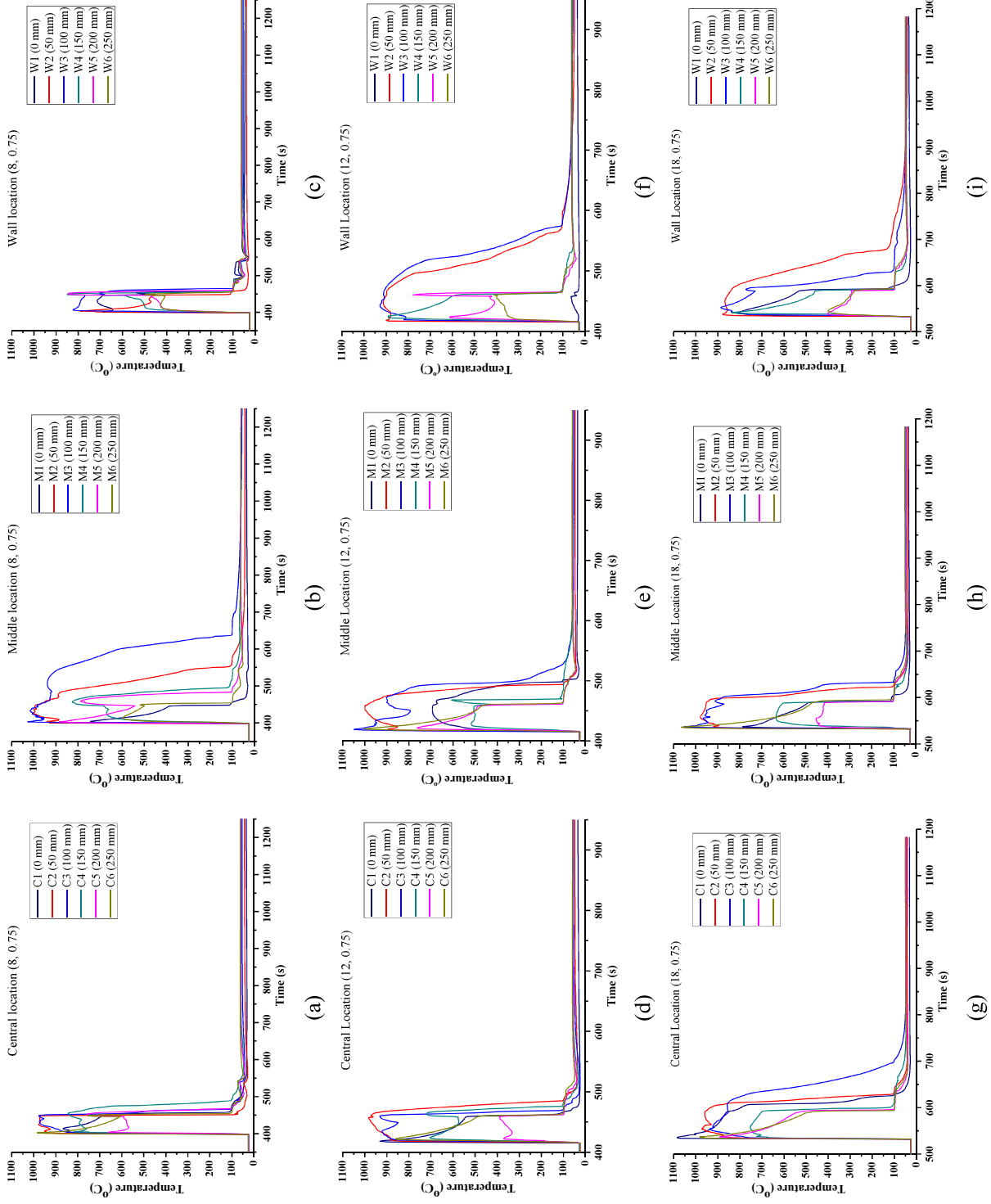


Figure 47: Temperature profiles for three different nozzle diameters at 0.75 bar inlet pressure.



(a) 8 mm



(b) 12 mm



(c) 18 mm

Figure 48: Effect of nozzle diameters on debris sizes for the experiment at 0.75

The entire melt was converted into porous debris in all the experiments, as shown in Figure 48. The gross behaviour of the debris was nearly the same. The measured porosities of the debris are found to be nearly similar in the experiments and ranged between 50-57%. A range of particle sizes were found. Small fine particles of size from 3-5 mm were typical from eruption formed mainly due to surface tension. This suggests that melt gets lifted upward while interacting with water during the eruption.

Figure 49 shows the variation of average quenching time and average measured porosity in different experiments conducted at 0.75 bar. It is evident from the figure that the time taken to quench the melt was least with 12 mm diameter nozzle and also the porosity measured for this case was the highest. It can thus be concluded that the melt can be cooled fastest with 12 mm diameter nozzle at 0.75 bar inlet pressure.

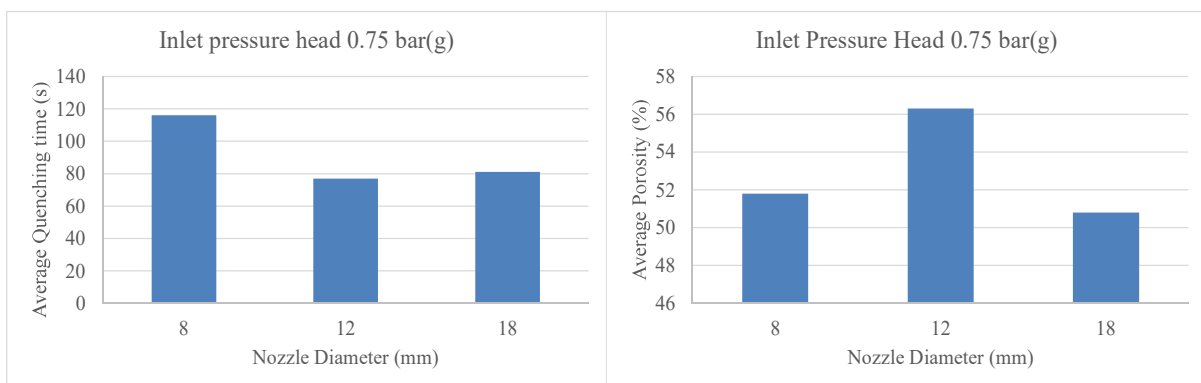


*Figure 49: Variation of average quenching time and average porosity with respect to nozzle diameter at inlet water pressure head of 0.75 bar(g)*

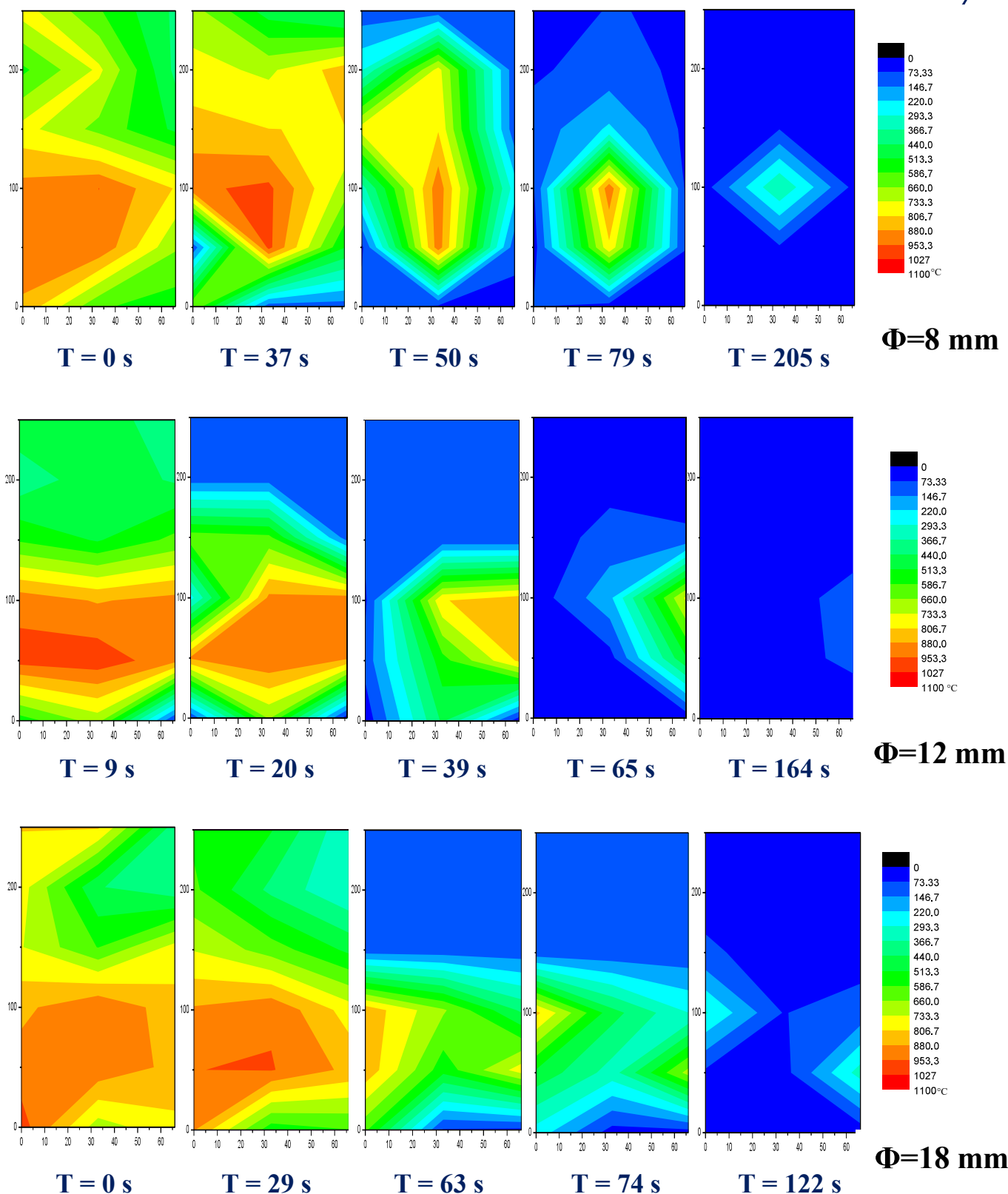


Figure 50: Quench-front propagation for different nozzle diameters.

#### 5.2.4. Quench-front analysis

The quench-front analysis as shown in Figure 50 indicates that it took longer time for melt to erupt in case of 8 mm nozzle diameter, which may be attributed to the lower inlet flow rates due to smaller opening area. The eruption occurred earliest in the case with 12 mm diameter. However, the difference in the time of eruption, in case with 12 mm and 18 mm diameters, is insignificant and the possible reason for the same could be that the mass flow rate at the 18 mm nozzle opening was higher, compared to 12 mm nozzle, due to larger cross section. Thus, the build-up time required to convert excess available water into steam, was a bit higher for 18 mm nozzle resulting in higher quenching time.

### 5.3. Influence of inlet pressures

#### 5.3.1. Details of the test sections

These experiments were performed in the small scale test facility and its details have been discussed in [section 2.4](#) of chapter 2. The facility consisted of test sections connected with inlet water injection arrangement and an overhead tank (OHT) from which inlet water comes under gravity to the test section inlet arrangement. To conduct experiments at two injection pressures viz. 0.35 bar and 0.75 bar, the heights of this OHT were varied to achieve these pressures. The test section of 500 mm height and 130 diameter was used in both the cases, and with same nozzle diameter of 12 mm.

#### 5.3.2. Experiments conducted

The experiments were conducted at two inlet water injection pressure, viz. 0.35 bar and 0.75 bar, to study their effect on melt coolability. The same simulant CaO-B<sub>2</sub>O<sub>3</sub> was used in all these experiments.

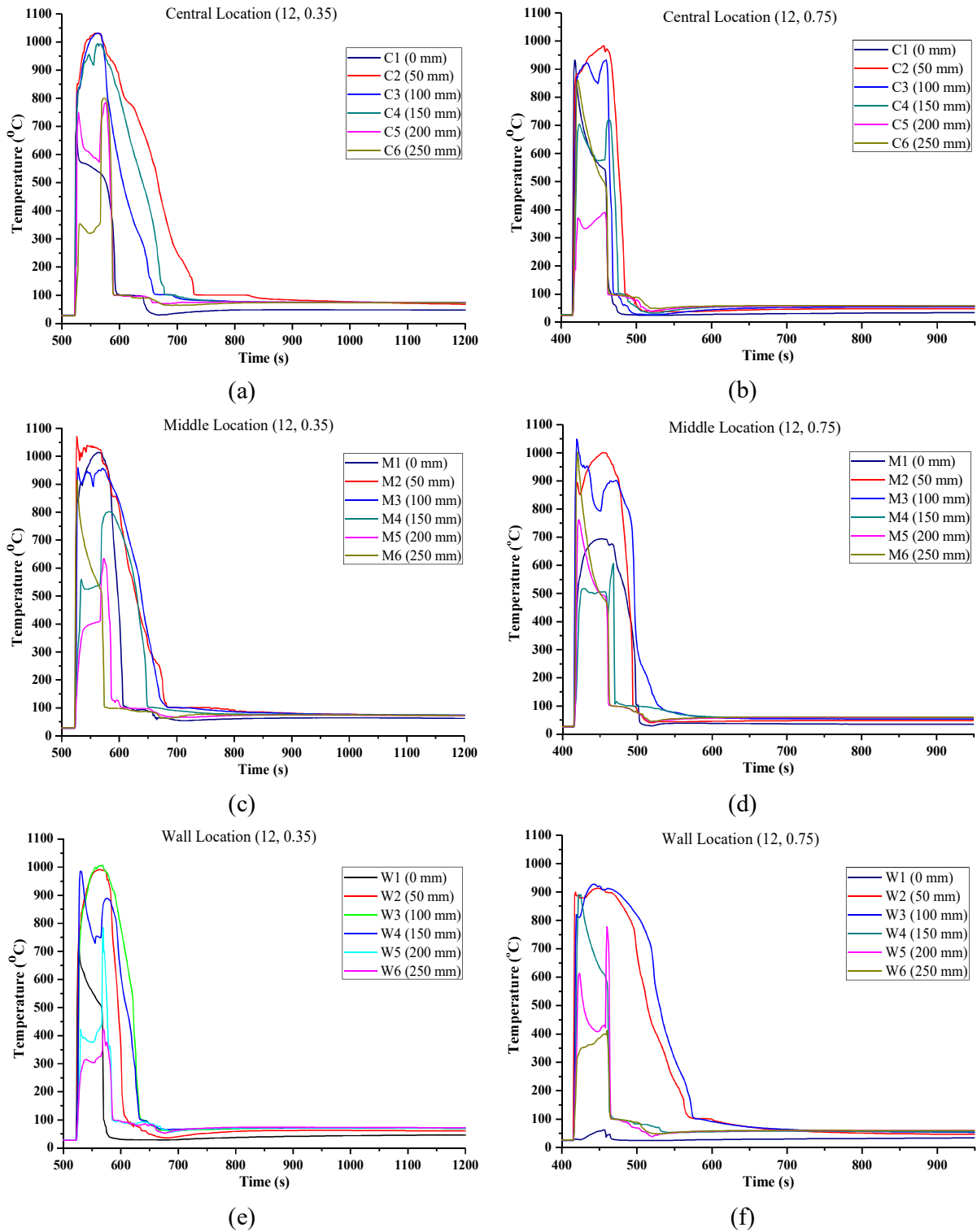


Figure 51: Temperature profiles for two inlet pressures at constant nozzle diameter of 12 mm.

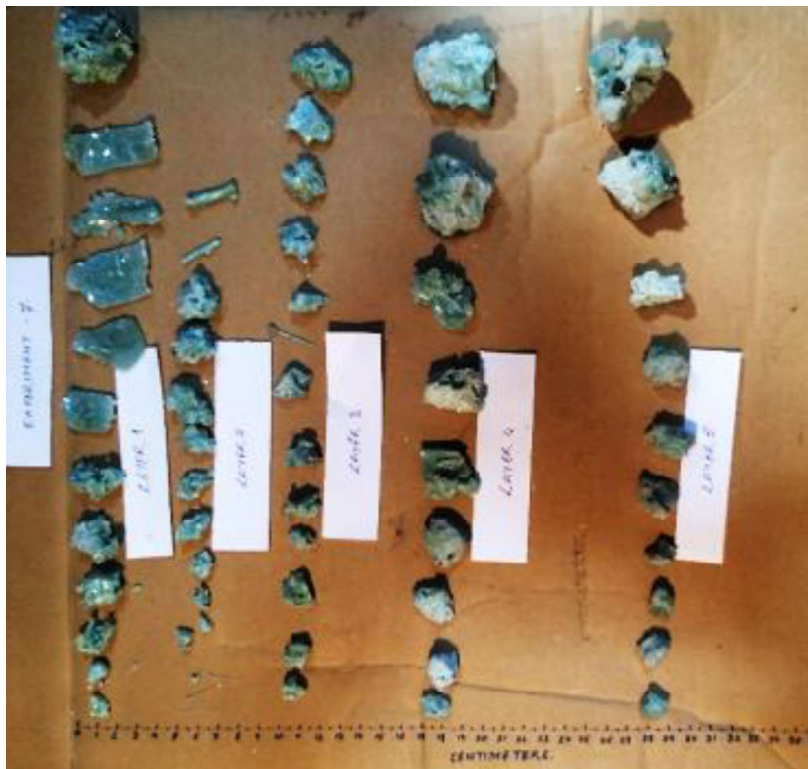
The experiments were conducted with similar initial melt temperatures and water injection conditions.

### 5.3.3. Comparative analysis

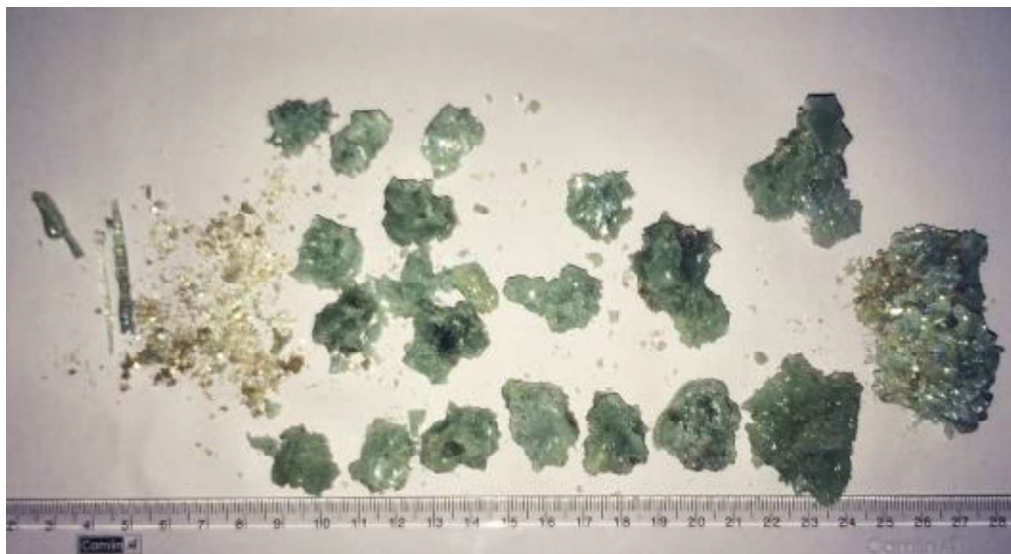
The temperatures profile of these experiments is shown in Figure 51. Figure 51(a), Figure 51(c) and Figure 51(e) shows the temperatures profile at central, middle and near wall locations for the experiment at 0.35 bar, respectively. The temperatures profile of the experiment at 0.75 bar is shown in Figure 51(b), Figure 51(d) and Figure 51(f) at central, middle and near wall locations respectively. As expected, the average quenching time was less (61 s) possibly due to higher flow velocities in case of 0.75 bar and higher (122 s) in 0.35 bar experiment. It can also be seen from the figure that the temperatures at central and middle locations, came down instantaneously for 0.75 bar case while there was a progressive delay in case of 0.35 bar experiment. Overall, the temperatures within the melt came down to 100°C within a few minutes.

Entire melt was converted into porous debris in all the experiments, as shown in Figure 52. The gross behaviour of the debris was nearly the same and has been discussed in earlier section.

The graphs in Figure 53 show that the melt gets cooled faster at higher inlet pressure for the constant nozzle diameter. Also, the average porosity was higher at the higher inlet pressure. This can be attributed to the fact that at higher inlet pressure, the overall pressure required by the steam to overcome the stresses in the crust and melt pressure head can be achieved faster due to higher mass flow rates. While it takes more time in case of lower inlet pressure. This condition is valid while keeping the nozzle diameter constant. Though, the porosities were found to be of similar order, yet the experiment at higher inlet pressure has higher measured porosity.



(a) 0.35 bar



(b) 0.75 bar

Figure 52: Effect of inlet velocities on debris sizes for the experiments with 12 mm nozzle diameter

Considering the minimum quenching time criteria, the combination of 12 mm nozzle diameter at 0.75 bar(g) inlet water pressure is most suitable for achieving quicker coolability of molten pool when flooded with water from bottom.

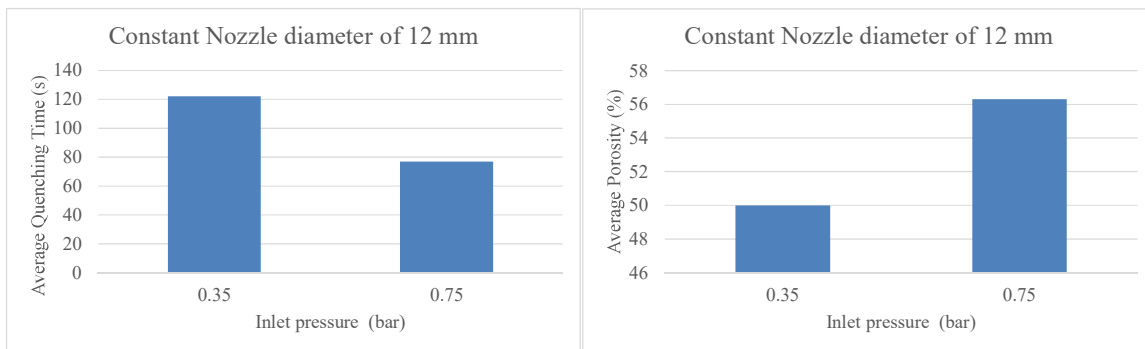


*Figure 53: Variation of average quenching time and average porosity with respect to inlet pressure at 12 mm nozzle diameter*

#### 5.4. Quench-front Analysis

Figure 54 shows the quench-front analysis to understand the effect of inlet water pressure on melt coolability under bottom flooding.

In case of the experiment with 0.35 bar injection pressure, it is evident from the figure that the steam build-up time ( $T=0s$  to  $T=35s$ ) required to erupt the melt was higher. After the eruption, it took nearly a minute to cool the melt. In case of higher injection pressure case with 0.75 bar, the steam build-up time ( $T=0s$  to  $T=20s$ ) was smaller compared to lower injection pressure case. The melt erupted within a few seconds of water injection and got cooled.

Due to this, melt erupted a bit late in low injection pressure case resulting in higher melt quenching time. Once erupted, both of them took nearly the same time to cool the melt.

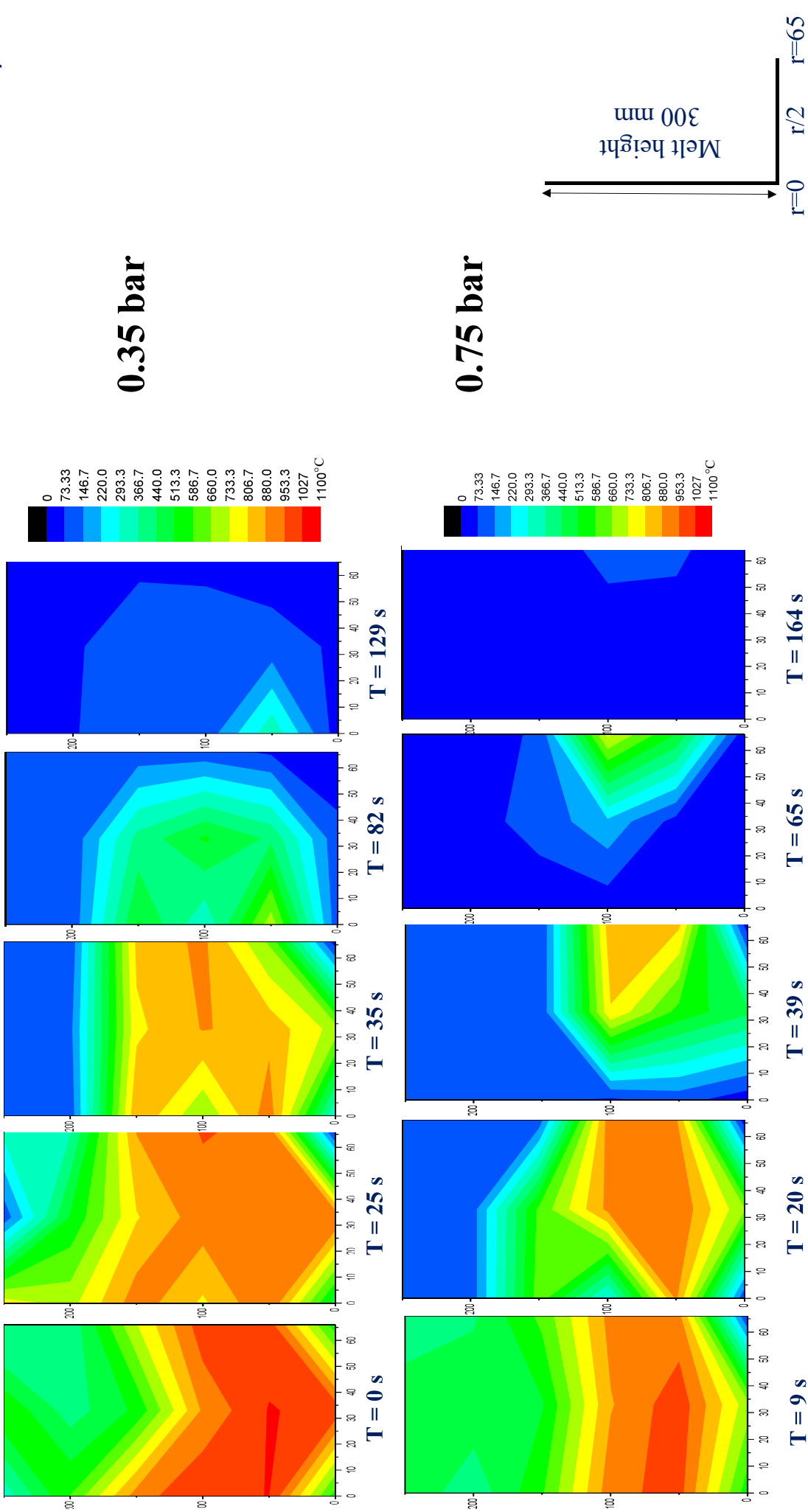


Figure 54: Quench-front propagation for different inlet pressures

Hence, it can be concluded that the effect of nozzle diameter and injection pressure on melt coolability behaviour is invariably small but they influence the melt quenching time due to change in mass flow rates.

### 5.5. Summary

Experimental studies have been conducted to study the effect of nozzle diameters and inlet pressure on the coolability of molten pool under bottom flooding.

It has been observed that the overall melt pool coolability behaviour under bottom flooding remains unaffected by any parameter. However, there is a certain effect of each parameter on time required for cooling the molten pool.

- In the experiment with 8 mm nozzle diameter, the quenching time was higher compared to experiments with 12 mm and 18 mm nozzle diameters for same inlet pressure. This is because of the low flow rates available due to smaller nozzle diameter. However, the melt quenching time was found minimum for 12 mm diameter nozzle at 0.75 bar inlet pressure.
- For the given nozzle diameter, the average quenching time was less for higher inlet pressure.
- The average porosities measured were found to be in the range of 50-60% for all the cases, which is sufficiently large for cooling any debris bed.

It can thus be concluded that the molten pool can be cooled within a few minutes under bottom flooding and the average quenching time can be optimized by selecting suitable combinations of physical and geometrical parameters.



# Chapter

*“It doesn't matter how beautiful your theory is, it doesn't matter how smart you are. If it doesn't agree with experiment, it's wrong”*

— *Richard Phillips Feynman (May 11, 1918 – February 15, 1988)*  
*American theoretical physicist*



## **Chapter 6. DEVELOPMENT OF MATHEMATICAL MODEL TO SIMULATE MELT COOLABILITY UNDER BOTTOM FLOODING**

### **6.1. Introduction of the model**

The series of experiments on melt coolability with bottom flooding revealed that steam build-up below the melt is primarily responsible for melt eruption which forms an inverted cone of porous debris. It was also observed that the porosity within this cone varies radially. On the basis of these findings, a mathematical model has been developed from first principle to simulate the phenomenology of the melt coolability under bottom flooding. In the model, the average particle size has been used from the experimental measurements as it is very difficult to model debris formation with a distribution of particle sizes formed during the melt eruption. Empirical correlation developed for the radial variation in porosity has been plugged into the model.

### **6.2. Model Development**

#### **6.2.1. Limitations of Existing Model**

There are not much information available in open literature about modelling the complex behaviour of melt coolability under bottom flooding. Kulkarni and Nayak[44] were probably the first to develop a simple model to study the transient coolability of melt pool under bottom flooding. This simple mathematical model was based on the model proposed by Paladino et al.[38], and was validated against the DECOBI experimental data. It assumes that vertical porous channels form with uniform porosity in the melt pool when water is injected through the nozzle from the bottom of the melt pool; the diameters of the channels are of the same order of magnitude as the nozzle

diameter. The assumptions worked reasonably well for the small scale experiment of DECOBI wherein the melt height was 50 mm only and no decay heat was present in the melt pool. This model was subsequently used to predict the melt coolability under bottom flooding in another facility with molten glass as melt simulant having a pool height of 300 mm, but without decay heat. The temperature predictions were found closer to the experimental measurements. However, the model had the following limitations:

- a) In the model of Kulkarni and Nayak[44], it was assumed that the melt eruption forms the vertical porous channels with uniform porosity throughout this eruption zone, as shown in Figure 55. One of the important limitations was the unaccountability of heat sink. The heat transfer from porous debris to coolant was considered to be by convection only and no phase change was considered. However, boiling heat transfer is substantial.

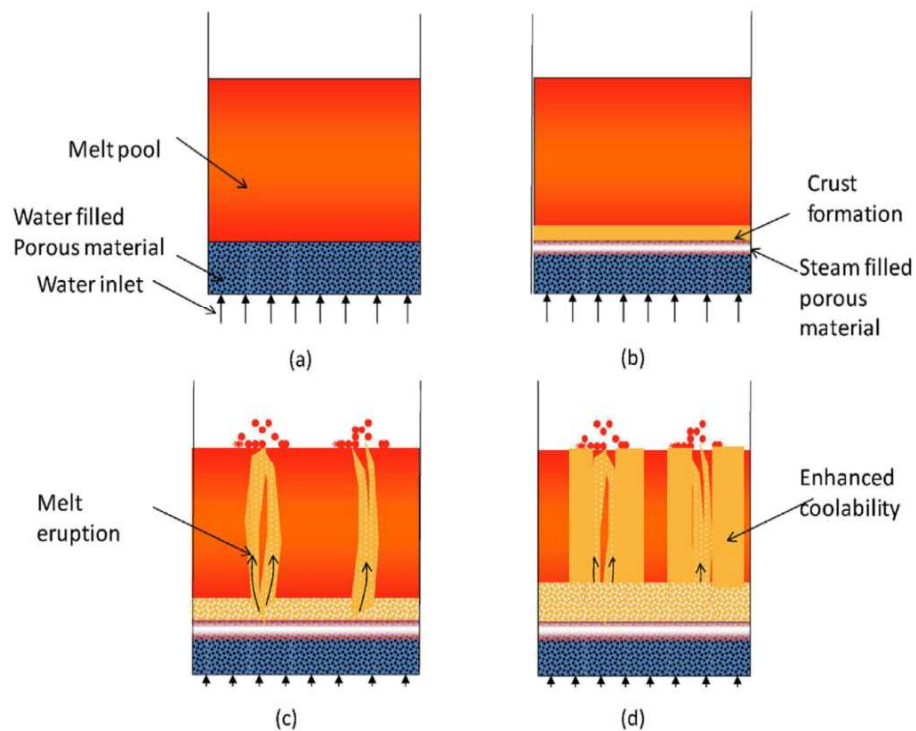


Figure 55: Melt coolability model by Kulkarni and Nayak (2013)

b) In the present experiments, a porous eruption cone was observed instead of vertical porous channels. Also, it was observed that the porosity follows the radial variation in the eruption zone unlike uniform porosity assumed in the model of Kulkarni and Nayak[44]. Measurements of porosity show that the variation was radially decreasing within the eruption zone, as shown in Figure 56.

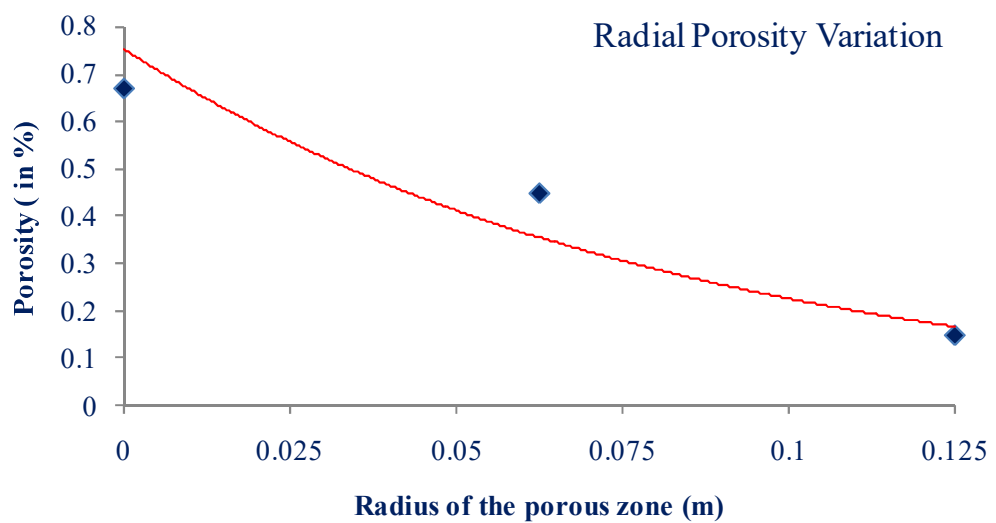


Figure 56: Variation in porosity along the radius of the porous zone within the test section

Due to this variation in porosity, the melt coolability also varies along the radius of the eruption zone. It was observed that the cooling rate was much faster at the centre of the eruption site as compared to that at the wall of the eruption zone.

### 6.2.2. Postulations

Considering the above discussed factors and the inferences of experiments, the model was postulated in the present work. The basic postulates of this model are as follows, and depicted pictorially in Figure 57.

- When water is flooded into the melt through nozzles it interacts with water and cools down while forming a thin crust (Figure 57(a)).
- This crust starts growing further upon addition of water (Figure 57(b)).
- Due to intense heat transfer, steam forms and expands below the crust and exerts pressure on it in all directions.
- The crust is now subjected to stresses
  - Steam pressure on one side
  - Hydrostatic head of the melt pool on the other side
  - Thermal stresses generated due to temperature gradient across the thickness
- When the total stresses exceed fracture stress, numerous fine cracks occurs on the crust surface due to brittle nature of the material, which acts as the eruption locations (Figure 57(c)).
- The principal conical eruption occurs along with numerous secondary eruptions. This inverted cone shaped porous zone is termed as ‘eruption cone’ (Figure 57(d)).
- These eruptions convert melt into debris due to intense shear between up-flowing steam and the melt. The cones formed act as the passage for cooling fluids.
- The porosity within these eruption zones varies spatially.
- Boling heat transfer occurs between the melt and the cooling fluids in this eruption cone which is quite significant and rapid.
- These result in significant enhancement in melt coolability.

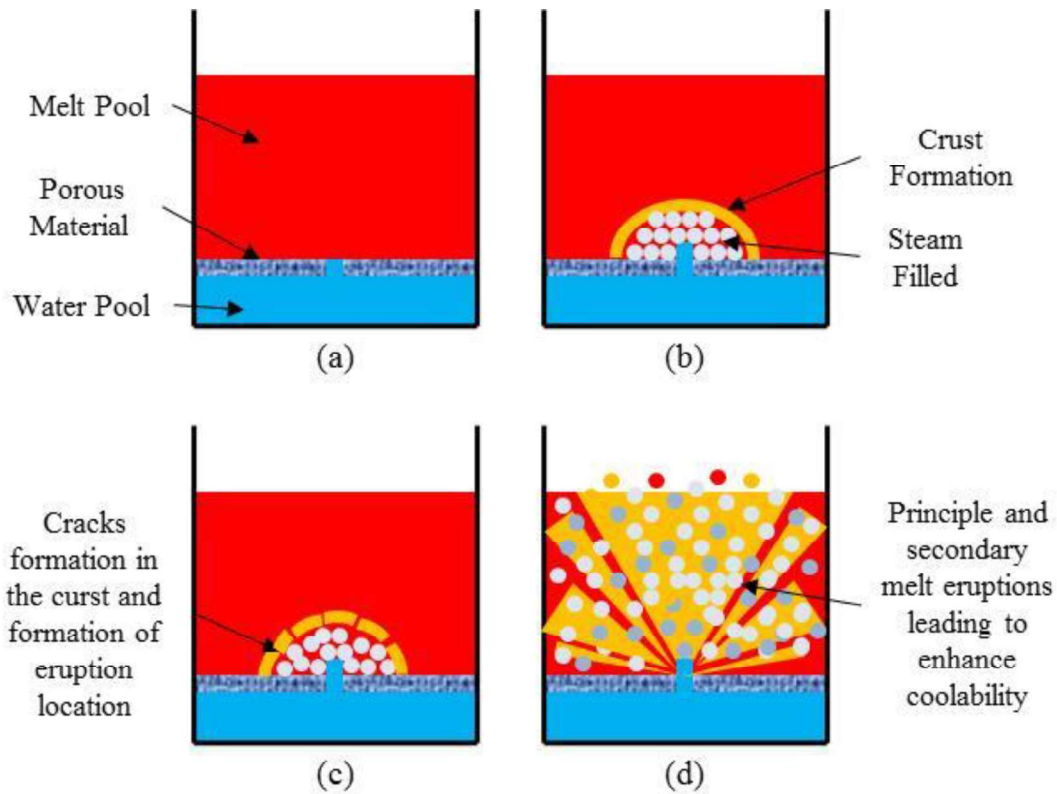


Figure 57: Melt coolability under bottom flooding with decay heat, the eruption model

### 6.2.3. Model Assumptions

Modelling of melt coolability under bottom flooding is a challenging and complex phenomena. It involves multi-physics, multicomponent and multiphase which are difficult to model from first principles. In order to deal with such a situation, following assumptions were made:

- a) In the melt pool, dominant mode of heat transfer is conduction due to the assumption that melt is near to the saturation (liquidus) condition having high viscosity.
- b) In the porous zone, the mean particle diameter to calculate interfacial area is taken from experiments while assuming that all debris particles maintain the spherical symmetry of that particular diameter.
- c) The steam generated at the time of melt eruption is superheated.

- d) In the porous zone; within a unit volume, porous medium completely transfers the heat to the cooling fluid passing through it. This acts a heat sink for the system.
- e) Heat transfer coefficient, h, is evaluated from the surface temperature based on heat transfer regime (boiling heat transfer here).
- f) Local thermal non-equilibrium has been considered in the porous zone. However, convective boundary condition has been used at porous-solid cone interface.

#### 6.2.4. Description of Model

##### 6.2.4.1. Governing equations for molten pool

Once the melt pool is formed in the ex-vessel severe accident scenario, conduction is the dominating mode of heat transfer. The transient two dimensional axi-symmetric heat conduction equation for the melt pool can be written as the following,

$$\rho C_p \frac{\partial T}{\partial t} = \frac{1}{r} \frac{\partial}{\partial r} r \left( k \frac{\partial T}{\partial r} \right) + k \frac{\partial^2 T}{\partial z^2} + q''' \quad \dots(1)$$

In the crust layer also, similar heat conduction equation is obeyed,

$$\rho C_p \frac{\partial T}{\partial t} = \frac{1}{r} \frac{\partial}{\partial r} r \left( k \frac{\partial T}{\partial r} \right) + k \frac{\partial^2 T}{\partial z^2} + q''' \quad \dots(2)$$

Where,

$\rho$  is the melt density,

$C_p$  is the specific heat capacity of the melt,

$k$  is the thermal conductivity of melt

$q'''$  is the volumetric heat generation rate

The boundary conditions for the above equations are given in Figure 58.

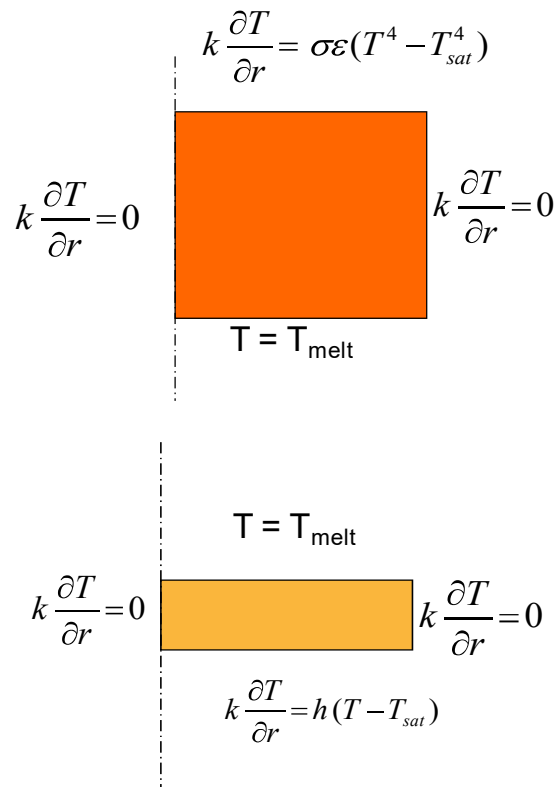


Figure 58: Boundary conditions for melt (upper) and crust layer (lower).

#### 6.2.4.2. Eruption Model

Once the water comes in contact with the melt, it cools the melt and a lot of steam is formed below the melt. As a result a thin crust is formed due to cooling of the melt above the nozzle outlet. This crust is then subjected to various stresses as shown in Figure 59. The melt pool exerts hydrostatic head on the top of the crust while at the bottom of it, steam pressurizes it.

This pressure developed is calculated using the equation of state,

$$p = f(\vartheta) \quad \dots (3)$$

Where,

p is the steam pressure

The specific volume of the steam is obtained as,

$$\vartheta = \frac{M_{st}}{V_p} \quad \dots (4)$$

Where,

$V_p$  is the volume of the porous zone

The mass of steam generated in the a given time is obtained from

$$M_{st} = \Gamma \cdot dt \quad \dots (5)$$

Where,

t is the time

The rate of vaporisation is calculated as,

$$\Gamma = \frac{v \cdot A \cdot \rho \cdot (h_{in} - h_{fs}) + h \cdot A \cdot (T_{melt} - T_{sat})}{h_{fg}} \quad \dots (6)$$

Where,

v is the velocity of steam

A is the area of cross section

$h_{in}$  is inlet enthalpy

$h_{fs}$  is liquid saturation enthalpy

$h_{fg}$  is latent heat of vaporisation

$T_{melt}$  is melt temperature

$T_{sat}$  is saturation temperature

The velocity is predicted by using Darcy's equation,

$$v = -\frac{dp}{dz} \frac{\kappa}{\mu} \quad \dots (7)$$

Where,

$\kappa$  is bed permeability

$\mu$  is dynamic viscosity

In addition to this, the top edge of the crust is at melting temperature whereas; the bottom end is at much lower water temperature. This exerts thermal as well as mechanical stresses to the crust.

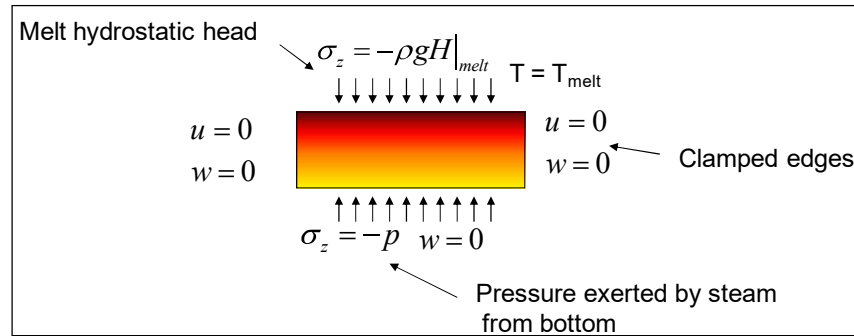


Figure 59: Stresses in the crust.

The bending stresses on the circular plate type crust as a result of clamped edges are given as (Timoshenko,[99])

$$\sigma_b = 0.75 \cdot \frac{(\Delta p \cdot r^2)}{t_{cr}^2} \quad \dots (8)$$

Where,

p is the pressure of steam

r is the radius

t<sub>cr</sub> is the crust thickness

The thermal stresses as a result of temperature gradient are given as

$$\sigma_{th} = \frac{\alpha \cdot \Delta T \cdot E}{2(1-\nu)} \quad \dots (9)$$

Where,

T is the temperature

α is the linear expansion coefficient

E is the Young's modulus of elasticity

ν is the Poisson's ratio

Since the total strain is additive and the material, being brittle, remains in elastic region, hence, we can add the individual stresses to obtain the total maximum stress acting on the crust as

$$\sigma_{tot} = \sigma_{th} + \sigma_b \quad \dots (10)$$

The crust will break if the total stress exceeds the strength of the crust  
i.e.

$$\sigma_{tot} > \sigma_{max} \quad \dots (11)$$

Now, the crust fracture at numerous sites which become the eruption location on the surface of the crust. The principal eruption ( $\hat{E}$ ) is favoured in the central region due to cumulative axial momentum. Along with this principal eruption, a series of secondary eruptions ( $\hat{E}1, \hat{E}2, \dots, \hat{E}n$ ) also occur on other fracture locations of the crust. This, within no time converts the entire melt pool into the porous debris. These eruptions form porous conical zone in their respective directions. Using Bursik[100] model, we can write mass continuity for the principal eruption as:

$$\frac{d}{dz} (r_{erup}^2 \cdot \rho_{erup} \cdot v_{erup}) = 2 \cdot \rho_{st} \cdot r_{erup} \cdot v_{st} + \sum_{i=1}^N \frac{dM_i}{dh} \quad \dots (12)$$

Where,

$r_{erup}$  is radius of eruption

$\rho_{erup}$  is density of eruption

$v_{erup}$  is velocity of eruption

$\rho_{st}$  is density of steam

$v_{st}$  is velocity of steam

$M_i$  is the mass flux of debris of size fraction  $i$  within eruption zone

$h$  is melt height

The right hand side of the equation (12) represents the mass flux of steam entrainment and the mass flux of debris, respectively. The radius of eruption varies as the function eruption cone angle and is given as,

$$r_{erup} = h \cdot \tan \frac{\theta}{2} \quad \dots (13)$$

Where,

$\theta$  is cone angle of eruption

The principal eruption cone angle can be evaluated using the simple correlation given by Abramovich[101] using the jet mixing theory assuming that the eruption of melt acts as an inverted jet spray. Thus, the cone angle is given as,

$$\tan \theta = 0.13 \left( 1 + \frac{\rho_m}{\rho_{st}} \right) \quad \dots (14)$$

Where,

$\rho_m$  is melt density

$\rho_{st}$  is steam density

Using Barsotti[102] model, we can calculate

$$\frac{dM_i}{dh} = \rho_{erup} r_{erup} (1 - \varepsilon) w_i M_i \quad \dots (15)$$

Where,

$\varepsilon$  is porosity

$w_i$  is settling velocity of a debris the given size class

And the conservation of momentum for the principal melt eruption zone can be written as follows,

$$\begin{aligned} & \frac{d}{dh}(\rho_{erup} \cdot r_{erup}^2 \cdot v_{erup}^2) \\ & = g \cdot r_{erup}^2 \cdot (\rho_m - \rho_{erup}) + v_{erup} \cdot \sum_{i=1}^N \frac{dM_i}{dh} \end{aligned} \quad \dots (16)$$

Where,

g is the acceleration due to gravity

The two terms on the right hand side of the equation (16) are related to acceleration due to gravity and the segregation of particles, respectively.

The eruption density used throughout comprises the mass fraction of debris and vapour at atmospheric temperature. The mass fraction of liquid has been neglected for the sake of simplicity as the temperature difference is so large that the steam will be in superheated regime at the time of eruption.

$$\rho_{erup} = \frac{1}{\frac{x_{debris}}{\rho_{debris}} + \frac{x_{vapor}}{(\rho_{vapor})_{atm}}} \quad \dots (17)$$

Where,  $\rho_{erup}$  is the density of the mixture comprised of vapours and melt debris.

Along with the principal eruption, the series of secondary eruption taking place can also be evaluated using the same philosophy as of the principal eruption.

The total eruption =  $\hat{E} + \hat{E}_1 + \hat{E}_2 + \dots + \hat{E}_n$ .

And, the total momentum (vector sum) due to these eruptions =  $P + P_1 + P_2 + \dots + P_n$ .

The number of secondary eruption locations on the crust surface can be evaluated by using Zubers'[103] modified Critical Taylor Wavelength

formula. The average density of eruption locations per unit area of the crust surface can be given as

$$\gamma = \frac{1}{\xi^2} \quad \dots (18)$$

Where,  $\xi$  is the spacing between the eruption locations given by

$$\xi = 2\pi \sqrt{\frac{\sigma_{mc}}{(\rho_m - \rho_{st})g}} \quad \dots (19)$$

Where,  $\sigma_{mc}$  is the surface tension between melt and steam.

Once the melt is erupted, the melt pool is considered to be made of two zones, mainly porous zone and non-porous zone.

#### 6.2.4.3. Equation in porous zone:

Energy balance equation for the porous zone can be written as below

$$\rho C_p \frac{\partial T}{\partial t} = \frac{1}{r} \frac{\partial}{\partial r} r \left( k \frac{\partial T}{\partial r} \right) + k \frac{\partial^2 T}{\partial z^2} + q''' - q'''_{s,f} \quad \dots (20)$$

This equation includes the decay heat term,  $q'''$ , and the heat sink term,  $q'''_{s,f}$ , considering that a unit volume of porous medium completely transfers the heat to the cooling fluid passing through it, as shown in Figure 60.

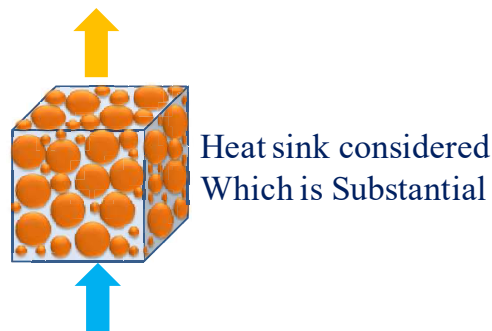


Figure 60: Philosophy of boiling heat transfer in the present model

The interfacial area density is obtained from porosity and the particle diameter within heat sink (as shown in Figure 60 above),  $d_p$  is,

$$\dot{a} = 6 \frac{(1 - \varepsilon)}{d_p} \quad \dots (21)$$

Where,

$\varepsilon$  is porosity

$d_p$  is particle diameter

The heat transfer from solid to fluid acts as a heat sink term,

$$q'''_{s,f} = h \cdot \dot{a} \cdot (T - T_{inf}) \quad \dots (22)$$

Where,

$h$  is heat transfer coefficient evaluated from surface temperature based on heat transfer regime i.e. film boiling or nucleate boiling.

In the model, for film boiling, Berenson's[104] model is used and for nucleate boiling Rohsenow[105] correlation is used.

As observed in the experiments, porosity varies as a function of radius of the porous zone,  $\varepsilon = \mathcal{F}(r)$ . The correlation for the radial porosity variation has been deduced from the test data and is given by

$$\varepsilon = 0.753 e^{-11.9 r} \quad \dots (23)$$

Where,

$r$  is the radius of porous zone

The model predicts the temperatures in the melt pool by modifying the initial domain and governing equations by using effective properties as

$$\rho_{eff} = \rho_{fluid} \cdot \varepsilon + \rho_{solid} \cdot (1 - \varepsilon) \quad \dots (24)$$

Similar to equation (24), other properties like thermal conductivity,  $k_{eff}$ ,

$$k_{eff} = k_{fluid} \cdot \varepsilon + k_{solid} \cdot (1 - \varepsilon) \quad \dots (24a)$$

and specific heat capacity,  $C_p$ , are modified.

$$C_{p_{eff}} = C_{p_{fluid}} \cdot \varepsilon + C_{p_{solid}} \cdot (1 - \varepsilon) \quad \dots (24b)$$

The equation for porous medium is modified as

$$\begin{aligned} \rho_{eff} \cdot C_{p_{eff}} \cdot \frac{\partial T}{\partial t} = \frac{1}{r} \frac{\partial}{\partial r} r \left( k_{eff} \frac{\partial T}{\partial r} \right) + k_{eff} \cdot \frac{\partial^2 T}{\partial z^2} + q''' \\ - h \cdot 6 \frac{(1 - \varepsilon)}{d_p} \cdot (T - T_{inf}) \end{aligned} \quad \dots (25)$$

The effective properties are volume averaged in the bed. With boundary conditions as

$$k_{eff} \frac{\partial T}{\partial z} = h(T - T_{\infty}) \quad \dots (26)$$

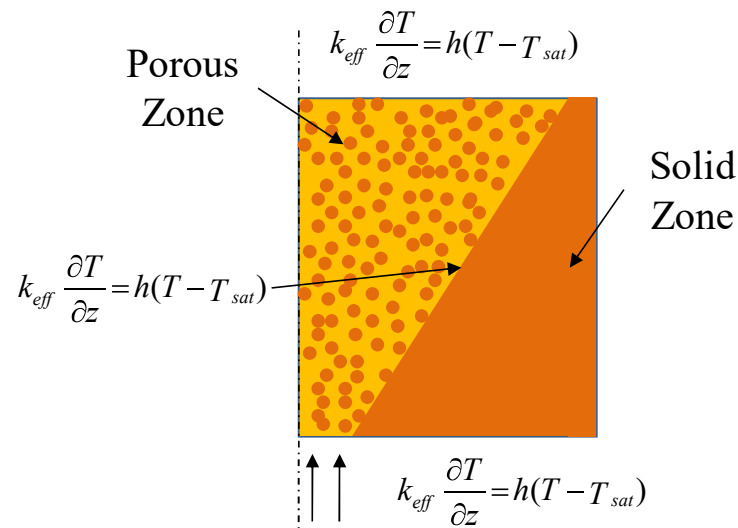


Figure 61: Modified boundary conditions for solid region

For the solid region, the boundary conditions are modified as shown in Figure 61. In addition to top and bottom, now the span of the solid zone has reduced and additional convective boundary condition at one side

has been introduced which makes it coolable from two dimensions. As a result, the overall coolability is greatly enhanced.

### 6.3. Solution Procedure

The governing equations in melt pool and solid crust region are discretized using finite difference method and solved implicitly using Gauss-Siedel iterative method to obtain temperature distribution in the melt pool. After evaluating the temperatures, the crust growth rate is calculated and subsequently the thickness of the solid crust region is updated. After the temperature distribution has been obtained, the stresses are calculated. With the stresses, the fracture conditions are evaluated. When the crust breaks, it is considered to be a porous zone with experimentally observed porosity and calculated number of eruption sites and diameter of eruption sites are calculated. After that, the domain is modified and the equations for porous zone and solid zones are recalculated using modified governing equations using similar technique.

### 6.4. Results and Discussion

The model has been applied to the large scale melt coolability experiments with and without decay heat simulation as described in chapter 3. The initial conditions of the melt were considered to be the same as in the experiment just before water was injected. Water injection pressure in the nozzle was also kept the same in the model. The predicted and measured melt temperatures during quenching have been compared and discussed below.

#### 6.4.1. Case I: Decay heat scenario

The variation in melt pool temperatures at the central region of the melt pool is shown in Figure 62. Both, numerical prediction and experimental measurements follow the same trend and are in good agreement with each other.

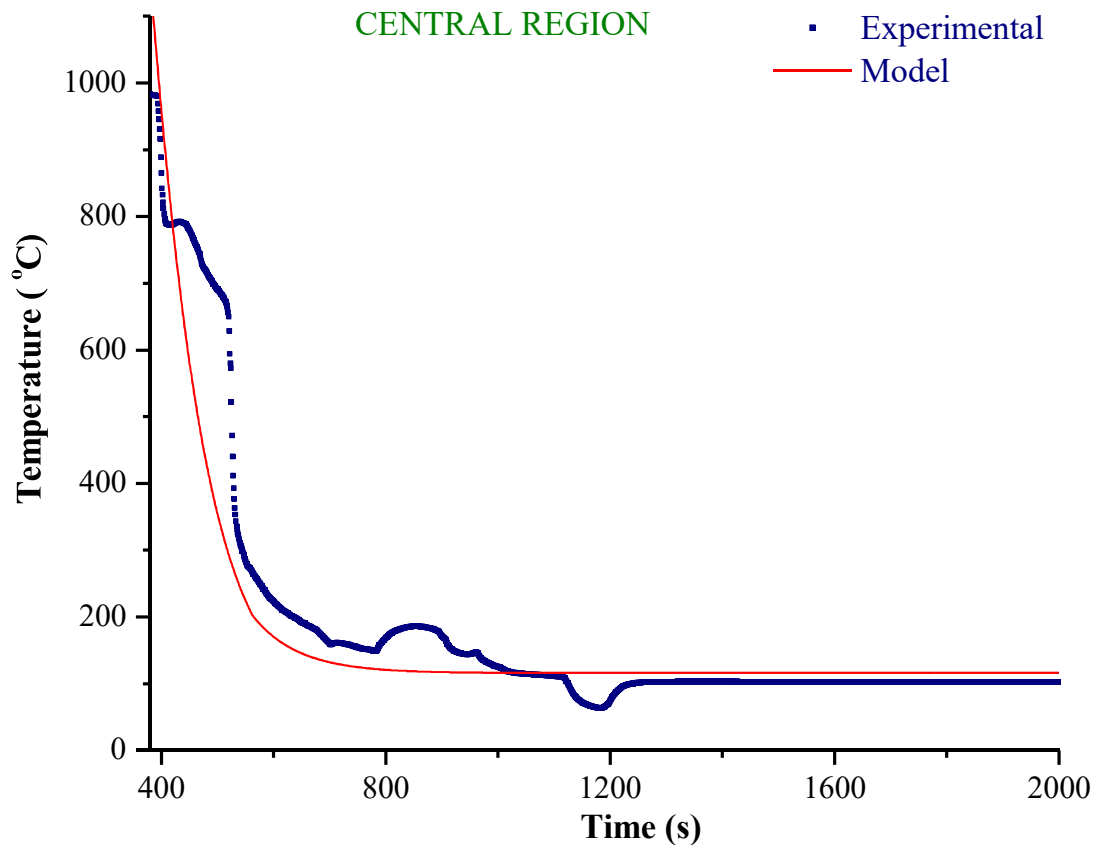


Figure 62: Modeled vis-à-vis measured temperatures at central location of the test section (with decay heat)

The melt pool temperatures variation at half radius region is shown in Figure 63. This is the region of highest porosity and implies to be the eruption site both numerically and experimentally. Due to the highest porosity in this region, there is sharp fall of temperatures. After the sharp fall in the experimental temperature, there is a rise in temperature due to the steady state water inlet flow rate which equals to the rate of steam formation. This has been modeled by changing the boundary condition as sink temperature, i.e.  $T_{inf} = T_{sat}$  (water saturation temperature). Hence, there is a jump in temperature. The plot shows a good agreement in prediction and experimental measurements.

Figure 64 shows the variation in melt pool temperatures near wall region. The porosity was found to be the least in this region and hence the fall of temperatures was slower than other regions.

In this particular region near the wall, the model predictions are slightly away due to the reason that the model considers the debris particles of particular diameters while in actual scenario larger chunks are present in this region because it is away from eruption zone. Also, the effective properties i.e. thermal conductivity ( $k_{\text{eff}}$ ), density ( $\rho_{\text{eff}}$ ) and specific heat ( $C_{p_{\text{eff}}}$ ) have been considered and they all are function of porosity which is difficult to estimate accurately in this region. Thus, model over predicts the temperature variations in this region and hence the gap is seen.

The model predictions in this region too are following the experimental trend.

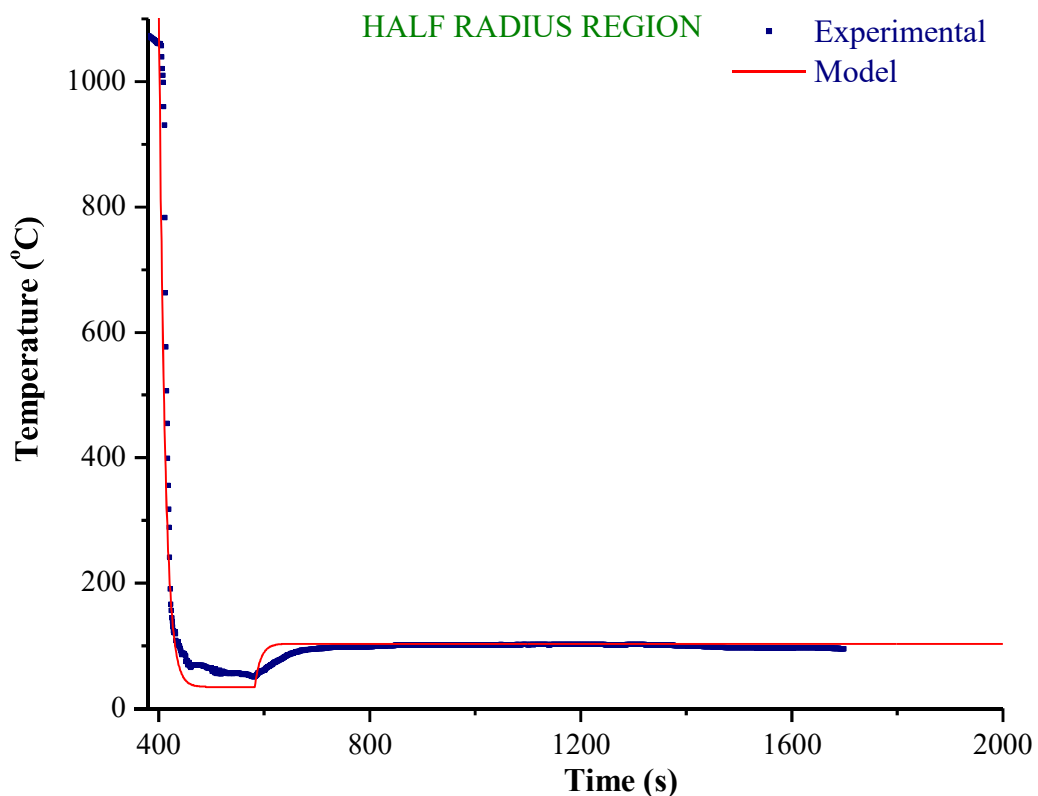


Figure 63: Modeled vis-à-vis measured temperatures at Half Radius of the test section (with decay heat)

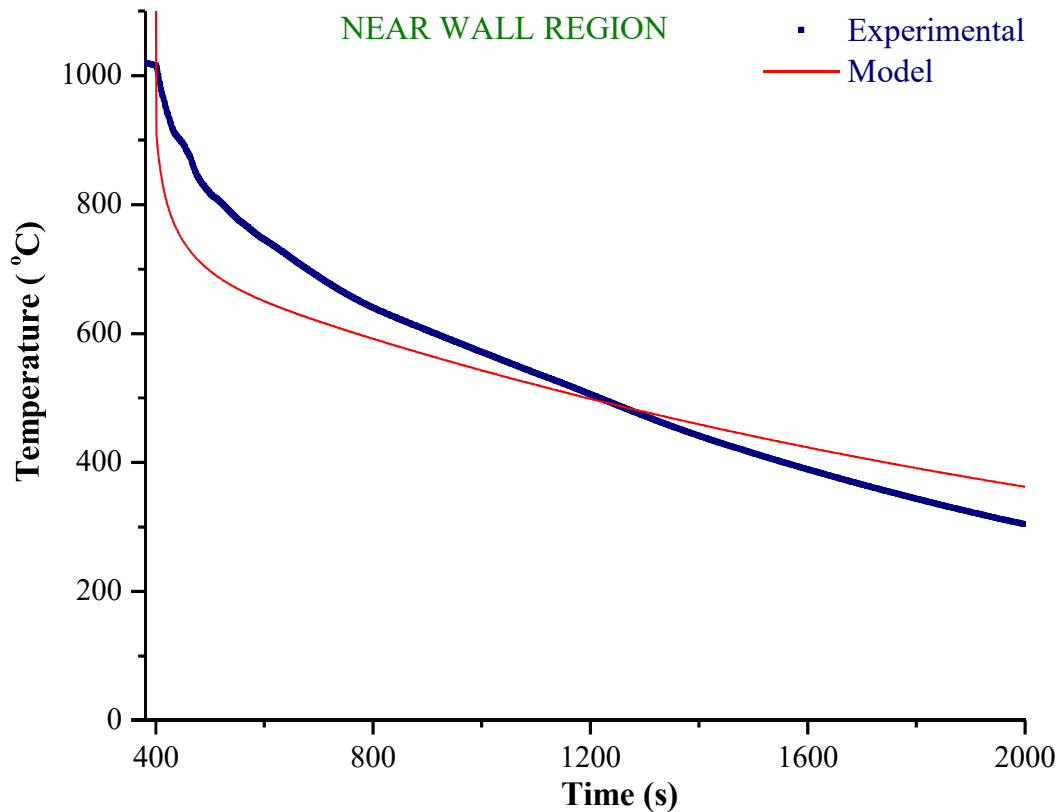


Figure 64: Modeled vis-à-vis measured temperatures near inner wall of the test section (with decay heat)

#### 6.4.2. Case II: Without decay heat scenario

This model was also used to predict the temperature variation in the absence of decay heat. This also was compared with the experimental measurements of the experiment conducted for melt coolability under bottom flooding without decay heat.

Figure 65 shows the variation in melt pool temperatures at the central region. Principal melt eruption occurred at this location in the experiment, so there is a sharp dip in this graph as discussed earlier as well. Present model changes the boundary condition as sink temperature, i.e.  $T_{\text{inf}} = T_{\text{sat}}$  (water saturation temperature) to capture this. Both, numerical prediction and experimental measurements follow the same trend and are in good agreement with each other.

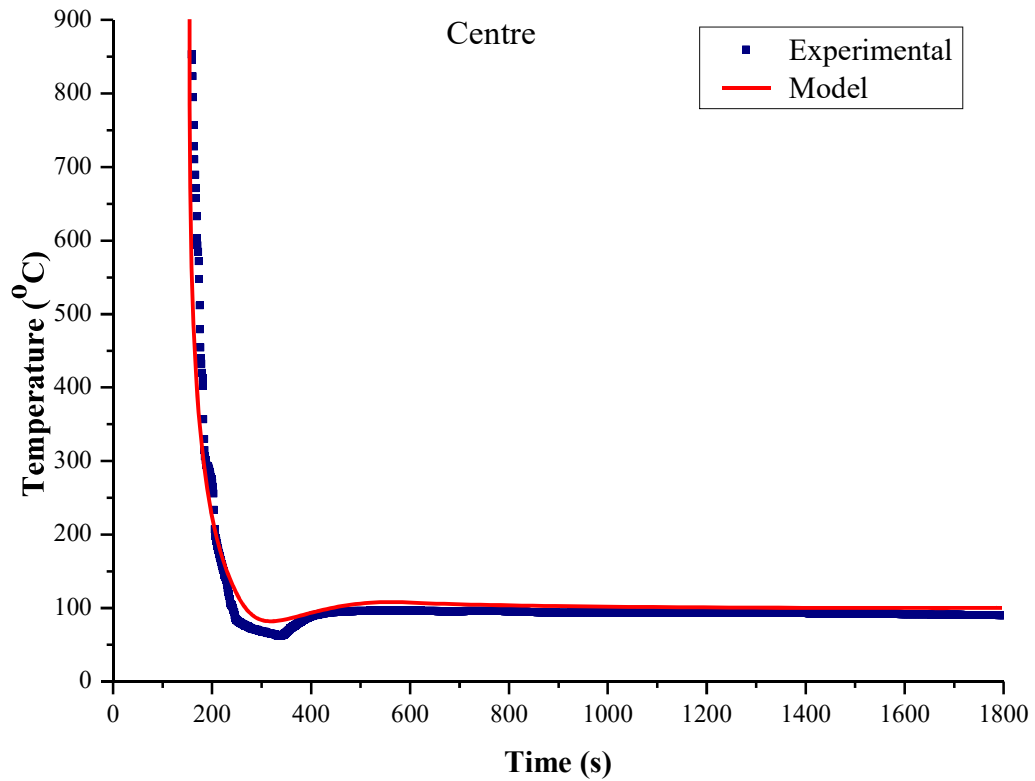


Figure 65: Modeled vis-à-vis measured temperatures at central location of the test section (without decay heat)

The variation in melt pool temperatures at the half radius region is shown Figure 66. Numerical prediction follows the similar trend as the experimental measurements.

The porosity in the region near to the inner wall is lower compared to other regions. This leads to slower fall of temperatures in near wall region as shown in Figure 67. The model predictions in this region as well follow the experimental trend.

In all the cases discussed, the model predictions follow the similar trend as of experimental measurements. However, they are not exact recreations of the measured data. This is because of the various assumptions used to model the phenomenology.

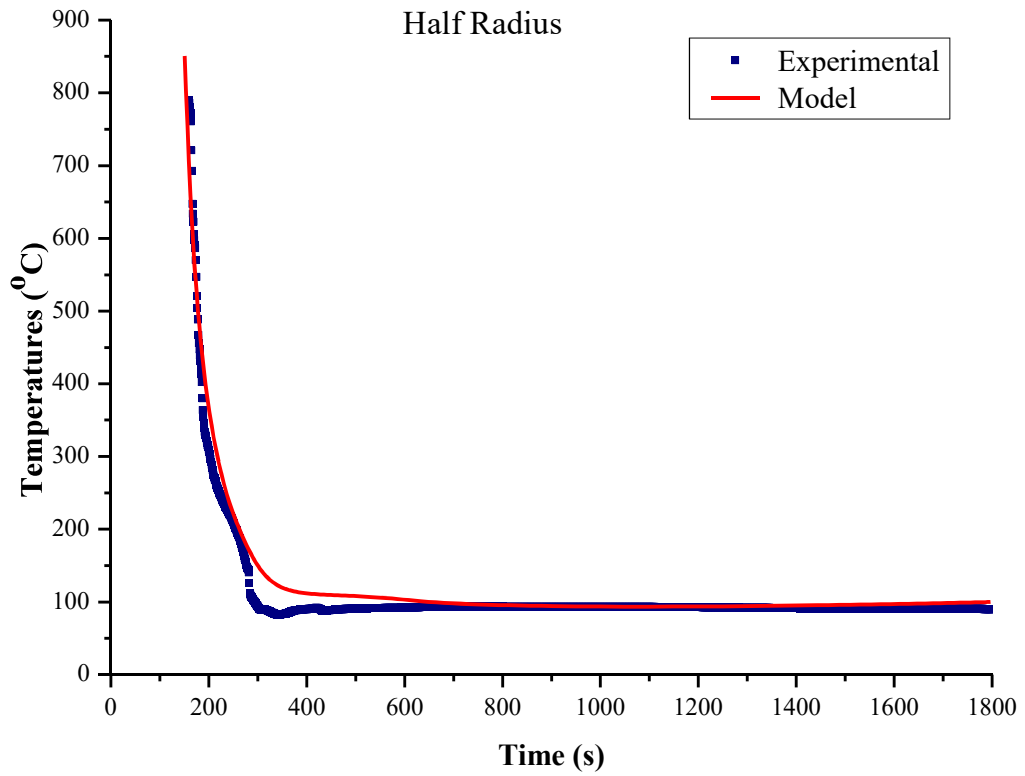


Figure 66: Modeled vis-à-vis measured temperatures at Half Radius of the test section (without decay heat)

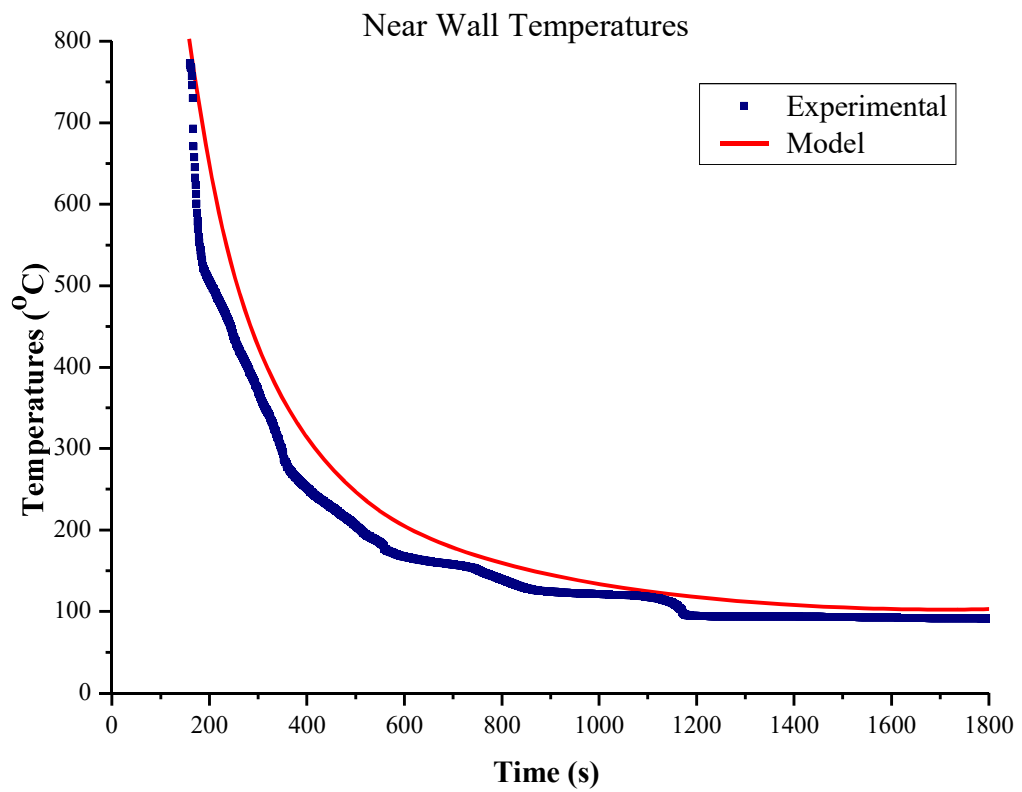


Figure 67: Modeled vis-à-vis measured temperatures near inner wall of the test section (without decay heat)

### 6.5. Summary

A numerical model has been developed to simulate and better understand the melt coolability under bottom flooding with decay heat. The model postulates the formation of crust below the melt pool when water is being inserted from the bottom. The model predicts the failure of this crust due to various stresses, resulting in the inverted cone shaped melt eruption. The model captures this ‘eruption cone’ along with radial variation in porosity. The key inferences obtained from these experimental measurements and numerical predictions are as follows:

- The melt eruption model is able to capture the formation of inverted conical shaped porous zone.
- The radial variation in porosity follows the below mentioned empirical relation within the eruption zone.

$$\varepsilon = 0.753 e^{-11.9 r}$$

- The heat transfer between melt and the cooling fluid is through boiling. Accounting the heat sink term in the energy balance equation predicts better estimates of melt pool temperature variations.
- It has been observed both numerically and experimentally, that the quenching of the melt takes place within a few seconds and the cooling of the debris also achieved within a few minutes under bottom flooding even in the presence of decay heat.

It can thus be concluded that the present model is able to capture the phenomenology of melt eruption and the melt coolability under bottom flooding with and without decay heat simulation.



# Chapter

*“Only those who attempt the absurd will  
achieve the impossible”*

— *Maurits Cornelis Escher (17 June 1898 – 27 March 1972)*  
*Dutch graphic artist*

## CANON'S YEOMAN'S TALE

- Geoffrey Chaucer, "The Canterbury Tales"

*"And how, d'you think? It happens, like as not,  
There's an explosion and goodbye the pot!  
These metals are so violent when they split  
Our very walls can scarce stand up to it.  
Unless well-built and made of stone and lime,  
Bang go the metals through them every time  
And some are driven down into ground  
- That way we used to lose them by the pound-  
And some are scattered all about the floor;  
Some even jump into the roof, what's more.*

.....

*Some said the way the fire was made was wrong;  
Others said, 'No - the bellows. Blown too strong.'  
That frightened me, I blew them as a rule  
'Stuff!' said a third. 'You're nothing but a fool,  
It wasn't tempered as it ought to be.'  
'No!' said a fourth. 'Shut up and listen to me;  
I say it should have been a beech-wood fire  
And that's the real cause, or I'm a liar.'  
I've no idea why the thing went wrong;  
Recriminations though were hot and strong.  
Well,' said my lord, 'there's nothing more to do.  
I'll note these dangers for another brew;  
I'm pretty certain that the pot was cracked,  
Be that as may, don't gape! We've got to act.  
Don't be alarmed, help to sweep up the floor  
Just as we always do, and try once more."*

## **Chapter 7. MELT COOLABILITY DURING WET CONDITIONS IN A CORE CATCHER: FUEL COOLANT INTERACTION**

### **7.1. Introduction**

In a nuclear reactor, water may present in the reactor containment due to various possible reasons like leakage accidents, etc. During severe accidents involving core melting, the corium may relocate into the containment and may interact with this already present water. This situation is regarded as wet containment or wet core catcher (in case water is present in the core catcher) condition. This interaction of corium with the coolant water present in the containment is generally termed as fuel-coolant interaction (FCI). After Fukushima Daiichi accident, it is clear that the structural integrity of containment during such accidents has to be maintained[106]. There is a concern that due to FCI, steam explosions may occur, which may threaten the integrity of containment due to dynamic pressure loads. Thus, phenomenology of steam explosion should be understood and should be avoided to occur so as to minimize its consequences.

Steam explosion[107]–[109] occurs when rapid and coherent heat transfer between the melt and coolant occurs. It progresses in four distinct phases as described:

1. Premixing phase

In this phase, the melt and coolant interact and undergo fragmentation owing to the hydrodynamic forces which results from Rayleigh-Taylor and Kelvin-Helmholtz instabilities of the system. Due to high melt temperature, a vapour blanket insulates the melt from water and hinders subsequent heat transfer. This

meta-stable state is usually referred as the premixing phase, as shown in Figure 68(a).

## 2. Triggering phase

The event which destabilizes the vapour blanket such that the melt and coolant comes in contact is called as trigger. Due to this vapour film collapses; there is a rapid heat transfer and rapid rise in pressure in some local region. Film destabilization may occur due to external pressure pulse resulting from impact of melt on bottom of the tank or vessel, thermal film destabilization, and coolant entrapment within the melt. This stage is called as the triggering phase, as shown in Figure 68(b).

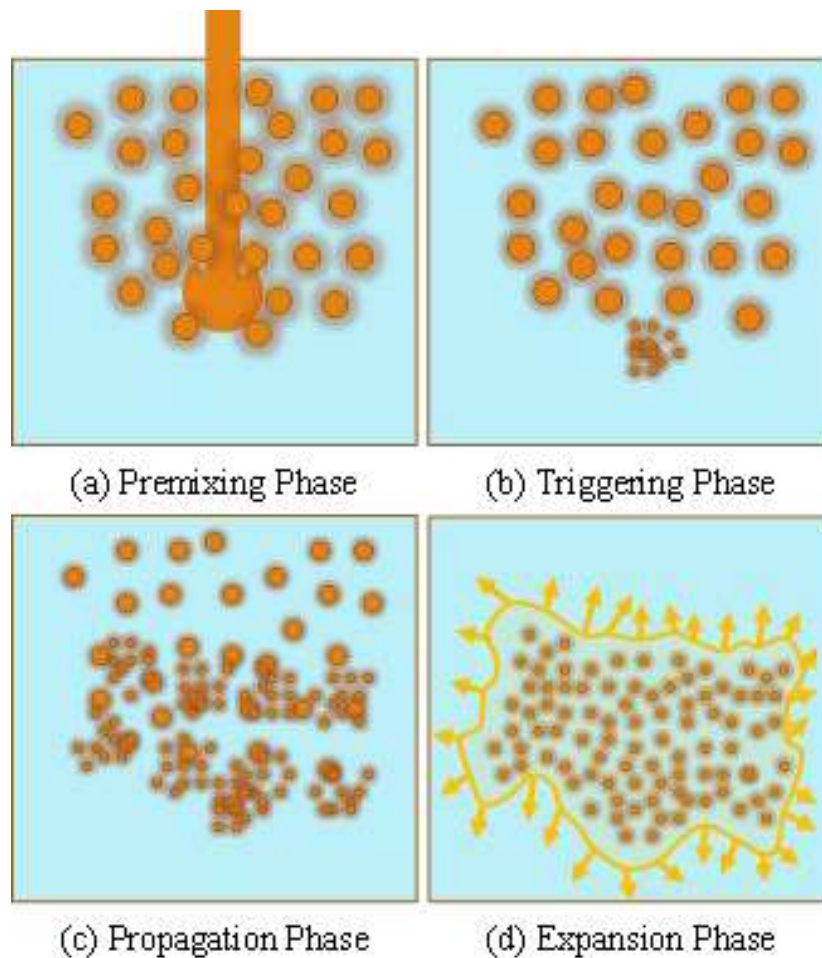


Figure 68: Steam explosion and its phases of occurrence

### 3. Propagation phase

In favourable circumstances, the pressure pulse from previous phase can escalate further vapour film collapse leading to further heat transfer and rapid pressure rise. This propagating pressure pulse collapses the vapour blankets around the melt fragments present in the premixture, causing coherent energy release and further fragmentation of melt. This results in intense heat transfer from the melt to coolant. This process is known as the propagation phase as shown in Figure 68(c).

### 4. Expansion phase

Further swelling of high pressure mixture behind the propagation front against the inertial constraints imposed by the surroundings leads to the potential to cause damage to any surrounding structures. This phase is generally called as the expansion phase, as shown in Figure 68(d).

Steam explosion has been studied intensively for a few decades, as discussed in [section 1.6.1](#) of chapter 1. In the literature, several experiments have been performed with simulants as well as with prototypic materials to evaluate the resulting pressure rise due to FCI and melt fragmentation behaviour. In all these studies, tests have been performed using simulant melts from a few grams to nearly 100 kg which were poured into varying amount of water to study this behaviour. In some cases, steam explosion occurred while in others it did not. However, all these studies are unable to explain the conditions for steam explosion. Moriyama[96] suggested that steam explosion occurs when the fine fragments i.e. the particles of the order of 0.1 mm in size or below formed during fragmentation and constitute about 10-50% on debris mass considering the history of melt fragmentation in the prior experiments, as shown in Figure 13. This raised a question, that, whether the presence of fine fragmentation is the root cause of

steam explosion? To investigate this, a series of experiments were performed by us to study the fragmentation behaviour of ceramic oxides in water and the effects of melt-to-water ratio on it. All these experiments were performed in two different facilities. In the following sections, results and insights from the experiments have been discussed.

## 7.2. Experiments conducted

Experiments were conducted using the CaO-B<sub>2</sub>O<sub>3</sub> melt with varying masses, i.e. 50g, 500g, 700g, 1000g, 2000g and 2300g, poured into the water pool of 4.5 litres.

### 7.2.1. Test section details

Two different test set-ups were used to conduct experiments with different melt masses. These experimental set-ups are discussed in detail in [section 2.5](#) of chapter 2. Experiment with 50g of melt was performed in the small scale test set-up. The melt generated using induction furnace was poured into the test section of 6 litres water capacity (150mm x 150mm x 300mm) as shown in Figure 20. Experiments with higher melt masses were performed in the large scale set-up. Its test section was having 12 litres capacity made of a steel vessel of 130 mm diameter and 500 mm height as shown in Figure 21. Both these set-ups were instrumented with piezoelectric dynamic pressure transducers to measure the dynamic pressure peak within the water pool. These transducers were connected to a computer based fast acting data acquisition system, which was used to record the dynamic pressure history.

### 7.2.2. Operating procedures

The water pool of 4.5 litres was maintained at about 300 K temperature in all the experiments. CaO-B<sub>2</sub>O<sub>3</sub> was used to be melted in the furnace and poured into the test section once temperature close to 1200°C was reached. About 50 g

to 2500 g of varying melt mass was poured into the water pool in different set of experiments to understand the influence of melt-to-water ratio on FCI. Just before pouring, the fast data acquisition to record dynamic pressure was activated. After the experiment, the debris were brought out of the test section for analysis and related studies.

### 7.3. Results and discussions

#### 7.3.1. Melt-to-water Ratio of 0.011 (Melt mass = 50 g; water mass = 4500 g)

About 50g of CaO-B<sub>2</sub>O<sub>3</sub> was melted and heated up to 1500 °C so as to ensure that the mixture is completely melted and having sufficient super-heat before pouring.

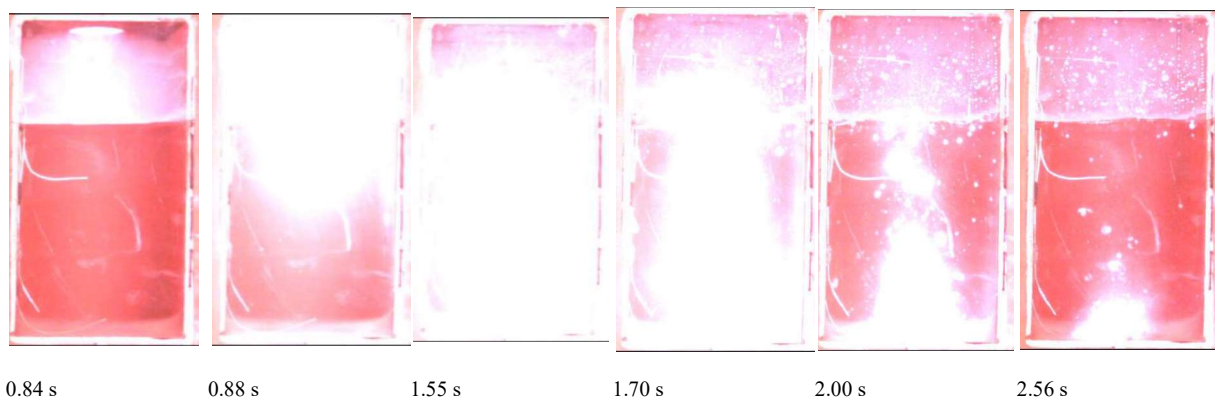


*Figure 69: Visuals from high speed shooting of FCI*

The molten simulant was then poured into the test section having the water pool as shown in Figure 69. It can be seen from the figure that the melt interacts with water at 1.55s. The bright light covering the entire face of test section was the heat coming out of the steam formed upon FCI. It seems that huge energetic interaction occurred, water was also seen sloshing within the test section; but no energetic pressure spike was measured. No dynamic pressure peak was observed in this case, as shown in Figure 70.

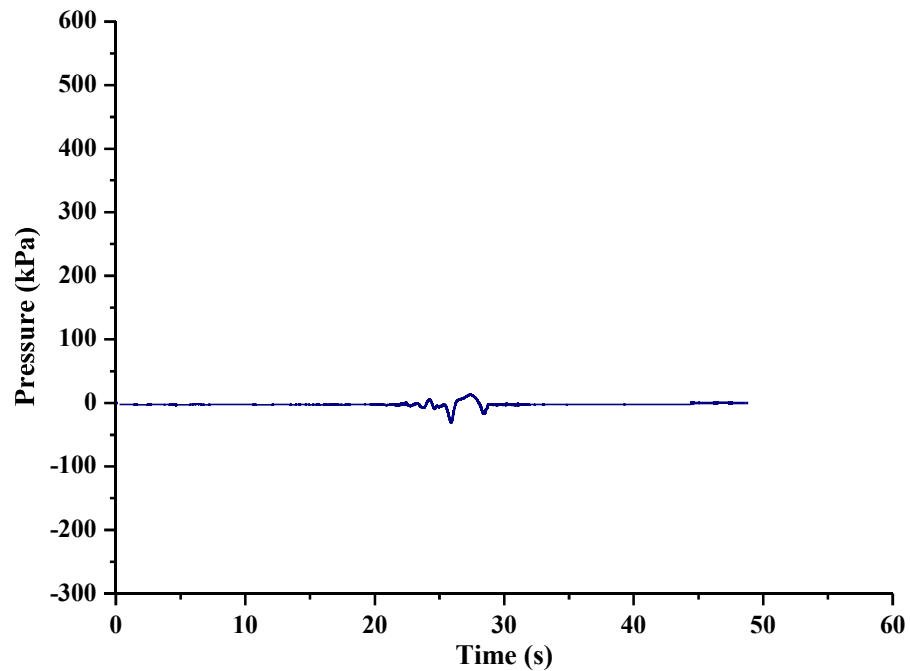
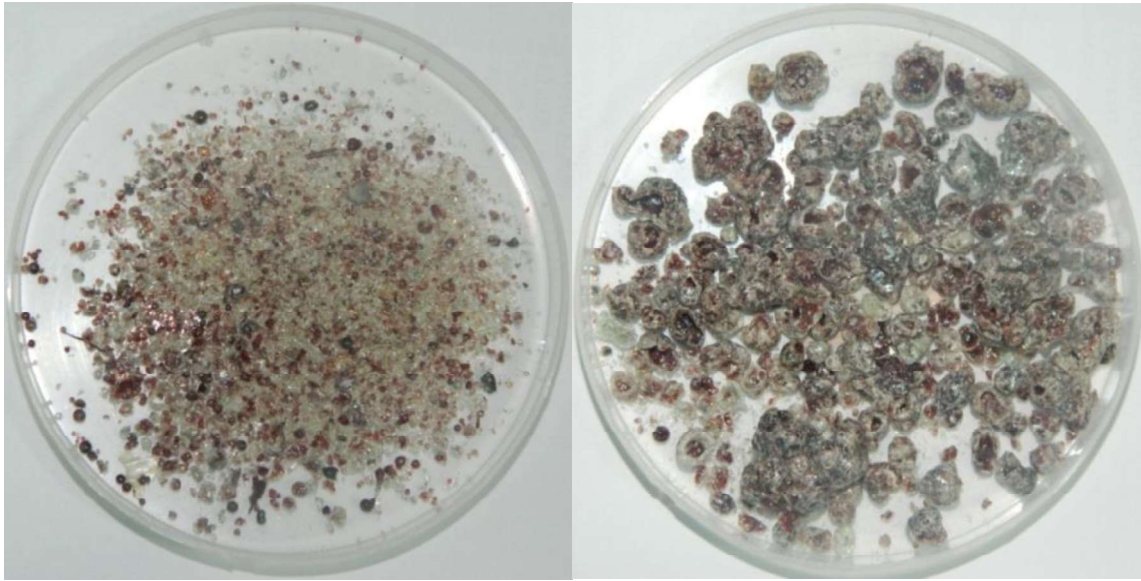


Figure 70: Dynamic pressure peak versus time curve for  $M/W$  ratio=0.011

After opening the test section, fine particulate and porous globular debris were obtained as shown in Figure 71. The debris mainly constituted large porous globular structure and some fine crystals (formed mainly because of crushing of surfaces of larger debris). Such globular debris may have been formed due to ballooning effect caused by the generated steam while interacting with molten material. This also has led to the formation of porosity within these debris. Due to this ballooning effect, there is an increase in area of melt-water contact from both sides (inside and outside walls of globular debris), and hence rapid heat transfer from melt to the water. The debris were so fragile that most of them were breaking even while handled softly, and contributed to fine particulates. To further analyse the debris, microscopic analysis was performed as shown in Figure 72, which shows the morphology and particulate diameters. It is clearly visible that along with the porous and globular debris, some fine solid round particles were also present.



*Figure 71: Fine particulate and porous globular debris of small volume experiment*

*(Scale: 1cm of image = 2 cm of actual size)*

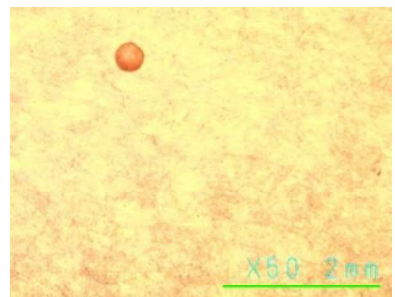
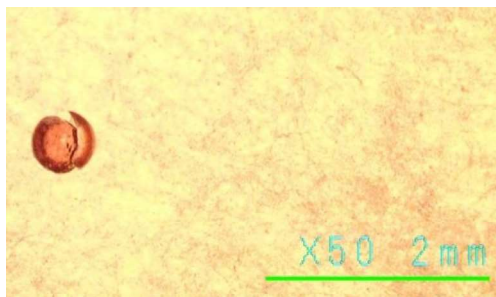
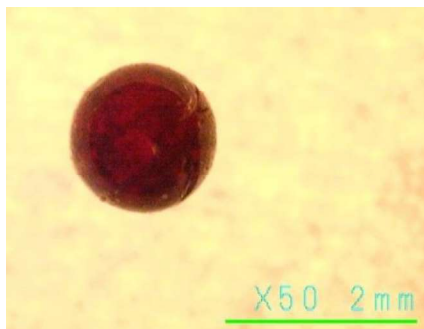


*Figure 72: Microscopic analysis of debris from small melt volume experiment*

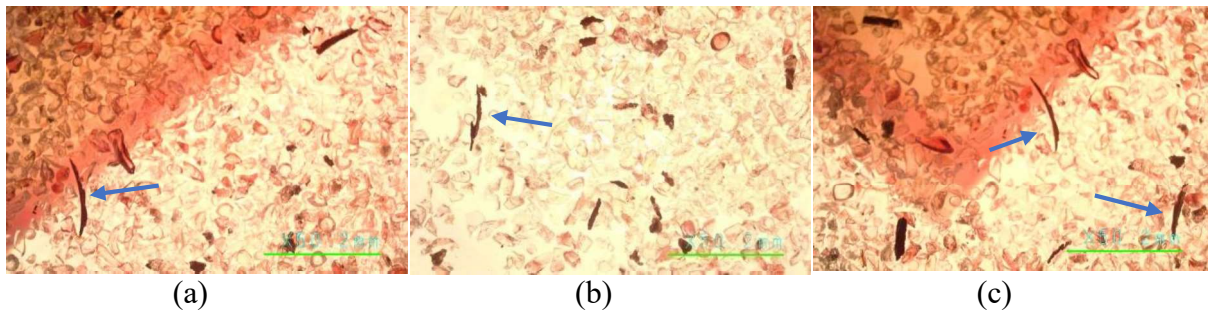


Figure 73: Microscopic analysis of fine particulate of small melt volume experiment (Scale: 1 cm = 8 mm)

However, the diameter of these solid round particles were close to 0.5-1 mm. Figure 73 presents the enlarged images of fine particulates in different regions of the petri-dish they were kept in. This figure contains small strands known as Pele's hair (marked with an arrow in the figure), observed during the experiment. The presence of Pele's hairs suggests high shear between the melt and steam formed during the interaction.

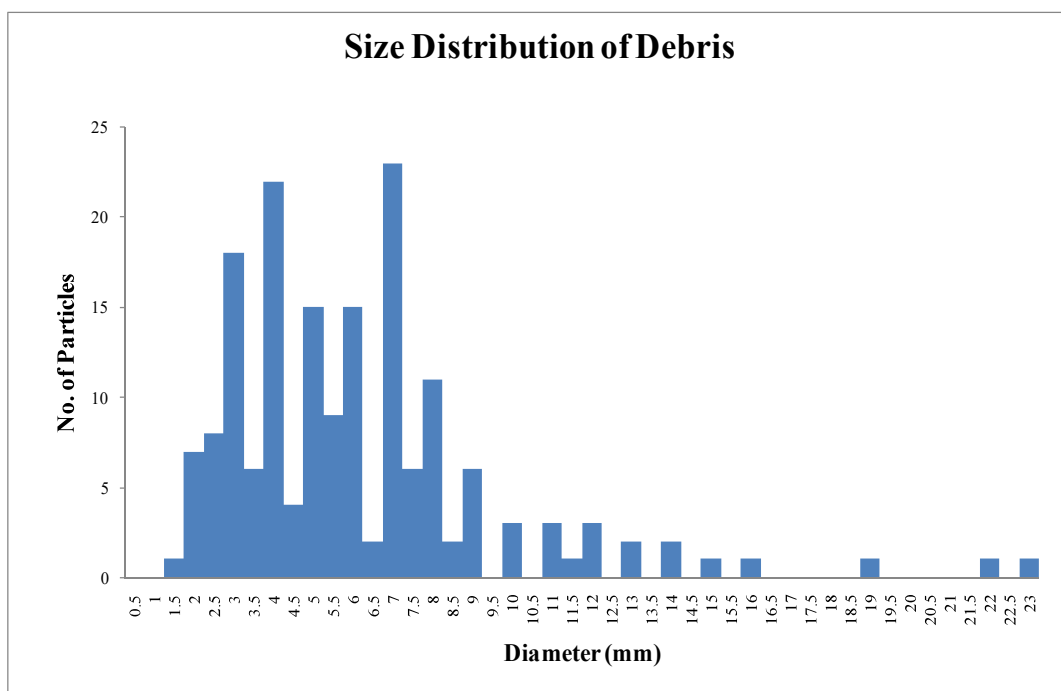


Figure 74: Debris particle size distribution of small melt volume experiment

The size distribution of the globules is shown in Figure 74. It was observed that porous globule sizes ranging from 1.5 mm diameter to 23 mm diameter were observed, most of them lie in between 2 mm to 9 mm diameter.

### 7.3.2. Melt-to-water Ratio of 0.11 (Melt mass = 515 g; water mass = 4500 g)

In this case, about 515 g of CaO-B<sub>2</sub>O<sub>3</sub> was melted and heated nearly up to 1200 °C and was poured into 4.5 litres of water pool. No dynamic pressure peak was observed in this case, shown in Figure 75.

The debris obtained after opening the test section were analysed. Porous globular debris of sizes ranging from a few mm to 25 mm were obtained; along with long thread like structures formed due to shear between melt and steam known as Pele's hair were obtained (Figure 76). Most prominent range of particles was observed between 5 to 15 mm as shown in Figure 77.

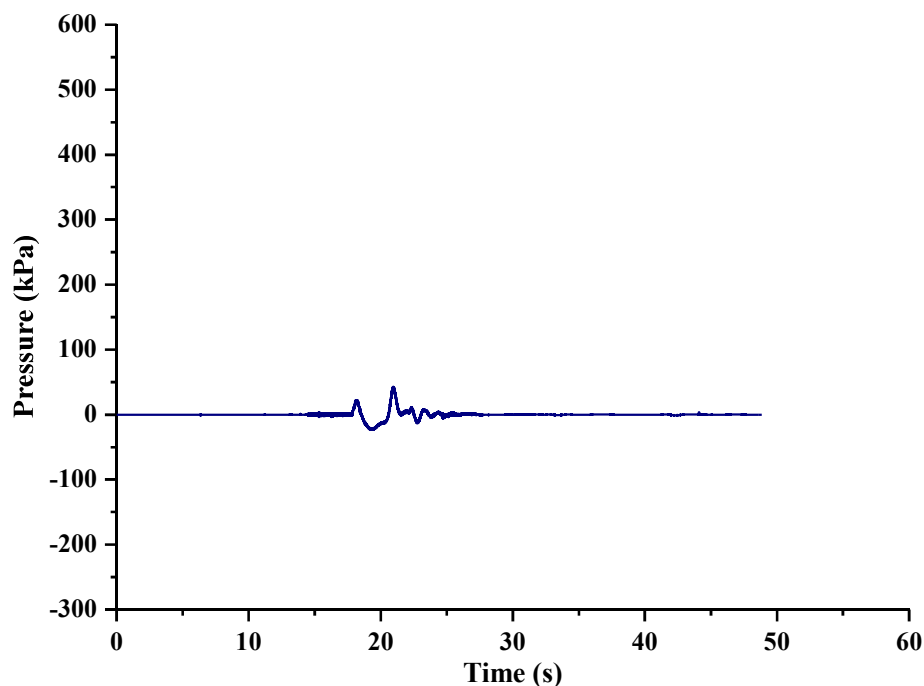


Figure 75: Dynamic pressure peak versus time curve for M/W ratio=0.11



Figure 76: Debris obtained from experiment with  $M/W=0.11$

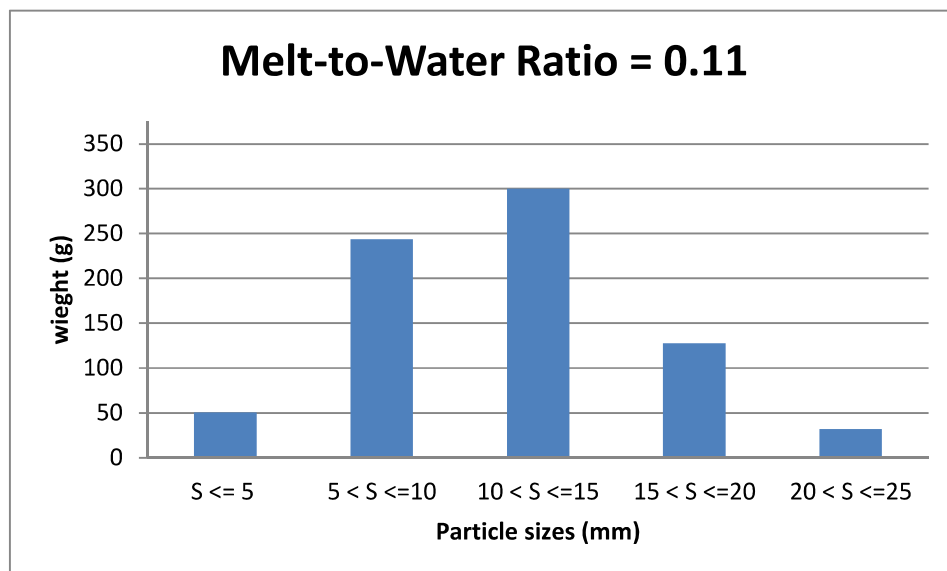


Figure 77: Debris particle size distribution of experiment with  $M/W=0.11$

### 7.3.3. Melt-to-water Ratio of 0.16 (Melt mass = 710 g; water mass = 4500 g)

About 710 g of CaO-B<sub>2</sub>O<sub>3</sub> was melted and heated nearly up to 1200 °C and was poured into similar 4.5 litres of water pool. No dynamic pressure peak was observed in this case, shown in Figure 78.

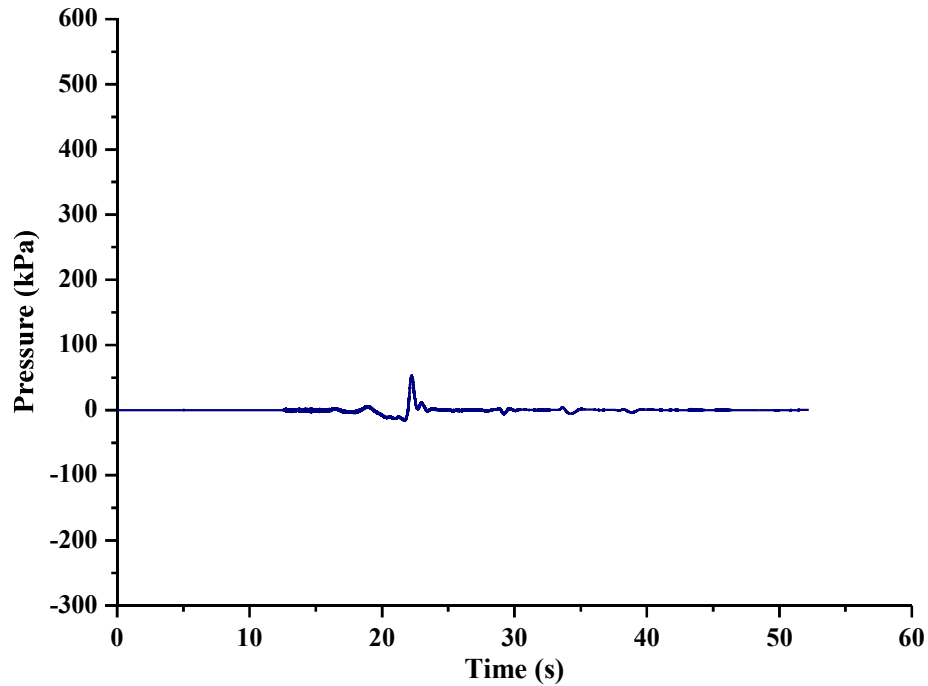


Figure 78: Dynamic pressure peak versus time curve for  $M/W$  ratio=0.16

The debris obtained in this case were porous globular of sizes ranging from a few mm to 38 mm; along with long thread like structures formed due to high shear between melt and steam known as Pele's hair (Figure 79). Most prominent range of particles was observed between 5 to 20 mm, as shown in Figure 80.



Figure 79: Debris obtained from experiment with  $M/W=0.16$

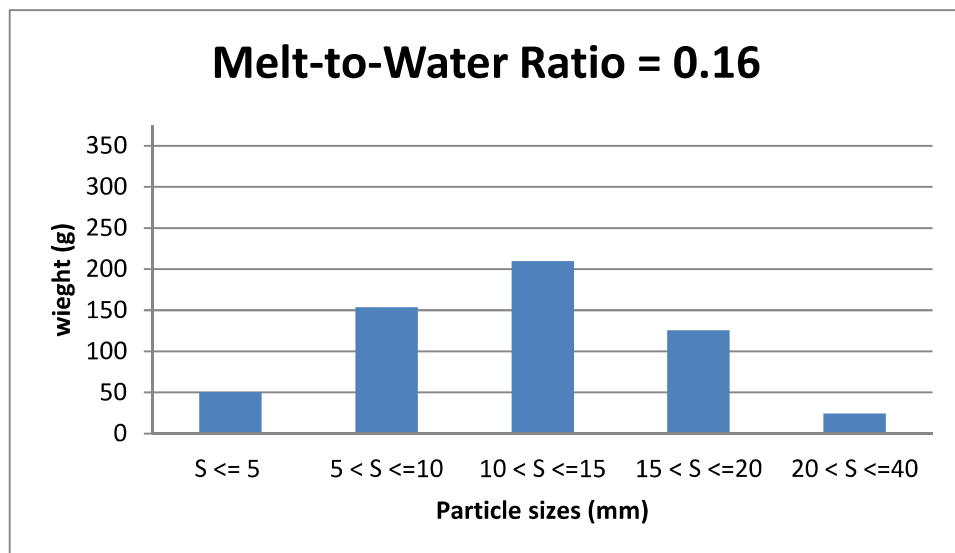
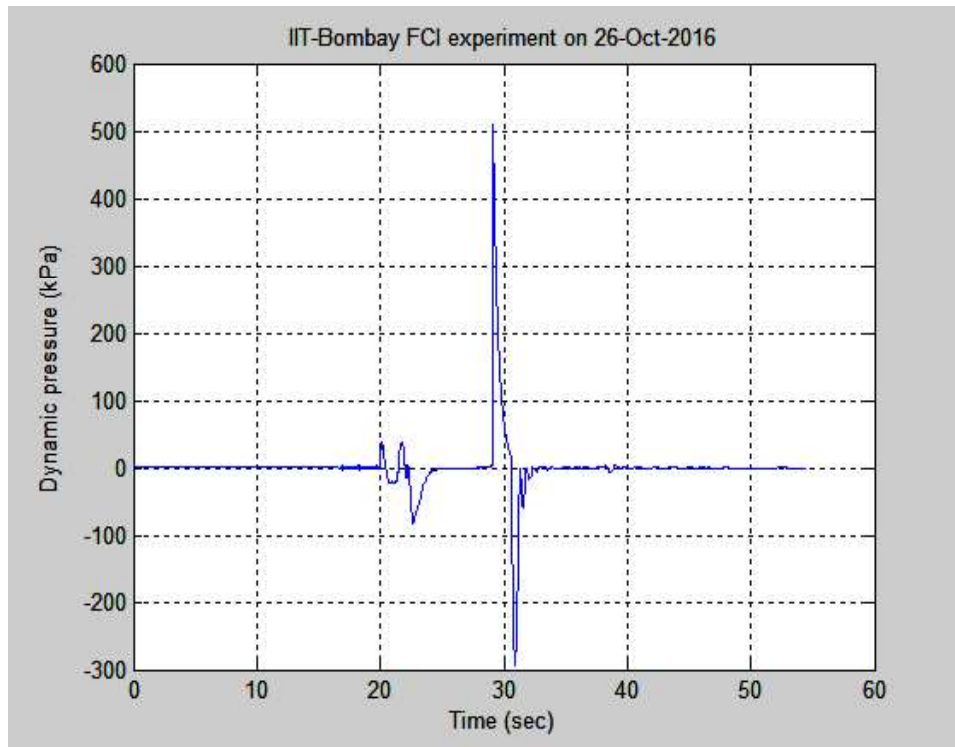


Figure 80: Debris particle size distribution of experiment with  $M/W=0.16$

#### 7.3.4. Melt-to-water Ratio of 0.21 (Melt mass = 925 g; water mass = 4500 g)

About 925 g of  $\text{CaO-B}_2\text{O}_3$  was melted and heated nearly up to  $1200^\circ\text{C}$  and was poured into similar 4.5 litres of water pool. Dynamic pressure peak of 506 kPa

was observed in this case, shown in Figure 81. This peak has two parts, positive and negative, which aroused mainly due to compression and rarefaction of the pressure wave. This is discussed in detail in the last section of this article.



*Figure 81: Dynamic pressure peak versus time curve for  $M/W$  ratio=0.21*

The debris obtained in this case were porous globular debris of sizes ranging from a few mm to 42 mm; along with Pele's hair as shown in Figure 82. Number of agglomerated debris was more in this case. Most prominent range of particles was observed between 5 to 20 mm.



*Figure 82: Debris obtained from experiment with  $M/W=0.21$*

#### 7.3.5. Melt-to-water Ratio of 0.41 (Melt mass = 1846 g; water mass = 4500 g)

About 1846 g of  $\text{CaO-B}_2\text{O}_3$  was melted and heated nearly up to  $1200\text{ }^\circ\text{C}$  and was poured into similar 4.5 litres of water pool. Dynamic pressure peak of 467 kPa was observed in this case, shown in Figure 83. Behaviour of the peak was similar to the previous case.

Mostly porous globular debris of sizes ranging from a few mm to 42 mm were obtained as shown in Figure 84. Most prominent range of particles was observed between 5 to 30 mm.

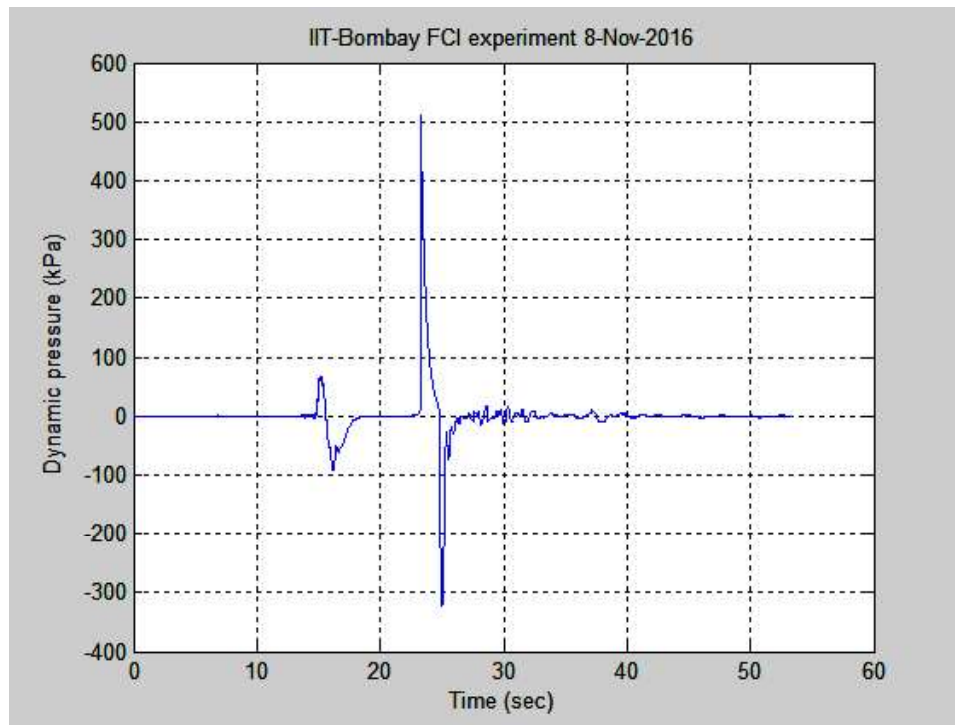


Figure 83: Dynamic pressure peak versus time curve for  $M/W$  ratio=0.41



Figure 84: Debris obtained from experiment with  $M/W=0.41$

### 7.3.6. Melt-to-water Ratio of 0.51 (Melt mass = 2285 g; water mass = 4500 g)

About 2285 g of CaO-B<sub>2</sub>O<sub>3</sub> was melted and heated nearly up to 1200 °C and was poured into similar 4.5 litres of water pool. Dynamic pressure peak of 510 kPa was observed in this case, shown in Figure 85; with the similar behaviour as it was in previous case.

Porous globular debris of sizes ranging from a few mm to 42 mm were obtained as shown in Figure 86. Most prominent range of particles was observed between 5 to 20 mm.

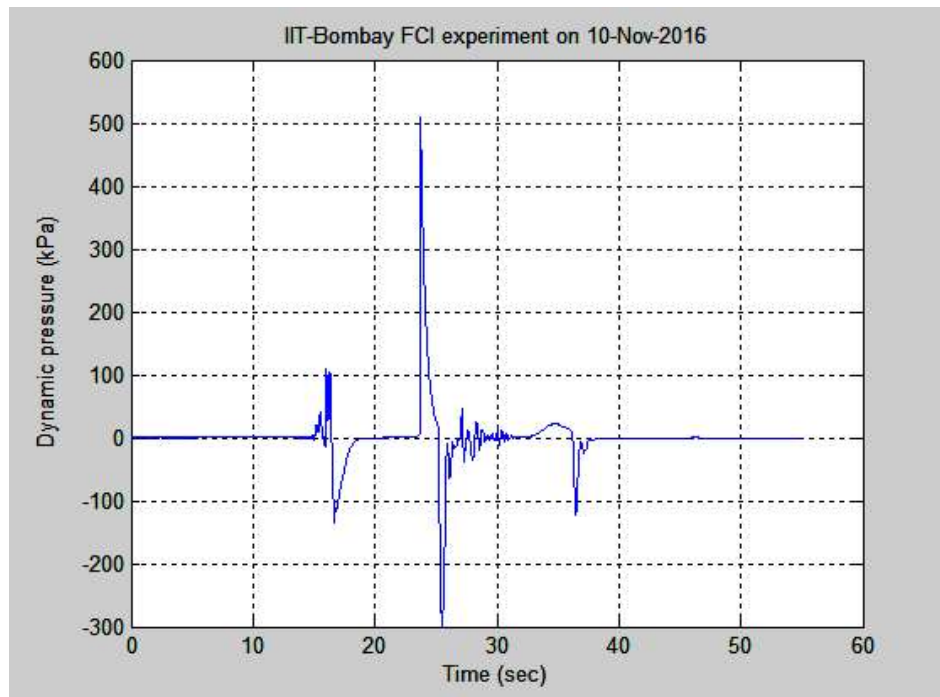


Figure 85: Dynamic pressure peak versus time curve for M/W ratio=0.51



*Figure 86: Debris obtained from experiment with  $M/W=0.51$*

The results obtained from the presented study show the following

- Sudden pressure spike was observed for the melt-to-water ratio greater than 0.21.
- Larger melt-to-water ratio leads to the increase in number of agglomerated debris.

#### 7.4. Role of conversion efficiency

It was observed that large pressure spikes occurred in the cases with larger melt-to-water ratio, even though fine fragments were absent in these cases. If we consider the conclusions from the Moriyama's[96] fine fragmentation theory saying that fine fragments present during FCI leads to steam explosion; the pressure spikes observed in the present study were found unexplainable as fine fragments were not present in this case. When our results were plotted on the Moriyama's curve, it is found that the results of the present study are lying in the no explosion zone as shown in Figure 87.

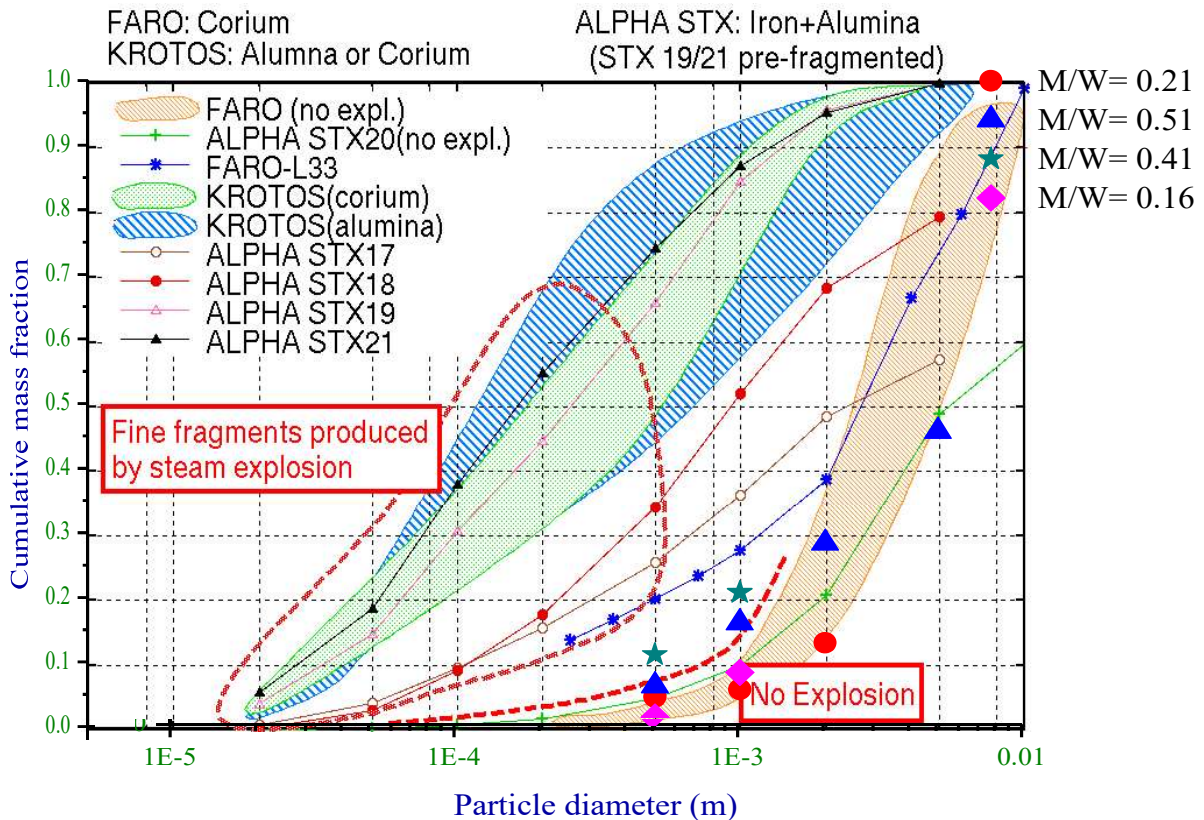


Figure 87: Analysis of present experiments using Moriyama's theory

Since the fragmentation theory could not explain the pressure spike observed during the FCI, we have attempted to explain the physics using the concept of conversion efficiency.

Sehgal[106] has explained the conversion efficiency as *the ratio of the mechanical energy output to the total thermal energy content of the molten mass mixed with water at the time the explosion occurs. 'Efficiency' is the conversion ratio expressed as a percentage of the melt thermal energy.*

To evaluate the mechanical energy imparted by the dynamic pressure wave, the wave power was evaluated. In a medium, the wave power is given by Landau and Lifshitz[110] as

$$P = \frac{Ap^2}{\rho c} \cos \theta \quad \dots (27)$$

Where,

- $A$  is the area of the surface;
- $p$  is the pressure of the peak;
- $\rho$  is the mass density of medium;
- $c$  is the sound velocity in the medium;
- $\theta$  is the angle between the direction of propagation of the wave and the normal to the surface (it is  $0^\circ$  here).

This power was then converted into the total mechanical energy output by dividing it by the duration of the peak in all cases. Evaluation of the ratio of mechanical energy over total thermal energy gives the conversion efficiency.

The conversion efficiencies for all the prior experiments were calculated from the literature and were found lying in the range of 0.3-12.7% (Table 5 and Table 6), and most of them were close to 0.8%. The duration of their peaks were lying in the range of 2-200 milliseconds. The conversion efficiencies for our tests were also found to be in the range of 0.3 to 0.70%, which is of similar order (Table 7).

Table 5: Conversion efficiencies for Alumina melt as given in the KROTOS literature

S. No	Melt mass	Melt Temperature	Thermal energy	Water volume	Mechanical Energy	Conversion efficiency	Explosion
			$E_{\text{thermal}}$		$E_{\text{pressure}}$	$\eta$	
	<b>Kg</b>	<b>K</b>	<b>kJ</b>	<b>l</b>	<b>kJ</b>	<b>%</b>	
1.	1.522	2665	5040.0	34	95.3	1.52	Yes
2.	1.47	3073	5707.4	34.6	60.1	0.87	
3.	1.539	2465	4665.3	34.6	109.1	2.13	
4.	1.5	2625	4883.1	34.6	76.8	12.7	
5.	1.5	2673	4983.9	33.2	153.2	2.48	
6.	1.47	2688	4915.1	34	46.1	2.41	

Table 6: Conversion efficiencies of  $ZrO_2$  and corium melts as given in TROI literature

S.No	Melt mass	Melt Temperature	Thermal energy	Water volume	Pressure peak	Peak duration	Mechanical Energy	Conversion efficiency	Explosion
			$E_{thermal}$				$E_{pressure}$	$\eta$	
	Kg	K	kJ	l	kPa	s	kJ	%	
1.	5	>3373	12524.5	~280	1000	0.02	11084.2	0.885	Yes
2.	4.2	>3373	10520.6	~280	2100	0.0025	8942.5	0.85	
3.	2.9	3373	7264.2	~280	900	0.008	3588.5	0.494	
4.	8.4	3800	16614.0	~280	1000	0.02	11081.5	0.667	
5.	7.7	2600	10008.9	~280	7000	0.02	90470.7	9.039*	
6.	6.5	3000	9918.1	~280	800	0.02	7418.7	0.748	
*this was a triggered explosion									

Table 7: Conversion efficiencies for the present tests

S.No	Melt mass	Melt Temperature	Thermal Energy	Water volume	Water height	Pressure peak	Mechanical Energy	Conversion efficiency	Explosion
			$E_{thermal}$				$E_{pressure}$	$\eta$	
	kg	K	kJ	l	m	kPa	kJ	%	
1.	0.925	1409	1982.2	4.5	0.27	506	13.1	0.7	Yes
2.	1.846	1407	3955.9	4.5	0.27	467	13.1	0.33	
3.	2.285	1399	4896.7	4.5	0.27	510	13.0	0.3	

So, using 0.8% as the conversion efficiency and respective peak durations, the mechanical energy imparted in the form of dynamic pressure peak was estimated for all previous experiments and presented in Table 8. It was observed that the estimated peak value is close to that of measured peak value. This explains that the amount of thermal energy converting into mechanical energy, is more important deciding factor for steam explosion to occur compared to the presence of fine fragments.

### 7.5. Role of thermal cavitation in explaining steam explosion

As discussed above, during the fuel coolant interaction, the thermal energy of the melt gets dissipated locally into the water pool, which forms a large bubble locally. This leads to thermal cavitation (Brennen[111]).

Table 8: Analysis of various experimental studies performed so far using conversion efficiency theory

Obtaining Pressure Peak From Conversion Ratio														
Expt	Melt	Melt mass	Melt Temperature	Energy IN	Water volume	Water height	Test section Diameter	Area	Conversion efficiency	Mech Energy	Estimated Pressure peak	Explosion	Measured Pressure peak	
				$E_{\text{internal}}$					$\eta$	$E_{\text{pressure}}$				
		kg	K	kJ	l	m	m	m <sup>2</sup>	%	kJ	kPa		kPa	
5	CaO-B <sub>2</sub> O <sub>3</sub>	0.925	1409	1982.3	4.5	0.27	0.13	0.11	0.8	1585.8	462	Pressure Spike	506	
7		1.846	1407	3956.0	4.5	0.27	0.13	0.11	0.8	3164.8	413		467	
8		2.285	1399	4896.8	4.5	0.27	0.13	0.11	0.8	3917.4	459		510	
9	Sodium Borosilicate Glass	1.885	1406	1856.7	4.5	0.27	0.13	0.11	0.8	1485.4	447		510	
38	KROTOS	1.522	2665	5040.0	34	1.1	0.2	0.691	0.8	4032.0	930		1000	
40		1.47	3073	5707.4	34.6	1.1	0.2	0.691	0.8	4565.9	990	Yes	1000	
42		1.539	2465	4665.3	34.6	1.1	0.2	0.691	0.8	3732.3	895		1000	
43		Alumina	1.5	2625	4883.1	34.6	1.1	0.2	0.691	0.8	3906.5	916		1000
44		1.5	2673	4983.9	33.2	1.1	0.2	0.691	0.8	3987.1	925	Yes	1000	
49		1.47	2688	4915.1	34	1.1	0.2	0.691	0.8	3932.1	919		1000	
1	TROI	5	>3373	12524.6		0.67	0.65	1.37	0.8	10019.7	737		1000	
4		ZrO <sub>2</sub>	4.2	>3373	10520.7		0.67	0.65	1.37	0.8	8416.5	1911		2100
5		2.9	3373	7264.3		0.67	0.65	1.37	0.8	5811.4	888		900	
12		8.4	3800	16614.0		0.67	0.65	1.37	0.8	13291.2	849	Yes	1000	
13		Corium	7.7	2600	10008.9		0.67	0.65	1.37	0.8	8007.2	659*		7000*
14		6.5	3000	9918.1		0.67	0.65	1.37	0.8	7934.5	656		800	

\*Triggered explosion

At the interaction surface between steam and water, the steam gets trapped (may be due to pressure exerted by the water or due to localized condensation at this interface). Thus, the bubble formed here is not a perfect vacuum but a region with relatively low steam pressure. This kind of low pressure bubble in a liquid begins to collapse due to the higher pressure of the surrounding water. As this bubble collapses, the vapour pressure increases within it. The bubble eventually collapses to a minute fraction of its original size, at which point the steam within dissipates energy into the surrounding liquid via a rather violent mechanism which releases a significant amount of energy in the form of an acoustic shock wave. This phenomenon occurs within the fractions of a second. The shock wave or dynamic pressure peak obtained due to bubble collapse has a typical nature and contains two parts, positive and negative (Brennen[111]). Once bubble collapses, it gives rise to the positive part of the peak representing the shock to walls of the vessel (bubble compresses until the pressure inside it is higher than outside of its boundary and then explodes leading to compression of the surrounding water). After the collapse, the surrounding water re-settles (rarefaction of the surrounding water) to occupy the volume held by the bubble, which contributes to the negative part of the peak. Peak of similar kinds were also obtained in the present experiments. Thus, steam explosion is caused by the formation and collapse of vapour bubble formed due to local deposition of thermal energy by the melt into the water. The conversion efficiency plays a key role in deciding the size of the bubble formed and hence the occurrence of steam explosion.

This phenomenology also explains the case that presence of metals in the melt increases the probability of steam explosion compared to that of oxidic melts. Metals have higher thermal conductivity compared to oxidic materials. Due to this, metallic melts transfer their thermal energies nearly instantaneously to the water and thus

forming the bubble quickly. Oxidic melts take longer time to transfer their thermal energies due to low conductivity. In case, the density of the material is very high (like corium), then it will reach to the bottom of the vessel before conducting its thermal energy completely to the water and thus doesn't undergo explosive interaction with water.

It may also be noted that the studies conducted so far are lacking to capture (photographically) the formation and collapse of this bubble, formed due to thermal cavitation, may be due to lower temporal resolution in voided environment.

### 7.6. Summary

The phenomenology of fuel-coolant interaction has been studied to investigate the cause and the condition for steam explosion to occur. Several experiments have been performed and analysed to find out the root cause of the steam explosion. Following are the key findings of the present study:

- Keeping the water volume constant and varying melt amount i.e. with increase in melt-to-water ratio, after a threshold a mild steam explosion occurred.
- In all the experiments, the debris found were globular and larger in sizes (ranged between a few mm to 42 mm agglomerations) which could not be explained by the fact that fine fragments are needed for steam explosion to occur.
- Conversion efficiency analysis has shown that steam explosion could occur even in the absence of fine fragments. This is so because of the significant transfer of thermal energy which helps in formation of bubble.
- Conversion efficiency plays the key role in deciding the pressure spike occurred during FCI.
- Thermal cavitation gives us much clear picture of steam explosion phenomenology and it could also explain various associated phenomena.

It can thus be concluded that fine fragmentation is not the root cause for the steam explosion. It is necessary to investigate further in the direction of thermal cavitation phenomenology to understand steam explosion at fundamental state. Role of conversion efficiency is profound in deciding the pressure spike observed during steam explosion and this phenomenology can be used to estimate the safety margins for the systems involving possible melt-water interactions.



# Chapter

*“The combination of experience and experimentation will ultimately yield a personal sound”*

— *Mark Wells White Jr. (March 17, 1940 – August 5, 2017)*  
*American politician and lawyer*



## Chapter 8. CONCLUSIONS

The present study is focused to resolve several scientifically unexplained aspects of molten corium coolability which are important for the design of core catchers for advanced nuclear reactors. The physics behind melt coolability for dry and wet conditions of the core catcher has been brought out. Detailed phenomenology of melt coolability under bottom flooding and the influences of various parameters were determined. Insights on root cause of steam explosion which may occur during fuel-coolant interaction in case of wet conditions of core catcher has been brought out. The main conclusions drawn out from the study are as follows:

### 8.1. Influence of decay heat on melt coolability under bottom flooding

To understand the influence of decay heat on coolability of molten corium under bottom flooding, experiments were performed, without decay heat and with decay heat, using Sodium borosilicate glass as the stimulant material under similar initial conditions. To simulate the decay heat radiative heaters were used to heat the molten pool.

These experiments resulted in following insights.

- Without decay heat, the quenching of melt lasted for very short period of time. The entire melt was converted into fine debris which resulted in early stabilization of all temperatures up to saturation level and further to ambient temperature. A porous bed of 51% porosity and particle sizes ranging from very fine particles to 10 mm size chunks was obtained which resulted in rapid heat transfer. Along with them, numerous Pele's hairs of thickness ranging from a few microns to a millimetre were found in the debris. Presence of such particles validates the high shear between melt and generated steam as a results of an eruption.

- Results with decay heat simulation surprisingly showed that the quenching of the melt in this scenario took almost similar time as that in stored heat case (i.e. no decay heat). The entire melt was converted into fine and large sized porous debris which enhanced the coolability. However, the debris formed of sizes ranging from 0.5 to 50 mm sized porous chunks including “Pele’s hair” particles. Presence of these fine strands of debris confirms the eruption with high shear between melt and resulted steam. The average porosity was to be much higher than the stored heat case and was measured as 67%. Although, it took little more time for all temperatures to reach saturation due to presence of decay heat.

Thus, it can be concluded that the quenching characteristics of molten material with bottom flooding does not depend on decay heat, although stabilization of debris temperatures at saturation take longer duration as compared to stored heat scenarios. The bottom flooding technique for melt coolability is the most efficient technique even under actual decay heat scenario and can be effectively utilized for advanced core catcher designs.

## 8.2. Scalability of melt coolability under bottom flooding phenomena

To understand the scalability of melt coolability experiments, several experiments were conducted to understand the following aspects:

### (a) Influence of melt volume

Experiment was conducted with 20 litre of sodium borosilicate glass and then was repeated with 3 litre of the same melt.

### (b) Influence of melt composition

Experiment was conducted with 5 kg of sodium borosilicate glass and then was repeated with same amount of CaO-B<sub>2</sub>O<sub>3</sub> melt.

Following are the key insights of these experiments.

- Experiments performed with two different melt volumes having almost same melt heights, suggest that the average quenching time remains more or less same. The debris particles sizes and morphology were also found to be the same in both the cases. Hence, it can be concluded that the results of the experiments with small melt volumes can be safely extrapolated to the experiments with large volumes of melt.
- The quenching time was higher for CaO-B<sub>2</sub>O<sub>3</sub> compared to borosilicate glass. This difference in quenching time is attributed to more strength of CaO-B<sub>2</sub>O<sub>3</sub> compared to that of borosilicate glass. Thus, the time taken by the CaO-B<sub>2</sub>O<sub>3</sub> to erupt was more compared that to glass; but once the melt erupts and get converted to debris, it gets cooled within a few minutes. Hence, the coolability behaviour is not much affected by the debris structures.
- The porosity measured in all these cases was in the range of 50-60%.

Thus, it can be concluded that the the stimulant material having strength closer to the prototype should have similar melt coolability behaviour under bottom flooding.

### 8.3. Influence of nozzle diameter and injection pressure on melt coolability under bottom flooding

To understand the influence of geometric and operating parameters on melt coolability with bottom flooding, experiments have been performed by varying the nozzle diameter and inlet injection pressure. It has been observed that the overall coolability behaviour under bottom flooding remains unaffected by any of these parameters. However, there is a certain effect of each parameter on time required for cooling the molten pool.

- In the experiment with 8 mm nozzle diameter, the quenching time was higher compared to experiments with 12 mm and 18 mm nozzle diameters for same inlet pressure. This is because of the low flow rates available due to smaller nozzle diameter. However, the melt quenching time was found minimum for 12 mm diameter nozzle at 0.75 bar inlet pressure.
- For the given nozzle diameter, the average quenching time was less for higher inlet pressure.
- The average porosities measured were found to be in the range of 50-60% for all the cases, which is sufficiently large for cooling any debris bed.

It can thus be concluded that any molten pool can be cooled within a few minutes under bottom flooding and the average quenching time can be optimized by selecting suitable combinations of physical and geometrical parameters.

#### 8.4. [Development of model to understand melt coolability under bottom flooding](#)

Since there were no models available for simulation of this complex phenomenon, a new numerical model has been developed from first principle to simulate the melt coolability under bottom flooding with decay heat. The model postulates the formation of crust below the melt pool when water is being inserted from the bottom. The model predicts the failure of this crust due to various stresses, resulting in the inverted cone shaped melt eruption. The model captures this ‘eruption cone’ along with radial variation in porosity. The key inferences obtained from these experimental measurements and numerical predictions are as follows:

- The melt eruption model is able to capture the formation of inverted conical shaped porous zone.

- The radial variation in porosity follows the below mentioned empirical relation within the eruption zone.

$$\varepsilon = 0.753 e^{-11.9 r}$$

- The heat transfer between melt and the cooling fluid is through boiling. Accounting the heat sink term in the energy balance equation predicts better estimates of melt pool temperature variations.
- It have been observed both numerically and experimentally, that the quenching of the melt takes place within a few seconds and the cooling of the debris also achieved within a few minutes under bottom flooding even in the presence of decay heat.

It can thus be concluded that presented model is able to capture the physics of melt eruption during the coolability under bottom flooding with decay heat simulation. This model can be used for the estimation of actual reactor scenarios and the duration of melt pool cooling can be well predicted.

#### 8.5. Melt coolability during wet conditions in a core catcher: fuel coolant interaction

The phenomenology of steam explosion has been studied to investigate the cause and the condition for its occurrence. Several experiments have been performed and analysed to find out the root cause of the steam explosion. Following are the key findings of the present study:

- Keeping the water volume constant and varying melt amount i.e. with increase in melt-to-water ratio, after a threshold steam explosion occurred.
- In all the experiments, the debris found were globular and larger in sizes (ranged between a few mm to 42 mm agglomerations) which could not be explained by the fact that fine fragments are needed for steam explosion to occur.

- Conversion efficiency analysis has shown that steam explosion could occur even in the absence of fine fragments. This is so because of the significant transfer of thermal energy which helps in formation of bubble.
- Conversion efficiency plays the key role in deciding the pressure spike occurred during FCI.
- Thermal cavitation gives us much clear picture of steam explosion phenomenology and it could also explain various associated phenomena.

It can thus be concluded that fine fragmentation is not the root cause for the steam explosion. It is necessary to investigate further in the direction of thermal cavitation phenomenology to understand steam explosion at fundamental state. Role of conversion efficiency is profound in deciding the pressure spike observed during steam explosion and this phenomenology can be used to estimate the safety margins for the systems involving possible melt-water interactions.

#### 8.6. *Lessons learnt, Recommendations and Future work*

In the present work, the phenomenology of melt coolability under bottom flooding has been established. More than 30 experiments have been performed to understand the repeatability, scalability of melt volume and melt composition, effect of geometrical parameters and influence of decay heat using different corium simulants ( $\text{CaO-B}_2\text{O}_3$  and Sodium borosilicate glass). It was found that a large amount of melt can be cooled in a very short time.

However, the question arises whether these results are applicable to actual core catcher on reactor scale?

- In the experiments performed in 130 mm and 300 mm diameter test sections, it was observed that the eruption diameter was 300 mm achieved using a single nozzle. In the core catcher on reactor scale, numerous nozzles each placed with pitch less than 300 mm should be used to cover the entire core catcher area. In this scenario,

each segment with single nozzle will be similar to the present experiments. The above distribution function will then definitely remain valid for this and thus on reactor scale.

- As shown by the results on scalability of melt volume, the coolability behaviour remains similar when the melt volume is increased. This indicates that it will also remain same on reactor scale and the results from experiments can be safely extrapolated to reactor scale. In order to do that, on reactor scale, the core catcher will not be the single volume entity; rather, it will be the combination of multiple small volume units. For example, if 100 tonnes of corium is to be cooled in a core catcher on reactor scale. Then, considering  $8000 \text{ kgm}^{-3}$  (approx.) as its density, the total melt volume to be cooled is around 12,500 litres. In the experiments, 20 litres of melt has been cooled using single nozzle. Thus, using at least 625 nozzles, entire corium can be cooled as stated by the experimental results. Hence, even for several meters of core catcher diameter, the results can be safely used. The same is true for the model as well.

To gain such a confidence for actual nuclear reactor application, it is necessary to investigate further on following aspects:

In terms of technological development, the strength of melt coolability under bottom flooding could become its limitation.

- Due to faster melt cooling rate, it generates a lot of steam which could pressurise the containment of a reactor.
- Due to presence of metals in corium, hydrogen generation is an issue. In presence of steam, it may lead to hydrogen explosion in the containment.

In scientific terms, the phenomenology has been understood for limited melt parameters i.e. for fixed melt height and melt temperature.

- It is necessary to validate the phenomenology at higher melt temperature, higher melt heights and also for high density melts.
- It is also recommended to validate multi-nozzle system using multi-volume approach so as to become more confident of using the bottom flooding technique on reactor scale.
- Study of thermal cavitation approach for better understanding of fuel-coolant interaction phenomenology.
- Also, occurrence of stratified steam explosion at elevated melt temperature due to large temperature difference in case of bottom flooding needs to be investigated.

# References

*“If I had thought about it, I wouldn’t have done the experiment. The literature was full of examples that said you can’t do this”*

— *Spencer Ferguson Silver (06 February 1941 – today)*  
*American chemist*



**REFERENCES**

- [1] H. Tuomisto and T. G. Theofanous, “A consistent approach to severe accident management,” *Nucl. Eng. Des.*, vol. 148, no. 2–3, pp. 171–183, Jul. 1994.
- [2] I. V Kukhtevich *et al.*, “The concept of localization of the corium melt in the ex-vessel stage of a severe accident at a nuclear power station with a VVER-1000 reactor,” vol. 48, pp. 699–706, 2001.
- [3] M. Fischer, “The severe accident mitigation concept and the design measures for core melt retention of the European Pressurized Reactor (EPR),” in *Nuclear Engineering and Design*, 2004, vol. 230, no. 1–3, pp. 169–180.
- [4] H. Alsmeyer and W. Tromm, “Experiments for a core catcher concept based on fragmentation,” in *International Topical Meeting on Advanced Reactor Safety*, 1994.
- [5] H. Alsmeyer and W. Tromm, “Concept of a core cooling system and experiments performed,” *Nucl. Eng. Des.*, vol. 154, no. 1, pp. 69–72, 1995.
- [6] H. Alsmeyer, G. Albrecht, G. Fieg, U. Stegmaier, W. Tromm, and H. Werle, “Controlling and cooling core melts outside the pressure vessel,” *Nucl. Eng. Des.*, vol. 202, no. 2–3, pp. 269–278, 2000.
- [7] H. Alsmeyer and W. Tromm, “The COMET concept for cooling core melts: Evaluation of the experimental studies and use in the EPR,” 1999.
- [8] W. Tromm and A. Et., “Ex-vessel corium cooling by passive water addition through porous concrete,” in *ICONE 9*, 2001.
- [9] R. Hamazaki, Y. Kojima, and H. Yanagisawa, “The enhanced severe accident mitigation systems for a BWR.” 2009.
- [10] M. T. Farmer, S. Lomperski, and S. Basu, “Results of Reactor Materials Experiments Investigating 2-D Core-Concrete Interaction and Debris Coolability.” American Nuclear Society - ANS, La Grange Park (United States), 01-Jul-2004.

- [11] C. R. B. Lister, “On the Penetration of Water into Hot Rock,” *Geophys. J. R. Astron. Soc.*, vol. 39, no. 3, pp. 465–509, 1974.
- [12] H. Björnsson, S. Björnsson, and T. Sigurgeirsson, “Penetration of water into hot rock boundaries of magma at Grímsvötn,” *Nature*, vol. 295, no. 5850, pp. 580–581, Feb. 1982.
- [13] E. A. Jagla and A. G. Rojo, “Sequential fragmentation: The origin of columnar quasihexagonal patterns,” *Phys. Rev. E*, vol. 65, no. 2, p. 26203, Jan. 2002.
- [14] M. Epstein, “Dryout Heat Flux During Penetration of Water Into Solidifying Rock,” *J. Heat Transfer*, vol. 128, no. 8, p. 847, 2006.
- [15] B. R. Sehgal and B. W. Spencer, “ACE Program Phase D: Melt Attack and Coolability Experiments (MACE) Program,” *Second OECD Spec. Meet. Molten Core Debris-Concrete Interact.*, vol. I, pp. 345–356, 1992.
- [16] M. Merilo, M. T. Farmer, and B. W. Spencer, “Status report on the MACE M3B experiment,” in *CSARP Meeting*, 1997.
- [17] M. T. Farmer, R. W. Aeschlimann, D. J. Kilsdonk, and B. W. Spencer, “Results of MACE Test M3b posttest debris characterization. ACEX-TR-31.,” 2000.
- [18] M. T. Farmer and B. W. Spencer, “A review of database pertaining to ex-vessel debris coolability. ACEX-TR-C34,” 2001.
- [19] H. Nagasaka, I. Sakaki, M. Kato, Y. Vasilyev, A. Kolodeshnikov, and V. Zhdanov, “COTELS Project (3) : Ex-vessel Debris Cooling Tests,” vol. I, no. November 1999, pp. 3–10, 1999.
- [20] T. G. Theofanous, C. Liu, and W. W. Yuen, “Coolability and quench of corium–concrete interactions by top feeding. MACE-TR-D15.,” 1998.
- [21] K. B. Vladimir, G. S. Vladimir, B. V. Sevostian, and G. V. Victor, “Severe accident management concept of the VVER-1000 and the justification of corium retention in a

- crucible-type core catcher,” *Nucl. Eng. Technol.*, vol. 41, no. 5, pp. 561–574, 2009.
- [22] R. Wachowiak, “Management of Severe Accident Phenomena in the ESBWR Design,” 2006.
- [23] Westinghouse, “TITLE: AP1000 Pre-Construction Safety Report SIGNATURE / DATE (If processing electronic approval select option) Electronically Approved\*\*\* PATENT REVIEW SIGNATURE / DATE,” 2009.
- [24] D. A. Meneley, C. Blahnik, J. T. Rogers, V. G. Snell, and S. Nijhawan, “Coolability of Severely Degraded CANDU Cores.,” 1996.
- [25] B. R. Sehgal, A. Giri, U. Chikkanagoudar, and A. Karbojian, “Experiments on in-vessel melt coolability in the EC-FOREVER Program,” *Nucl. Eng. Des.*, vol. 236, no. 19–21, pp. 2199–2210, 2006.
- [26] D. A. Henry, R.E.; Dube, “Water in the RPV : a mechanism for cooling debris in the RPV lower head,” *Spec. Meet. Sel. Contain. Sev. Accid. Manag. Strateg.*, vol. I, p. 2, 1994.
- [27] R. E. Henry, “A scaling and experimental approach for investigating in-vessel cooling.,” in *Proceedings of 24th Water Reactor Safety Information Meeting*, 1996, pp. 141–159.
- [28] F. V. Asmolov (KI, Russia), A. Behbahani (NRC, USA), G. Hache (IPSN, R. H. Nakamura (JAERI, Japan), B. Raj Sehgal (SKI, Sweden), V. Strizhov (IBRAE, and F. K. Trambauer (GRS, Germany), H. Tuomisto (Fortum, Finland), C. Vitanza (NEA, “CSNI/NEA RASPLAV Seminar,” 2000.
- [29] T. G. Theofanous, M. Maguire, S. Angelini, and T. Salmassi, “The first results from the ACOPO experiment,” *Nucl. Eng. Des.*, vol. 169, no. 1–3, pp. 49–57, Jun. 1997.
- [30] M. Helle and A. Et, “Experimental COPO II data on natural convection in homogenous and stratified pools.,” in *International Topical Meeting on Nuclear Reactor Thermal Hydraulics (NURETH-9)*, 1999.

- [31] L. Bernaz, J.-M. Bonnet, B. Spindler, and C. Villiermaux, “Thermalhydraulic Phenomena in Corium Pools: Numerical Simulation with TOIBIAC and Experimental Validation with BALI.”
- [32] A. Stepanyan, A. K. Nayak, and B. R. Sehgal, “Experimental investigations of natural convection in a three layer stratified pool with internal heat generation,” *Am. Nucl. Soc. Embed. Top. Meet. - 2004 Int. Top. Meet. Oper. Nucl. Facil. Safety, ONFS*, no. i, pp. 1–8, 2004.
- [33] F. Kretzschmar and B. Fluhrer, “Behavior of the melt pool in the LP of the RPV\_FZKA7382,” no. April, 2008.
- [34] W. Tromm and H. Alsmeyer, “Experiments for a core catcher concept based on water addition from below,” *Nucl. Eng. Des.*, vol. 157, pp. 437–445, 1995.
- [35] H. Alsmeyer, M. Farmer, F. Ferderer, B. Spencer, and W. Tromm, “The COMET-concept for cooling of ex-vessel corium melts.” 1998.
- [36] J. J. Foit, M. Bürger, C. Journeau, H. Alsmeyer, and W. Tromm, “Quenching of melt layers by bottom injection of water in the COMET core-catcher concept,” in *Proceedings of the 3rd European Review Meeting on Severe Accident Research*, 2008, no. September, pp. 1–12.
- [37] W. Tromm, H. Alsmeyer, and H. Schneider, “Fragmentation of melts by waterinlet from below,” in *International Topical Meeting on Nuclear Reactor Thermal-Hydraulics (NURETH-6)*, 1993.
- [38] D. Paladino, S. A. Theerthan, and B. R. Sehgal, “DECOBI: Investigation of melt coolability with bottom coolant injection,” *Prog. Nucl. Energy*, vol. 40, no. 2, pp. 161–206, 2002.
- [39] D. Paladino, A. Theerthan, L. Yang, and B. R. Sehgal, “Experimental investigations on melt-coolant interaction characteristics during debris cooling by bottom injection,” in

- Proceedings of the OECD workshop on ex-vessel debris coolability*, 1999, vol. I.
- [40] D. Paladino, A. Theerthan, and B. R. Sehgal, “Experimental Investigation on Debris Coolability by Bottom Injection.,” in *ANS, Annual Meeting*, 1999.
- [41] W. Widmann, M. Bürger, G. Lohnert, H. Alsmeyer, and W. Tromm, “Experimental and theoretical investigations on the COMET concept for ex-vessel core melt retention,” *Nucl. Eng. Des.*, vol. 236, no. 19–21, pp. 2304–2327, 2006.
- [42] D. H. Cho, R. J. Page, S. H. Abdulla, M. H. Anderson, H. B. Klockow, and M. L. Corradini, “Melt quenching and coolability by water injection from below: Co-injection of water and non-condensable gas,” *Nucl. Eng. Des.*, vol. 236, no. 19–21, pp. 2296–2303, 2006.
- [43] S. Lomperski and M. T. Farmer, “Performance testing of engineered corium cooling systems,” *Nucl. Eng. Des.*, vol. 243, pp. 311–320, 2012.
- [44] P. P. Kulkarni and A. K. Nayak, “A simple model to understand physics of melt coolability under bottom flooding,” *Nucl. Eng. Des.*, vol. 262, pp. 81–87, 2013.
- [45] P. P. Kulkarni and A. K. Nayak, “Study on coolability of melt pool with different strategies,” *Nucl. Eng. Des.*, vol. 270, pp. 379–388, 2014.
- [46] J. M. Fyler and W. Wetherbee, “Geoffrey Chaucer: The Canterbury Tales.,” *Speculum*, vol. 68, no. 2, p. 575, 1993.
- [47] D. Magallon and I. Huhtiniemi, “Corium melt quenching tests at low pressure and subcooled water in FARO,” *Nucl. Eng. Des.*, vol. 204, no. 1–3, pp. 369–376, 2001.
- [48] D. Magallon, “Characteristics of corium debris bed generated in large-scale fuel-coolant interaction experiments,” *Nucl. Eng. Des.*, vol. 236, no. 19–21, pp. 1998–2009, 2006.
- [49] D. Magallon, I. Huhtiniemi, and H. Hohmann, “Lessons learnt from FARO/TERMOS corium melt quenching experiments,” *Nucl. Eng. Des.*, vol. 189, no. 1, pp. 223–238, 1999.

- [50] A. Kaiser, F. Huber, and D. Wilhelm, “Experiments on the behaviour of a hot melt injected into sodium,” *Exp. Therm. Fluid Sci.*, vol. 18, no. 1, pp. 48–69, 1998.
- [51] K. Moriyama, Y. Maruyama, and H. Nakamura, “A simple evaluation method of the molten fuel amount in a premixing region of fuel-coolant interactions,” *J. Nucl. Sci. Technol.*, vol. 39, no. 1, pp. 53–58, 2002.
- [52] M. L. Corradini, B. J. Kim, and M. D. Oh, “Vapor explosions in light water reactors: A review of theory and modeling,” *Prog. Nucl. Energy*, vol. 22, no. 1, pp. 1–117, 1988.
- [53] M. L. Corradini and R. Taleyarkhan, “Vapor explosions: {A} review of experiments for accident analysis,” *Nucl. Saf.*, vol. 32, Jul. 1991.
- [54] G. Berthoud, “Vapor Explosions,” *Annu. Rev. Fluid Mech.*, vol. 32, no. 1, pp. 573–611, Jan. 2000.
- [55] D. H. Cho, D. R. Armstrong, and R. P. Anderson, “Combined vapor and chemical explosions of metals and water,” *Nucl. Eng. Des.*, vol. 155, no. 1–2, pp. 405–412, 1995.
- [56] D. Magallon and H. Hohmann, “High pressure corium melt quenching tests in FARO,” *Nucl. Eng. Des.*, vol. 155, no. 1–2, pp. 253–270, 1995.
- [57] G. Hwang *et al.*, “FARO tests corium-melt cooling in water pool: Roles of melt superheat and sintering in sediment,” *Nucl. Eng. Des.*, vol. 305, pp. 569–581, 2016.
- [58] A. Annunziato, A. Yerkess, and C. Addabbo, “FARO and KROTOS code simulation and analysis at JRC Ispra,” *Nucl. Eng. Des.*, vol. 189, no. 1, pp. 359–378, 1999.
- [59] A. K. Nayak, H. S. Park, A. Annunziato, and B. R. Sehgal, “Investigations on Steam Explosion Phenomena with FARO and TROI Experiments,” no. iii, pp. 1–22.
- [60] G. Hwang *et al.*, “FARO tests corium-melt cooling in water pool: Roles of melt superheat and sintering in sediment,” *Nucl. Eng. Des.*, vol. 305, no. August, pp. 569–581, 2016.
- [61] Z. Magali *et al.*, “The KROTOS KFC and SERENA / KS1 tests : experimental results

- and MC3D calculations,” *7th Int. Conf. Multiph. Flow*, no. 7, pp. 1–11, 2010.
- [62] I. Huhtiniemi, D. Magallon, and H. Hohmann, “Results of recent KROTOS FCI tests: alumina versus corium melts,” *Nucl. Eng. Des.*, vol. 189, no. 1, pp. 379–389, 1999.
- [63] “Title : P2 . 10 - The KROTOS-SERENA tests : experimental results ans MC3D calculations URL : Site : University of Florida Digital Collections.”
- [64] I. Huhtiniemi and D. Magallon, “Insight into steam explosions with corium melts in KROTOS,” *Nucl. Eng. Des.*, vol. 204, no. 1–3, pp. 391–400, 2001.
- [65] R. Chen, J. Wang, G. H. Su, S. Qiu, and M. L. Corradini, “Analysis of KROTOS KS-2 and KS-4 steam explosion experiments with TEXAS-VI,” *Nucl. Eng. Des.*, vol. 309, pp. 104–112, 2016.
- [66] P. Piluso *et al.*, “Severe Accident Experiments on PLINIUS Platform Results of First Experiments on COLIMA Facility Related to VVER-440 - Presentation of Planned VULCANO and KROTOS Tests,” *Int. Conf. Nucl. Energy New Eur.*, pp. 1–12, 2005.
- [67] M. Uršič, M. Leskovar, and B. Mavko, “Simulations of KROTOS alumina and corium steam explosion experiments: Applicability of the improved solidification influence modelling,” *Nucl. Eng. Des.*, vol. 246, pp. 163–174, 2012.
- [68] H. Hohmann, D. Magallon, H. Schins, and A. Yerkess, “FCI experiments in the aluminum oxide/water system,” *Nucl. Eng. Des.*, vol. 155, no. 1–2, pp. 391–403, 1995.
- [69] D. Magallon, “Status and prospects of resolution of the vapour explosion issue in light water status and prospects of resolution of the vapour explosion issue in light water,” *Nucl. Eng. Technol.*, vol. 41, no. 5, pp. 603–616, 2017.
- [70] I. Huhtiniemi, H. Hohmann, and D. Magallon, “FCI experiments in the corium/water system,” *Nucl. Eng. Des.*, vol. 177, no. 1, pp. 339–349, 1997.
- [71] D. Magallon, “Status of International Programme SERENA on Fuel-Coolant Interaction,” *At. Energy*, vol. 33, no. 0, pp. 1–9, 2005.

- [72] J. H. Song *et al.*, “Experiments on the interactions of molten ZrO<sub>2</sub> with water using TROI facility,” *Nuclear Engineering and Design*, vol. 213, no. 2–3, pp. 97–110, 2002.
- [73] J. H. Kim *et al.*, “Steam explosion experiments using nuclear reactor materials in the TROI facilities,” in *Heat Transfer Engineering*, 2008, vol. 29, no. 8, pp. 748–756.
- [74] A. K. Nayak, H. S. Park, and B. R. Sehgal, “Simulation of the Faro and Troi Steam Explosion Behaviour Using the Cometa Code,” no. iii, pp. 1–16, 2005.
- [75] J. H. Song *et al.*, “Experiments on the interactions of molten ZrO<sub>2</sub> with water using TROI facility,” *Nucl. Eng. Des.*, vol. 213, no. 2–3, pp. 97–110, 2002.
- [76] J. H. Song *et al.*, “Insights from the recent steam explosion experiments in TROI,” *J. Nucl. Sci. Technol.*, vol. 40, no. 10, pp. 783–795, 2003.
- [77] J. H. Song *et al.*, “Fuel coolant interaction experiments in TROI using a UO<sub>2</sub>/ZrO<sub>2</sub> mixture,” *Nucl. Eng. Des.*, vol. 222, no. 1, pp. 1–15, 2003.
- [78] J. H. Kim *et al.*, “Results of the Triggered TROI Steam Explosion Experiments with a Narrow Interaction Vessel,” *At. Energy*, pp. 1322–1331, 2006.
- [79] S. W. Hong, S. H. Hong, K. S. Ha, J. H. Kim, and B. T. Min, “The measurement of void fraction by a differential pressure during a premixing stage in the TROI,” *Nucl. Eng. Des.*, vol. 265, pp. 846–855, 2013.
- [80] J. H. Kim *et al.*, “Layer inversion tests with metal-added corium in the TROI experiment,” in *Societe Francaise d’Energie Nucleaire - International Congress on Advances in Nuclear Power Plants - ICAPP 2007, “The Nuclear Renaissance at Work,”* 2008, vol. 3.
- [81] J. H. Kim *et al.*, “Triggered Steam Explosion Experiments in the TROI Facility,” *At. Energy*, pp. 1–9, 2005.
- [82] M. Uršič and M. Leskovar, “Analysis of TROI-13 steam explosion experiment,” *Sci. Technol. Nucl. Install.*, vol. 2008, 2008.

- [83] I. K. Park, J. H. Kim, B. T. Min, and S. W. Hong, “Thermal-hydraulic aspects of FCIs in TROI corium/water interaction tests,” *Nucl. Eng. Des.*, vol. 263, pp. 419–430, 2013.
- [84] K. D. Hee, K. H. Dong, K. T. Jong, K. B. Sang, S. H. Jin, and H. W. Seong, “Investigations on the resolution of severe accident issues for Korean nuclear power plants,” *Nucl. Eng. Technol.*, vol. 41, no. 5, pp. 617–648, 2009.
- [85] J. H. Song, S. B. Kim, and H. D. Kim, “On some salient unresolved issues in severe accidents for advanced light water reactors,” *Nucl. Eng. Des.*, vol. 235, no. 17–19, pp. 2055–2069, 2005.
- [86] Y. S. Na, S. H. Hong, J. H. Song, and S. W. Hong, “Fuel-Coolant Interaction Visualization Test for In-Vessel Corium Retention External Reactor Vessel Cooling (IVR-ERVC) Condition,” *Nucl. Eng. Technol.*, vol. 48, no. 6, pp. 1330–1337, 2016.
- [87] M. Leskovar, V. Centrih, and M. Uršič, “Analysis of oxidation influence on steam explosion energetics,” *Ann. Nucl. Energy*, vol. 90, pp. 441–449, 2016.
- [88] J. H. Song and J. H. Kim, “The effect of the UO<sub>2</sub>/ZrO<sub>2</sub> composition on fuel/coolant interaction,” *Nucl. Technol.*, vol. 149, no. 3, pp. 309–323, 2005.
- [89] D. E. Mitchell, M. L. Corradini, and W. W. Tarbell, “Intermediate Scale Steam Explosion Phenomena: Experiments and Analysis,” in *NUREG/CR-2145, SAND81-0124.*, 1981.
- [90] N. Yamano, Y. Maruyama, T. Kudo, A. Hidaka, and J. Sugimoto, “Phenomenological studies on melt-coolant interactions in the ALPHA program,” *Nucl. Eng. Des.*, vol. 155, no. 1–2, pp. 369–389, 1995.
- [91] P. Kudinov, A. Karbojian, W. Ma, and T.-N. Dinh, “The DEFOR-S Experimental Study of Debris Formation with Corium Simulant Materials,” *Nucl. Technol.*, vol. 170, no. 1, pp. 219–230, Apr. 2010.
- [92] P. Kudinov, M. Davydov, G. Pohlner, M. Bürger, M. Buck, and R. Meignen, “Validation

- of the FCI Codes against DEFOR-A Data on the Mass Fraction of Agglomerated Debris,” *th Eur. Rev. Meet. Sev. Accid. Res. Col.*, 2012.
- [93] P. Kudinov, A. Karbojian, C. T. Tran, and W. Villanueva, “Agglomeration and size distribution of debris in DEFOR-A experiments with Bi<sub>2</sub>O<sub>3</sub>-WO<sub>3</sub> corium simulant melt,” *Nucl. Eng. Des.*, vol. 263, pp. 284–295, Oct. 2013.
- [94] P. Kudinov, D. Grishchenko, A. Konovalenko, and A. Karbojian, “Experimental investigation of debris bed agglomeration and particle size distribution using W<sub>3</sub>-ZR<sub>2</sub> melt,” in *International Topical Meeting on Nuclear Reactor Thermal Hydraulics 2015, NURETH 2015*, 2015, vol. 10, pp. 8046–8054.
- [95] P. Kudinov and M. Davydov, “Development and validation of conservative-mechanistic and best estimate approaches to quantifying mass fractions of agglomerated debris,” *Nucl. Eng. Des.*, vol. 262, pp. 452–461, Sep. 2013.
- [96] K. Moriyama and H. S. Park, “Challenges in Thermohydraulic Analysis of LWR Severe Accidents : Steam Explosion,” in *IW-NRTHS 2014: international workshop on new horizons in nuclear reactor thermal hydraulics and safety*, 2014, vol. I, p. 91.
- [97] A. K. Nayak, R. K. Singh, P. P. Kulkarni, and B. R. Sehgal, “A numerical and experimental study of water ingression phenomena in melt pool coolability,” *Nucl. Eng. Des.*, vol. 239, no. 7, pp. 1285–1293, 2009.
- [98] D. Shimozuru, “Physical parameters governing the formation of Pele’s hair and tears,” *Bull. Volcanol.*, vol. 56, no. 3, pp. 217–219, 1994.
- [99] S. Timoshenko and S. Woinowsky-Krieger, *Theory of Plates and Shells*, Second. New York: McGraw-Hill, 1959.
- [100] M. Bursik, “Effect of Wind on the Rise Height of Volcanic Plumes,” *Geophys. Res. Lett.*, vol. 28, no. 18, pp. 3621–3624, 2001.
- [101] G. N. Abramovich, *The Theory of Turbulent Jets*. 1963.

- [102] S. Barsotti, A. Neri, and J. S. Scire, “The VOL-CALPUFF model for atmospheric ash dispersal: 1. Approach and physical formulation,” *J. Geophys. Res. Solid Earth*, vol. 113, no. 3, pp. 1–12, 2008.
- [103] N. Zuber, “On stability of boiling heat transfer.,” *ASME Trans.* 80, 711–720., vol. 80, pp. 711–720, 1958.
- [104] P. J. Berenson, “Film-Boiling Heat Transfer From a Horizontal Surface,” *J. Heat Transfer*, vol. 83, no. 3, p. 351, Aug. 1961.
- [105] W. M. Rohsenow, “A method of correlating heat transfer data for surface boiling of liquids,” (Technical Report No. 5), Publisher: Cambridge, Mass. : M.I.T. Division of Industrial Cooperation, 1951.
- [106] B. R. Sehgal, *Nuclear safety in light water reactors*. 1st edition, Elsevier Inc., ISBN-978-0-12-388446-6. 2012.
- [107] G. Berthoud, “Vapor explosions,” *Annu. Rev. Fluid Mech.* pp. 573–611, 2000.  
<https://doi.org/10.1146/annurev.fluid.32.1.573>
- [108] S. J. Board, R. W. Hall, and R. S. Hall, “Detonation of fuel coolant explosions,” *Nature*, vol. 254, pp. 319–321, 1975.
- [109] D. F. Fletcher and T. G. Theofanous, “Heat Transfer and Fluid Dynamic Aspects of Explosive Melt–Water Interactions,” in *Advances in Heat Transfer*, vol. 29, no. C, Elsevier Inc., pp. 129–213. 1997
- [110] L. D. Landau and E. M. Lifshitz, *Fluid mechanics: Landau and Lifshitz: course of theoretical physics*, vol. 6, no. 1. 1987.
- [111] E. Christopher, Brennen, C. E. Brennen, and E. Christopher, Brennen, *Cavitation and bubble dynamics*, vol. 9, no. 1. 1995.